Supplementary Information for

A Secondary-Sphere Proton Channel Accelerating Metal–Hydride Formation in Mn(I) Catalysts for Selective CO_2-to-Formate Conversion

Min-Jong Bong,[1,2,#] Wonjung Lee,[3,4,#] Daehan Lee,[1] Hyunuk Kim,[1,2] Junhyeok Seo,[3,4,*] and Ho-Jin Son[1,2,*]

[1]Department of Advanced Materials Chemistry, Korea University, Sejong 30019, Republic of Korea
[2]Division of Smart Energy Convergence Engineering, Korea University, Sejong 30019, Republic of Korea
[3]Department of Chemistry, Gwangju Institute of Science and Technology (GIST), Gwangju 61005, Republic of Korea
[4]Research Center for Innovative Energy and Carbon Optimized Synthesis for Chemicals (Inn-ECOSysChem), Gwangju Institute of Science and Technology (GIST), Gwangju 61005, Republic of Korea

*Correspondence and requests for materials should be addressed to

*E-mail: seojh@gist.ac.kr.
*E-mail: hjson@korea.ac.kr.

Table of contents

Experimental

General Procedures. All reagents were purchased from Aldrich and were used without further purification. All manipulations were performed under a dry nitrogen or argon atmosphere by using standard Schlenk techniques. *N,N*-Dimethylacetamide (DMA) and *N,N*-dimethylformamide (DMF) were distilled from calcium hydride and stored over molecular sieves. The other solvents used were distilled over sodium−benzophenone under nitrogen prior to use. Glassware, syringes, magnetic stirring bars, and needles were dried in a convection oven for over 4 hours before use. Reactions were monitored by thin-layer chromatography (TLC; Merck Co.). The spots developed onto TLC were identified under UV light at 254 or 365 nm. Column chromatography was performed on silica gel 60 G (particle size 5–40 μm; Merck Co.). The ^{1}H NMR spectra were recorded on a JEOL JNM-ECZ400S (400 MHz) spectrometer. The IR spectra were measured using a Nicolet 6700 Fourier Transform Infrared Spectrometer (FTIR) from Thermo Fisher Scientific. ESI-MS was performed by the linear ion trap of a LTQ XL ETD mass spectrometer (Thermo Fisher Scientific, LCQ Fleet Hyperbolic Ion Trap MS/MSn spectrometer). GC–MS spectra were recorded on an Agilent Technologies 7890A GC system equipped with a 5975C inert MSD with Triple-Axis detector, using an Agilent J&W DB-FFAP column. Elemental analyses (EA) were performed using a Thermo Scientific FlashSmart Elemental Analyzer.

Synthesis and Characterization. Ir(III) complex (IrPS) $[Ir(C^N)_2(N^N)]^+$ (C^N = 1-phenylisoquinoline (piq), N^N = 4,4′-dimethyl-2,2′-bipyridine),[S1] 4,4′-di-*tert*-butyl-6-methyl-2,2′-bipyridine (**bpy^{Me}**),[S2] 6-(alcholethyl)-4,4′-di-*tert*-butyl-2,2′-bipyridine (**bpy^{OH}**),[S3,S4] 4,4′-di-*tert*-butyl-6-(2-methoxyethyl)-2,2′-bipyridine (**bpy^{OMe}**),[S5] 4,4′-di-*tert*-butyl-6-(2-ethoxyethyl)-2,2′-bipyridine (**bpy^{OEt}**),[S5] 4,4′-di-*tert*-butyl-6-butyl-2,2′-bipyridine (**bpy^{Bu}**),[S6] 4,4′-di-*tert*-butyl-6,6′-dimethyl-2,2′-bipyridine (**bpy^{diMe}**),[S7] 6,6′-di-(alcholethyl)-4,4′-di-*tert*-butyl-2,2′-bipyridine (**bpy^{diOH}**),[S3,S4] 4,4′-di-*tert*-butyl-6,6′-bis(2-methoxyethyl)-2,2′-bipyridine (**bpy^{diOMe}**),[S5] and sacrificial

electron donor (BIH)[S8] were prepared according to the previously reported procedures. The functionalized Mn(I) complexes (**Mn-bpy^{OH}**, **Mn-bpy^{OMe}**, **Mn-bpy^{OEt}**, **Mn-bpy^{Bu}**, **Mn-bpy^{diOH}** and **Mn-bpy^{diOMe}**) were synthesized by modifying a previous protocol,[S9] details of which are described below (Scheme 1).

6-(alcholethyl)-4,4′-di-*tert*-butyl-2,2′-bipyridine (bpy^{OH}). To a solution of diisopropylamine (1.0 mL, 4.6 mmol) in THF (10 mL), cooled to –78 °C, was added dropwise *n*-butyllithium (2.5 M in *n*-hexane, 2.0 mL, 5.0 mmol) under a N_2 atmosphere. The resulting LDA solution was stirred at –78 °C for 20 min and subsequently transferred dropwise via cannula to a cold solution of 4,4′-di-*tert*-butyl-6-methyl-2,2′-bipyridine (**bpy^{Me}**; 1.0 g, 3.5 mmol) in THF (30 mL). After stirring at –78 °C for 3 h, paraformaldehyde (0.27 g, 8.9 mmol) was added, and the reaction mixture was allowed to warm to room temperature and stirred for an additional 10 h under a N_2 atmosphere. The reaction was quenched with water, and the aqueous phase was extracted with EtOAc (3 × 50 mL) and washed with brine. The combined organic layer was dried over Na_2SO_4, filtered, and concentrated under reduced pressure. The crude product was purified by silica gel chromatography (*n*-hexane/EtOAc = 2:1, *v*/*v*, containing 2 vol% triethylamine) to afford **bpy^{OH}** as an off-white solid (R_f = 0.4). Yield: 42% (0.47 g, 1.5 mmol). ^{1}H NMR (400.1 MHz, [D$_1$]CHCl$_3$): δ = 8.58 (d, J = 5.2 Hz, 1H), 8.29 (s, 2H), 7.31 (dd, J_1 = 5.4 Hz, J_2 = 1.8 Hz, 1H), 7.16 (s, 1H), 4.11 (t, J = 5.5 Hz, 2H), 3.09 (t, J = 5.4 Hz, 2H), 1.37 (s, 18H). ESI-MS (*m*/*z*): Calcd. for $C_{20}H_{28}N_2O$, 312.2202 [M]; found 313.5358 $[M + H]^+$, 335.4583 $[M + Na]^+$.

4,4′-di-*tert*-butyl-6-(2-methoxyethyl)-2,2′-bipyridine (bpy^{OMe}). A mixture of **bpy^{OH}** (1.0 g, 3.2 mmol), methyl iodide (0.30 mL, 3.7 mmol), and KOH (0.80 g, 14 mmol) in acetonitrile (50 mL) was stirred at room temperature for 5 h under a N_2 atmosphere. Upon completion, the reaction was quenched with water, and the mixture was extracted with CH_2Cl_2 (3 × 50 mL). The combined organic

layer was dried over Na_2SO_4, filtered, and concentrated under reduced pressure. The crude dark orange liquid was purified by silica gel chromatography (*n*-hexane/EtOAc = 4:1, *v*/*v*) to afford **bpy^{OMe}** as an off-white solid (R_f = 0.3). Yield: 78% (0.82 g, 2.5 mmol). ^{1}H NMR (400.1 MHz, [D$_1$]CHCl$_3$): δ = 8.58 (dd, J_1 = 5.1 Hz, J_2 = 0.8 Hz, 1H), 8.45 (s, 1H), 8.24 (s, 1H), 7.29 (dd, J_1 = 5.3 Hz, J_2 = 2.0 Hz, 1H), 7.21 (s, 1H), 3.89 (t, J = 6.7 Hz, 2H), 3.41 (s, 3H), 3.15 (t, J = 6.9 Hz, 2H), 1.38 (s, 9H), 1.37 (s, 9H). ESI-MS (*m*/*z*): Calcd. for $C_{21}H_{30}N_2O$, 326.2358 [M]; found 327.4708 $[M + H]^+$, 349.4468 $[M + Na]^+$.

4,4′-di-*tert*-butyl-6-(2-ethoxyethyl)-2,2′-bipyridine (bpy^{OEt}). A mixture of **bpy^{OH}** (1.0 g, 3.2 mmol), ethyl iodide (0.30 mL, 3.7 mmol), and KOH (0.80 g, 14 mmol) in acetonitrile (50 mL) was stirred at room temperature for 5 h under a N_2 atmosphere. The reaction was quenched with water, and the mixture was extracted with CH_2Cl_2 (3 × 50 mL). The combined organic extracts were dried over Na_2SO_4, filtered, and concentrated under reduced pressure. The resulting dark orange liquid was purified by silica gel column chromatography (*n*-hexane/EtOAc = 4:1, *v*/*v*) to afford **bpy^{OEt}** as an off-white solid (R_f = 0.3). Yield: 73% (0.79 g, 2.3 mmol). ^{1}H NMR (400.1 MHz, [D$_1$]CHCl$_3$): δ = 8.56 (dt, J_1 = 6.3 Hz, J_2 = 0.9 Hz, 1H), 8.42 (s, 1H), 8.20 (s, 1H), 7.25 (dt, J_1 = 5.6 Hz, J_2 = 1.2 Hz, 1H), 7.20 (s, 1H), 3.89 (t, J = 7.9 Hz, 2H), 3.52 (q, J = 6.7 Hz, 2H), 3.13 (t, J = 6.3 Hz, 2H), 1.35 (s, 9H), 1.34 (s, 9H), 1.19 (t, J = 6.3 Hz, 3H). ESI-MS (*m*/*z*): Calcd. for $C_{22}H_{32}N_2O$, 340.2515 [M]; found 341.5525 $[M + H]^+$, 363.5083 $[M + Na]^+$.

4,4′-di-*tert*-butyl-6-butyl-2,2′-bipyridine (bpy^{Bu}). A solution of bpy (1.0 g, 3.7 mmol) in THF (50 mL) was cooled to –78 °C under a nitrogen atmosphere, and *n*-butyllithium (2.5 M in *n*-hexane, 2.0 mL, 5.0 mmol) was added dropwise. The reaction mixture was stirred at –78 °C and monitored by TLC. Upon completion, the reaction was quenched with water, and the mixture was extracted with EtOAc (3 × 50 mL) and washed with brine. The combined organic layer was dried over Na_2SO_4,

filtered, and concentrated under reduced pressure. The crude orange liquid was purified by silica gel chromatography (*n*-hexane/EtOAc = 9:1, *v*/*v*) to afford **bpy^{Bu}** as a bright yellow liquid (R_f = 0.3). Yield: 36% (0.43 g, 1.3 mmol). ^{1}H NMR (400.1 MHz, [D$_1$]CHCl$_3$): δ = 8.58 (d, J = 5.2 Hz, 1H), 8.44 (s, 1H), 8.18 (s, 1H), 7.27 (d, J = 5.3 Hz, 1H), 7.1 (s, 1H), 2.87 (t, J = 7.6 Hz, 2H), 1.81 (p, J = 7.6 Hz, 2H), 1.46 (h, J = 7.5 Hz, 2H), 1.38 (s, 9H), 1.37 (s, 9H), 0.99 (t, J = 7.3 Hz, 3H). ESI-MS (*m*/*z*): Calcd. for $C_{22}H_{32}N_2$, 324.2565 [M]; found 325.4583 $[M + H]^+$, 353.4618 $[M + Na]^+$.

6,6′-di-(alcholethyl)-4,4′-di-*tert*-butyl-2,2′-bipyridine (bpy^{diOH}). To a solution of diisopropylamine (2.0 mL, 8.9 mmol) in THF (20 mL), cooled to –78 °C under a N_2 atmosphere, was added dropwise *n*-butyllithium (2.5 M in *n*-hexane, 4.0 mL, 8.9 mmol). The resulting solution was stirred at –78 °C for 20 min to generate LDA, which was then transferred dropwise via cannula to a cold solution of **bpy^{diMe}** (1.0 g, 3.5 mmol) in THF (30 mL). After stirring at –78 °C for 3 h, paraformaldehyde (0.48 g, 16 mmol) was added, and the reaction mixture was allowed to warm to room temperature and stirred for an additional 10 h under a N_2 atmosphere. The reaction was quenched with water, and the mixture was extracted with EtOAc (3 × 50 mL) and washed with brine. The combined organic layer was dried over Na_2SO_4, filtered, and concentrated under reduced pressure. The crude bright yellow liquid was purified by silica gel chromatography (*n*-hexane/EtOAc = 2:1, *v*/*v*, containing 4 vol% triethylamine) to afford **bpy^{diOH}** as an off-white solid (R_f = 0.3). Yield: 30% (0.38 g, 1.0 mmol). ^{1}H NMR (400.1 MHz, [D$_1$]CHCl$_3$): δ = 8.15 (s, 2H), 7.16 (s, 2H), 5.04 (br, 2H), 4.08 (t, J = 5.7 Hz, 4H), 3.08 (t, J = 5.4 Hz, 4H), 1.34 (s, 18H). ESI-MS (*m*/*z*): Calcd. for $C_{22}H_{32}N_2O_2$, 356.2464 [M]; found 357.3824 $[M + H]^+$, 379.3392 $[M + Na]^+$.

4,4′-di-*tert*-butyl-6,6′-bis(2-methoxyethyl)-2,2′-bipyridine (bpy^{diOMe}). A mixture of **bpy^{diOH}** (1.0 g, 2.8 mmol), methyl iodide (0.50 mL, 7.0 mmol), and KOH (0.80 g, 14 mmol) in acetonitrile (50 mL) was stirred at room temperature for 5 h under a N_2 atmosphere. The reaction was quenched with water,

and the mixture was extracted with CH_2Cl_2 (3 × 50 mL). The combined organic layers were dried over Na_2SO_4, filtered, and concentrated under reduced pressure. The resulting dark orange liquid was purified by silica gel column chromatography (*n*-hexane/EtOAc = 4:1, *v*/*v*) to afford **bpy^{diOMe}** as an off-white solid (R_f = 0.4). Yield: 80% (0.86 g, 2.2 mmol). ^{1}H NMR (400.1 MHz, [D$_1$]CHCl$_3$): δ = 8.22 (s, 2H), 7.17 (s, 2H), 3.87 (t, J = 7.1 Hz, 4H), 3.39 (s, 6H), 3.13 (t, J = 7.1 Hz, 4H) 1.34 (s, 18H). ESI-MS (*m*/*z*): Calcd. for $C_{24}H_{36}N_2O_2$, 384.2777 [M]; found 385.4338 $[M + H]^+$, 407.3335 $[M + Na]^+$.

Mn(6-(alcholethyl)-4,4′-di-*tert*-butyl-2,2'-bipyridine)(CO)$_3$Br (Mn-bpy^{OH}). A solution of **bpy^{OH}** (0.30 g, 0.96 mmol) and $Mn(CO)_5Br$ (0.27 g, 0.98 mmol) in Et_2O (50 mL) was refluxed at 40 °C for 10 h under a N_2 atmosphere. After evaporation of the solvent under reduced pressure, the residue was washed with *n*-hexane (3 × 50 mL). The resulting solid was collected by filtration and dried under vacuum to afford **Mn-bpy^{OH}** as an orange-yellow solid. Yield: 77% (0.39 g, 0.74 mmol). ^{1}H NMR (400.1 MHz, [D$_6$]DMSO): δ = 9.10 (d, J = 5.7 Hz, 1H), 8.58 (s, 1H), 8.49 (s, 1H), 7.71 (d, J = 5.7 Hz, 1H), 7.65 (s, 1H), 4.97 (t, J = 4.9 Hz, 2H), 3.99 (p, J = 5.0 Hz, 2H), 3.52 (t, J = 5.6 Hz, 2H), 1.42 (s, 9H), 1.41 (s, 9H). ESI-MS (*m*/*z*): Calcd. for $C_{23}H_{28}BrMnN_2O_4$, 530.0613 [M]; found 451.1165 $[M – Br]^+$. Anal. Found (%): C, 52.05; H, 5.32; N, 5.28 (Calcd (%): C, 51.99; H, 5.31; N, 5.27).

Mn(4,4'-di-*tert*-butyl-6-(2-methoxyethyl)-2,2'-bipyridine)(CO)$_3$Br (Mn-bpy^{OMe}). A solution of **bpy^{OMe}** (0.30 g, 0.92 mmol) and $Mn(CO)_5Br$ (0.26 g, 0.94 mmol) in Et_2O (50 mL) was refluxed at 40 °C for 10 h under a N_2 atmosphere. After evaporation of the solvent under reduced pressure, the residue was washed with *n*-hexane (3 × 50 mL). The resulting solid was collected by filtration and dried under vacuum to afford **Mn-bpy^{OMe}** as an orange-yellow solid. Yield: 78% (0.39 g, 0.72 mmol). ^{1}H NMR (400.1 MHz, [D$_6$]DMSO): δ = 9.12 (br, 1H), 8.58 (br, 1H), 8.49 (br, 1H), 7.72 (br, 1H), 7.63 (br, 1H), 3.90 (br, 2H), 3.60 (br, 2H), 3.31 (br, 3H), 1.42 (br, 18H). ESI-MS (*m*/*z*): Calcd. for $C_{24}H_{30}BrMnN_2O_4$, 544.0769 [M]; found 465.0848 $[M – Br]^+$. Anal. Found (%): C, 52.88; H, 5.56; N,

5.14 (Calcd (%): C, 52.86; H, 5.55; N, 5.14).

Mn(4,4′-di-*tert*-butyl-6-(2-ethoxyethyl)-2,2′-bipyridine)(CO)$_3$Br (Mn-bpy^{OEt}). A solution of **bpy^{OEt}** (0.30 g, 0.88 mmol) and Mn(CO)$_5$Br (0.25 g, 0.90 mmol) in Et$_2$O (50 mL) was refluxed at 40 °C for 10 h under a N_2 atmosphere. After evaporation of the solvent under reduced pressure, the residue was washed with *n*-hexane (3 × 50 mL). The resulting solid was collected by filtration and dried under vacuum to afford **Mn-bpy^{OEt}** as an orange-yellow solid. Yield: 83% (0.41 g, 0.73 mmol). ^{1}H NMR (400.1 MHz, [D$_6$]DMSO): δ = 9.12 (br, 1H), 8.58 (br, 1H), 8.49 (br, 1H), 7.71 (br, 1H), 7.65 (br, 1H), 3.94 (br, 2H), 3.58 (br, 2H), 3.49 (br, 2H), 1.42 (br, 18H), 1.11 (br, 3H). ESI-MS (*m*/*z*): Calcd. for $C_{25}H_{32}BrMnN_2O_4$, 558.0926 [M]; found 479.1725 [M – Br]$^+$. Anal. Found (%): C, 53.77; H, 5.77; N, 5.02 (Calcd (%): C, 53.68; H, 5.77; N, 5.01).

Mn(4,4′-di-*tert*-butyl-6-butyl-2,2′-bipyridine)(CO)$_3$Br (Mn-bpy^{Bu}). A solution of **bpy^{Bu}** (0.30 g, 0.93 mmol) and Mn(CO)$_5$Br (0.26 g, 0.95 mmol) in Et$_2$O (50 mL) was refluxed at 40 °C for 10 h under a N_2 atmosphere. After evaporation of the solvent under reduced pressure, the residue was washed with *n*-hexane (3 × 50 mL). The resulting solid was collected by filtration and dried under vacuum to afford **Mn-bpy^{Bu}** as an orange-yellow solid. Yield: 75% (0.38 g, 0.70 mmol). ^{1}H NMR (400.1 MHz, [D$_6$]DMSO): δ = 9.09 (br, 1H), 8.55 (br, 1H), 8.45 (br, 1H), 7.67 (br, 1H), 7.59 (br, 1H), 3.47 (br, 2H), 1.79 (br, 2H), 1.40 ppm (br, 18H), 1.38 (br, 2H), 0.87 (br, 3H). ESI-MS (*m*/*z*): Calcd. for $C_{25}H_{32}BrMnN_2O_3$, 542.0977 [M]; found 462.9864 [M - Br]$^+$. Anal. Found (%): C, 55.26; H, 5.93; N, 5.16 (Calcd (%): C, 55.26; H, 5.93; N, 5.16).

Mn(6,6′-di-(alcholethyl)-4,4′-di-*tert*-butyl-2,2′-bipyridine)(CO)$_3$Br (Mn-bpy^{diOH}). A solution of **bpy^{diOH}** (0.30 g, 0.84 mmol) and Mn(CO)$_5$Br (0.24 g, 0.86 mmol) in Et$_2$O (50 mL) was refluxed at 40 °C for 10 h under a N_2 atmosphere. After evaporation of the solvent under reduced pressure, the residue was washed with *n*-hexane (3 × 50 mL). The resulting solid was collected by filtration and

dried under vacuum to afford **Mn-bpy^{diOH}** as an orange-yellow solid. Yield: 63% (0.24 g, 0.67 mmol). ^{1}H NMR (400.1 MHz, [D$_6$]DMSO): δ = 8.34 (s, 2H), 7.60 (s, 2H), 4.93 (s, 2H), 3.87 (t, J = 5.7 Hz, 4H), 3.52 (m, J = 6.4 Hz, 4H), 1.37 ppm (s, 18H). ESI-MS (m/z): Calcd. for $C_{25}H_{32}BrMnN_2O_5$, 574.0875 [M]; found 494.9795 [M – Br]$^+$. Anal. Found (%): C, 52.11; H, 5.62; N, 4.87 (Calcd (%): C, 52.19; H, 5.61; N, 4.87).

Mn(4,4′-di-*tert*-butyl-6,6′-bis(2-methoxyethyl)-2,2′-bipyridine)(CO)$_3$Br (Mn-bpy^{diOMe}). A solution of **bpy^{diOMe}** (0.30 g, 0.78 mmol) and Mn(CO)$_5$Br (0.22 g, 0.80 mmol) in Et$_2$O (50 mL) was refluxed at 40 °C for 10 h under a N$_2$ atmosphere. After evaporation of the solvent under reduced pressure, the residue was washed with *n*-hexane (3 × 50 mL). The resulting solid was collected by filtration and dried under vacuum to afford **Mn-bpy^{diOMe}** as an orange-yellow solid. Yield: 46% (0.15 g, 0.39 mmol). ^{1}H NMR (400.1 MHz, [D$_6$]DMSO): δ = 8.38 (s, 2H), 7.62 (s, 2H), 3.83 (br, 4H), 3.65 (br, 4H), 3.29 (s, 6H), 1.40 ppm (s, 18H). ESI-MS (m/z): Calcd. for $C_{27}H_{36}BrMnN_2O_5$, 602.1188 [M]; found 522.2531 [M – Br]$^+$. Anal. Found (%): C, 53.83; H, 6.01; N, 4.63 (Calcd (%): C, 53.74; H, 6.01; N, 4.64).

Crystal Structure Determination. Orange crystals of **Mn-bpy^{OEt}** and **Mn-bpy^{diOMe}** were obtained from Ether/*n*-hexane solution, sealed in glass capillaries under argon, and mounted on the diffractometer. The preliminary examination and data collection were performed by a Bruker SMART CCD X-ray diffractometer equipped with a sealed-tube X-ray source (50 kV × 30 mA) using graphite-monochromated Mo-$K\alpha$ radiation (λ = 0.71073 Å). The preliminary unit cell constants were determined by using a set of 45 narrow-frame (0.3° in ω) scans. The double-pass method of scanning was used to exclude noise. The collected frames were integrated by using an orientation matrix determined from the narrow-frame scans. A SMART software package was used for data collection, and SAINT was used for frame integration.[S10] The final cell constants were determined through global

refinement of the xyz centroids of the reflections harvested from the entire data set. Structure solution and refinement were performed by using the SHELXTL-PLUS software package.[S11] Crystallographic data were deposited with the Cambridge Crystallographic Data Centre as supplementary publications (CCDC-2500003 **Mn-bpy^{OEt}** and CCDC-2500002 **Mn-bpy^{diOMe}**). Tables S1−S8 of the SI provide additional crystallographic data.

Photocatalytic CO_2 Reduction. The Mn(I) catalysts (0.1 mM) with Ir(III) photosensitizer (IrPS, 0.3 mM) in 3 mL of DMA or mixed DMA/additive solvent (additive = TEOA) containing 0.1 M BIH were placed in a Pyrex cell (1 cm pass length; 12.8 mL total volume), bubbled with CO_2 for 30 min, and sealed with a septum. A series of samples were set on a homemade merry-go-round apparatus and then irradiated under magnetic stirring with an LED lamp (60 W, model Fc-6051, Cree Inc.). For the LED lamp, the incident light (λ >500 nm) was obtained by passing the light through a K_2CrO_4 solution layer of 1.0 cm path length. The gaseous products that evolved in the overhead space of the cell were identified by GC (7890B GC equipped with a TCD detector) using a SUPELCO Carboxen™ 1010 PLOT fused silica capillary column. The liquid phase of the irradiated samples was subjected to HPLC analysis using a Waters 515 pump, a Waters 486 UV detector operated at 210 nm, an RSpak KC-811 column (Shodex), and 0.05 M H_3PO_4 aqueous solution eluent.

Quantum Yields Measurement. The quantum yields for formate production ($\Phi_{formate}$) were determined for the homogeneous system composed of IrPS and the Mn(I) catalysts (**Mn-bpy**, **Mn-bpy^{OH}**, **Mn-bpy^{OMe}**, **Mn-bpy^{OEt}**, **Mn-bpy^{diOH}**, and **Mn-bpy^{diOMe}**). A 495–505 nm band-pass filter was used to isolate 500 nm excitation light from the emission of a 300 W Xe lamp (Asahi Spectra, MAX-350). The quantum yields were measured using an Asahi Spectra PRA-201 apparatus equipped with a Xe lamp (Asahi Spectra, MAX-350) and calculated according to Eq. 1.

$$\text{QY}\ (\%) = \frac{\text{amount of formate generated per unit time}}{\text{number of incident photons per unit time}} \times 100 \qquad (1)$$

Electrochemical Measurements. The cyclic voltammetry (CV) experiment was performed in distilled, Ar- or CO_2-degassed DMF containing 1 mM Mn(I) catalysts (**Mn-bpy**, **Mn-bpy^{OH}**, **Mn-bpy^{OMe}**, **Mn-bpy^{OEt}**, **Mn-bpy^{Bu}**, **Mn-bpy^{diOH}**, or **Mn-bpy^{diOMe}**) and 0.1 M tetrabutylammonium perchlorate (TBAP) at room temperature by using an electrochemical analyzer (CH Instruments, CHI660e). All experiments were recorded by using a glassy carbon working electrode (d = 2.0 mm), a platinum wire counter electrode, and a nonaqueous $Ag/AgNO_3$ (with inner electrolyte: 0.01 M $AgNO_3$ and 0.1 M Bu_4NPF_6 in DMF) reference electrode. Ferrocene/ferrocenium (Fc/Fc^+) was used as an internal potential marker. The potential values of compounds were calibrated in reference to the ferrocene/ferrocenium (Fc/Fc^+) redox couple and then corrected to the saturated calomel electrode (SCE) on the basis of the Fc/Fc^+ redox potential of 0.38 V vs SCE for direct comparison with the values in the literature.

In Situ FTIR Spectroscopy. A homemade in situ FTIR spectroscopy tool was designed and fabricated to analyze the chemical intermediates of Mn(I) catalysts in an environment similar to the actual photolysis conditions of the mixed homogeneous system.[S12] Fig. S1 and S2† show the details of the accessory parts that were specialized for this study. Three mirror reflectance accessories were put in the Nicolet 6700 FTIR spectrometer (Thermo Fisher Scientific). After the PTFE gasket-type ring was placed in the cell base body, a CaF_2 window was inserted, and a Teflon spacer was positioned on the CaF_2 window. After the DMA or mixed DMA/additive solution (additive = 5 vol% TEOA) containing 1 mM IrPS, 1 mM Mn(I) catalysts, and 0.1 M BIH was purged with Ar or CO_2 gas in the dark for 30 min, 0.05 mL of purged solution was injected into the active spacer, through which the IR beam passes with simultaneous LED irradiation (see Fig. S2†). Changes in the IR peaks under LED irradiation (>495 nm) were traced for (0−180) min.

Computational details. The geometries were optimized with the starting structure taken from the single-crystal structure of **Mn-bpy^{diOMe}**. Geometry optimizations and frequency calculations were performed with the unrestricted B3LYP functional and def2-SVP basis set using Orca 5.01 software.[S13] Solvation free energies in DMF were calculated by using the polarizable continuum model (C-PCM) using Bondi atomic radii.[S14-S16] DMF was selected due to its structure and dielectric constant, which are similar to those of the DMA solvent used in the experimental conditions. Single point energy of optimized geometries was calculated with the unrestricted B3LYP functional, def2-TZVPPD basis set,[S17] and dispersion correction. Frequency calculations were done on all the stationary points, and IRC calculations were done on transition states, followed by geometry optimizations to the nearest minimum, to ensure that the reactant-TS-product triads were always on a connected surface. We calculated Gibbs free energies (ΔG) including zero-point vibrational energies (ΔZ_0), vibrational energies at 298K ($\Delta E_{thermal}$), entropy at 298K ($-T\Delta S$), dispersion (ΔDisp), and complexation energies compensating for comparing one model with a two separated molecule reference (ΔG^o for change in standard state).[S18] The reduction potentials of Mn complexes were calculated by Eq. 2 and 3, where n represents the number of electrons transferred to the Mn complex.[S19]

$$E^o = -\frac{\Delta G_{solv}^{redox}}{nF}\left(F = 23.06\frac{kcal}{mol * V}\right) \quad (2)$$

$$\Delta G_{solv}^{redox} = \Delta G_{solv}^{red} - \Delta G_{solv}^{ox} \quad (3)$$

All reduction potentials were converted to values against absolute reduction potential of ferrocenium/ferrocene (Fc^+/Fc) redox couple by Eq. 4.[S20-21]

$$E^o(\text{vs } Fc^+/Fc) = E^o(Fc^+/Fc) - \frac{\Delta G_{solv}^{redox}}{nF} \quad (4)$$

Geometry optimizations and electronic energy calculations were compared using both the unrestricted Kohn–Sham (UKS) and broken-symmetry (BS) approaches (Table S11). For the two-electron-

reduced Mn complex, both singlet and triplet spin states are possible. Our calculations indicate that, in Mn-bpy^{diOMe}, the triplet state is higher in energy than the singlet state by 3.65 kcal/mol. The singlet state can be further classified into two distinct electronic configurations. One corresponds to a closed-shell configuration with paired electrons localized at the Mn center, while the other corresponds to an antiferromagnetic configuration in which an unpaired electron at the Mn center is antiferromagnetically coupled with another unpaired electron residing in the π* orbital of the bipyridine ligand. Among these, the open-shell Mn_-1_1_BS exhibits the lowest Gibbs free energy. Furthermore, Mulliken spin population and spin density analyses of the open-shell Mn_-1_1_BS (isovalue: 0.003 a.u.) reveal clear antiferromagnetic coupling.

Details regarding Fig. S46, S47, and S48

To computationally demonstrate a reduction pathway involving a chemical structural change of the Mn catalyst (Br^- dissociation), we optimized a structure of **Mn-bpy^{diOMe}** in which the Br^- ion is sufficiently separated from the Mn center (8.03 Å) after the one-electron reduction. We then calculated the Gibbs free energy associated with Br^- dissociation following this one-electron reduction. The calculated Gibbs free energy change for the reaction Mn(I)–Br + $e^- \rightarrow$ Mn(0) + Br^- was $\Delta G = -71.22$ kcal/mol, corresponding to $E_{calc} = -1.89$ V vs. Fc^+/Fc (Fig. S46a). This value is in good agreement with the experimentally observed reduction potential of **Mn-bpy^{diOMe}** ($E_{exp} = -1.98$ V vs. Fc^+/Fc) shown in Fig. 6d, supporting the validity of our computational approach. Inclusion of the Gibbs free energy associated with Br^- dissociation after the two-electron reduction Mn(I)–Br + $2e^- \rightarrow [Mn(0)L^{\bullet-}]^{1-} + Br^-$ yields $\Delta G = -130.07$ kcal/mol ($E_{calc} = -2.16$ V vs Fc^+/Fc), which closely matches the experimental value (Fig. S47). Using the same method as that applied to **Mn-bpy^{diOMe}**, the reduction potential of **Mn-bpy^{OMe}** was also evaluated (Fig. S48). Incorporation of the Gibbs free energy for Br^- dissociation following the two-electron reduction gives $\Delta G = -135.43$ kcal/mol ($E_{calc} = -2.04$ V vs. Fc^+/Fc), in good agreement with the experimental value ($E_{exp} = -1.88$ V vs. Fc^+/Fc).

Table S1 Crystal data and structure refinement for **Mn-bpy^{OEt}**.

	Mn-bpy^{OEt}
Identification code	**Mn-bpy^{OEt}**
Empirical formula	C50 H64 Br2 Mn2 N4 O8
Formula weight	1118.74
Temperature	296(2) K
Wavelength	0.71073 Å
Crystal system	Monoclinic
Space group	$P2_1/n$
Unit cell dimensions	a= 20.729(6) Å
	b= 12.375(3) Å
	c= 21.623(6) Å
Volume	5331(3) Å3
Z	4
Density (calculated)	1.394 g/cm3
Absorption coefficient	2.025 mm-1
F(000)	2304
Crystal size	0.370 ×0.100 ×0.050 mm3
Theta range for data collection	1.915 to 25.056°
Index ranges	-24≤h≤24, -14≤k≤14, -25≤l≤25
Reflections collected	182790
Independent reflections	9292 [R(int) = 0.0748]
Completeness to theta = 25.056°	98.3 %
Absorption correction	Semi-empirical from equivalents
Max. and min. transmission	0.7492 and 0.2412
Refinement method	Full-matrix least-squares on F2
Data / restraints / parameters	9292 / 143 / 623
Goodness-of-fit on F2	1.011
Final R indices [I>2sigma(I)]	R_1=0.0830,wR_2=0.2274
R indices (all data)	R_1=0.1020,wR_2=0.2488
Largest diff. peak and hole	1.392 and -0.669 e.Å-3

[a] $R_1 = \sum||F_o|-|F_c|| / \sum|F_o|$ (based on reflections with $F_o^2 > 2\sigma F^2$), [b] $wR_2 = [\sum[w (F_o^2-F_c^2)^2] / \sum[w (F_o^2)^2]]^{1/2}$; $w = 1/[\sigma^2 (F_o^2) + (0.095P)^2]$; $P = [\max(F_o^2, 0) + 2F_c^2]/3$(also with $F_o^2>2\sigma F^2$)

Table S2 Bond lengths [Å] for **Mn-bpy^{OEt}**.

Br(1)-Mn(1)	2.5352(14)	C(5)-C(8)	1.518(10)
Br(2)-Mn(2)	2.5162(14)	C(5)-C(7)	1.542(11)
Mn(1)-C(24)	1.790(9)	C(6)-H(6A)	0.9600
Mn(1)-C(1)	1.790(8)	C(6)-H(6B)	0.9600
Mn(1)-C(25)	1.783(10)	C(6)-H(6C)	0.9600
Mn(1)-N(1)	2.042(6)	C(7)-H(7A)	0.9600
Mn(1)-N(2)	2.112(5)	C(7)-H(7B)	0.9600
Mn(2)-C(50)	1.787(8)	C(7)-H(7C)	0.9600
Mn(2)-C(48)	1.818(9)	C(8)-H(8A)	0.9600
Mn(2)-C(49)	1.825(8)	C(8)-H(8B)	0.9600
Mn(2)-N(4)	2.034(5)	C(8)-H(8C)	0.9600
Mn(2)-N(3)	2.118(5)	C(9)-C(10)	1.392(9)
O(1)-C(1)	1.144(9)	C(9)-H(31)	0.9300
O(2)-C(24)	1.156(10)	C(10)-C(11)	1.468(8)
O(3)-C(25)	1.145(10)	C(11)-C(12)	1.385(8)
O(4)-C(48)	1.097(9)	C(12)-C(13)	1.375(9)
O(5)-C(49)	1.116(9)	C(12)-H(10)	0.9300
O(6)-C(50)	1.147(9)	C(13)-C(18)	1.385(10)
O(7)-C(22)	1.356(11)	C(13)-C(14)	1.520(9)
O(7)-C(21)	1.478(12)	C(14)-C(17A)	1.510(16)
N(1)-C(10)	1.340(8)	C(14)-C(15A)	1.524(16)
N(1)-C(2)	1.336(9)	C(14)-C(16A)	1.530(16)
N(2)-C(19)	1.349(9)	C(14)-C(16B)	1.529(11)
N(2)-C(11)	1.360(8)	C(14)-C(17B)	1.523(11)
N(3)-C(38)	1.345(8)	C(14)-C(15B)	1.516(11)
N(3)-C(27)	1.360(9)	C(15A)-H(15A)	0.9600
N(4)-C(47)	1.351(8)	C(15A)-H(15B)	0.9600
N(4)-C(39)	1.346(7)	C(15A)-H(15C)	0.9600
C(2)-C(3)	1.371(10)	C(16A)-H(16A)	0.9600
C(2)-H(33)	0.9300	C(16A)-H(16B)	0.9600
C(3)-C(4)	1.389(9)	C(16A)-H(16C)	0.9600
C(3)-H(32)	0.9300	C(17A)-H(17A)	0.9600
C(4)-C(9)	1.391(9)	C(17A)-H(17B)	0.9600
C(4)-C(5)	1.527(9)	C(17A)-H(17C)	0.9600
C(5)-C(6)	1.488(12)	C(15B)-H(15D)	0.9600
C(15B)-H(15E)	0.9600	C(35)-H(35B)	0.9600
C(15B)-H(15F)	0.9600	C(35)-H(35C)	0.9600
C(16B)-H(16D)	0.9600	C(36)-H(36A)	0.9600
C(16B)-H(16E)	0.9600	C(36)-H(36B)	0.9600
C(16B)-H(16F)	0.9600	C(36)-H(36C)	0.9600
C(17B)-H(17D)	0.9600	C(37)-C(38)	1.378(8)
C(17B)-H(17E)	0.9600	C(37)-H(61)	0.9300
C(17B)-H(17F)	0.9600	C(38)-C(39)	1.475(8)
C(18)-C(19)	1.387(11)	C(39)-C(40)	1.394(8)
C(18)-H(20)	0.9300	C(40)-C(41)	1.384(9)
C(19)-C(20)	1.562(12)	C(40)-H(60)	0.9300
C(20)-C(21)	1.435(14)	C(41)-C(46)	1.396(9)
C(20)-H(30)	0.9700	C(41)-C(42)	1.519(9)
C(20)-H(29)	0.9700	C(42)-C(44)	1.500(12)
C(21)-H(22)	0.9700	C(42)-C(43)	1.522(11)

C(21)-H(28)	0.9700	C(42)-C(45)	1.537(12)
C(22)-C(23)	1.493(13)	C(43)-H(43A)	0.9600
C(22)-H(22A)	0.9700	C(43)-H(43B)	0.9600
C(22)-H(22B)	0.9700	C(43)-H(43C)	0.9600
C(23)-H(23A)	0.9600	C(44)-H(44A)	0.9600
C(23)-H(23B)	0.9600	C(44)-H(44B)	0.9600
C(23)-H(23C)	0.9600	C(44)-H(44C)	0.9600
C(27)-C(31)	1.387(11)	C(45)-H(45A)	0.9600
C(27)-C(26)	1.503(13)	C(45)-H(45B)	0.9600
C(31)-C(32)	1.370(10)	C(45)-H(45C)	0.9600
C(31)-H(39)	0.9300	C(46)-C(47)	1.362(10)
C(32)-C(37)	1.377(9)	C(46)-H(58)	0.9300
C(32)-C(33)	1.523(9)	C(47)-H(59)	0.9300
C(33)-C(35)	1.500(12)	O(8)-C(52)	1.313(14)
C(33)-C(36)	1.520(11)	O(8)-C(51)	1.367(13)
C(33)-C(34)	1.545(12)	C(26)-C(51)	1.443(14)
C(34)-H(34A)	0.9600	C(26)-H(26A)	0.9700
C(34)-H(34B)	0.9600	C(26)-H(26B)	0.9700
C(34)-H(34C)	0.9600	C(51)-H(51A)	0.9700
C(35)-H(35A)	0.9600	C(51)-H(51B)	0.9700
C(52)-C(53)	1.400(15)	C(53)-H(53A)	0.9600
C(52)-H(52A)	0.9700	C(53)-H(53B)	0.9600
C(52)-H(52B)	0.9700	C(53)-H(53C)	0.9600

Table S3 Angles [°] for **Mn-bpy^{OEt}**.

C(24)-Mn(1)-C(1)	83.8(4)	C(3)-C(2)-H(33)	117.9
C(24)-Mn(1)-C(25)	89.5(4)	C(2)-C(3)-C(4)	119.9(6)
C(1)-Mn(1)-C(25)	88.7(4)	C(2)-C(3)-H(32)	120.0
C(24)-Mn(1)-N(1)	175.3(4)	C(4)-C(3)-H(32)	120.0
C(1)-Mn(1)-N(1)	94.0(3)	C(9)-C(4)-C(3)	115.9(6)
C(25)-Mn(1)-N(1)	94.6(3)	C(9)-C(4)-C(5)	122.7(6)
C(24)-Mn(1)-N(2)	103.8(3)	C(3)-C(4)-C(5)	121.4(6)
C(1)-Mn(1)-N(2)	172.3(3)	C(6)-C(5)-C(8)	110.1(7)
C(25)-Mn(1)-N(2)	92.3(3)	C(6)-C(5)-C(7)	109.7(8)
N(1)-Mn(1)-N(2)	78.3(2)	C(8)-C(5)-C(7)	107.9(6)
C(24)-Mn(1)-Br(1)	88.9(3)	C(6)-C(5)-C(4)	107.9(6)
C(1)-Mn(1)-Br(1)	92.1(3)	C(8)-C(5)-C(4)	109.8(6)
C(25)-Mn(1)-Br(1)	178.1(3)	C(7)-C(5)-C(4)	111.5(6)
N(1)-Mn(1)-Br(1)	87.04(17)	C(5)-C(6)-H(6A)	109.5
N(2)-Mn(1)-Br(1)	87.11(17)	C(5)-C(6)-H(6B)	109.5
C(50)-Mn(2)-C(48)	89.8(3)	H(6A)-C(6)-H(6B)	109.5
C(50)-Mn(2)-C(49)	84.1(4)	C(5)-C(6)-H(6C)	109.5
C(48)-Mn(2)-C(49)	87.9(3)	H(6A)-C(6)-H(6C)	109.5
C(50)-Mn(2)-N(4)	93.0(3)	H(6B)-C(6)-H(6C)	109.5
C(48)-Mn(2)-N(4)	93.9(3)	C(5)-C(7)-H(7A)	109.5
C(49)-Mn(2)-N(4)	176.6(3)	C(5)-C(7)-H(7B)	109.5
C(50)-Mn(2)-N(3)	170.7(3)	H(7A)-C(7)-H(7B)	109.5
C(48)-Mn(2)-N(3)	92.6(3)	C(5)-C(7)-H(7C)	109.5
C(49)-Mn(2)-N(3)	105.0(3)	H(7A)-C(7)-H(7C)	109.5
N(4)-Mn(2)-N(3)	77.8(2)	H(7B)-C(7)-H(7C)	109.5
C(50)-Mn(2)-Br(2)	91.9(2)	C(5)-C(8)-H(8A)	109.5
C(48)-Mn(2)-Br(2)	176.1(2)	C(5)-C(8)-H(8B)	109.5
C(49)-Mn(2)-Br(2)	88.8(3)	H(8A)-C(8)-H(8B)	109.5
N(4)-Mn(2)-Br(2)	89.51(17)	C(5)-C(8)-H(8C)	109.5
N(3)-Mn(2)-Br(2)	86.21(16)	H(8A)-C(8)-H(8C)	109.5
C(22)-O(7)-C(21)	118.5(10)	H(8B)-C(8)-H(8C)	109.5
C(10)-N(1)-C(2)	117.0(6)	C(4)-C(9)-C(10)	121.0(6)
C(10)-N(1)-Mn(1)	116.9(4)	C(4)-C(9)-H(31)	119.5
C(2)-N(1)-Mn(1)	126.0(4)	C(10)-C(9)-H(31)	119.5
C(19)-N(2)-C(11)	115.9(6)	N(1)-C(10)-C(9)	121.9(6)
C(19)-N(2)-Mn(1)	130.3(5)	N(1)-C(10)-C(11)	115.4(5)
C(11)-N(2)-Mn(1)	113.8(4)	C(9)-C(10)-C(11)	122.4(5)
C(38)-N(3)-C(27)	116.1(6)	N(2)-C(11)-C(12)	122.6(5)
C(38)-N(3)-Mn(2)	114.0(4)	N(2)-C(11)-C(10)	115.1(5)
C(27)-N(3)-Mn(2)	129.8(5)	C(12)-C(11)-C(10)	122.3(5)
C(47)-N(4)-C(39)	116.8(5)	C(13)-C(12)-C(11)	121.9(6)
C(47)-N(4)-Mn(2)	125.6(4)	C(13)-C(12)-H(10)	119.0
C(39)-N(4)-Mn(2)	117.5(4)	C(11)-C(12)-H(10)	119.0
O(1)-C(1)-Mn(1)	177.6(8)	C(12)-C(13)-C(18)	114.7(6)
N(1)-C(2)-C(3)	124.2(6)	C(12)-C(13)-C(14)	122.7(6)
N(1)-C(2)-H(33)	117.9	C(18)-C(13)-C(14)	122.6(6)
C(17A)-C(14)-C(15A)	114(3)	H(17D)-C(17B)-H(17F)	109.5
C(17A)-C(14)-C(16A)	102(3)	H(17E)-C(17B)-H(17F)	109.5
C(15A)-C(14)-C(16A)	106(3)	C(13)-C(18)-C(19)	122.2(7)
C(17A)-C(14)-C(13)	117.3(15)	C(13)-C(18)-H(20)	118.9
C(15A)-C(14)-C(13)	107.1(15)	C(19)-C(18)-H(20)	118.9

C(16A)-C(14)-C(13)	109.2(17)	N(2)-C(19)-C(18)	122.4(7)
C(13)-C(14)-C(16B)	106.9(7)	N(2)-C(19)-C(20)	118.7(7)
C(13)-C(14)-C(17B)	109.9(6)	C(18)-C(19)-C(20)	116.7(8)
C(16B)-C(14)-C(17B)	107.2(9)	C(21)-C(20)-C(19)	105.7(10)
C(13)-C(14)-C(15B)	113.2(7)	C(21)-C(20)-H(30)	110.6
C(16B)-C(14)-C(15B)	108.8(10)	C(19)-C(20)-H(30)	110.6
C(17B)-C(14)-C(15B)	110.6(10)	C(21)-C(20)-H(29)	110.6
C(14)-C(15A)-H(15A)	109.5	C(19)-C(20)-H(29)	110.6
C(14)-C(15A)-H(15B)	109.5	H(30)-C(20)-H(29)	108.7
H(15A)-C(15A)-H(15B)	109.5	C(20)-C(21)-O(7)	105.7(11)
C(14)-C(15A)-H(15C)	109.5	C(20)-C(21)-H(22)	110.6
H(15A)-C(15A)-H(15C)	109.5	O(7)-C(21)-H(22)	110.6
H(15B)-C(15A)-H(15C)	109.5	C(20)-C(21)-H(28)	110.6
C(14)-C(16A)-H(16A)	109.5	O(7)-C(21)-H(28)	110.6
C(14)-C(16A)-H(16B)	109.5	H(22)-C(21)-H(28)	108.7
H(16A)-C(16A)-H(16B)	109.5	O(7)-C(22)-C(23)	109.1(9)
C(14)-C(16A)-H(16C)	109.5	O(7)-C(22)-H(22A)	109.9
H(16A)-C(16A)-H(16C)	109.5	C(23)-C(22)-H(22A)	109.9
H(16B)-C(16A)-H(16C)	109.5	O(7)-C(22)-H(22B)	109.9
C(14)-C(17A)-H(17A)	109.5	C(23)-C(22)-H(22B)	109.9
C(14)-C(17A)-H(17B)	109.5	H(22A)-C(22)-H(22B)	108.3
H(17A)-C(17A)-H(17B)	109.5	C(22)-C(23)-H(23A)	109.5
C(14)-C(17A)-H(17C)	109.5	C(22)-C(23)-H(23B)	109.5
H(17A)-C(17A)-H(17C)	109.5	H(23A)-C(23)-H(23B)	109.5
H(17B)-C(17A)-H(17C)	109.5	C(22)-C(23)-H(23C)	109.5
C(14)-C(15B)-H(15D)	109.5	H(23A)-C(23)-H(23C)	109.5
C(14)-C(15B)-H(15E)	109.5	H(23B)-C(23)-H(23C)	109.5
H(15D)-C(15B)-H(15E)	109.5	O(2)-C(24)-Mn(1)	173.1(7)
C(14)-C(15B)-H(15F)	109.5	O(3)-C(25)-Mn(1)	176.3(8)
H(15D)-C(15B)-H(15F)	109.5	N(3)-C(27)-C(31)	121.7(7)
H(15E)-C(15B)-H(15F)	109.5	N(3)-C(27)-C(26)	119.4(8)
C(14)-C(16B)-H(16D)	109.5	C(31)-C(27)-C(26)	118.6(8)
C(14)-C(16B)-H(16E)	109.5	C(32)-C(31)-C(27)	121.9(7)
H(16D)-C(16B)-H(16E)	109.5	C(32)-C(31)-H(39)	119.1
C(14)-C(16B)-H(16F)	109.5	C(27)-C(31)-H(39)	119.1
H(16D)-C(16B)-H(16F)	109.5	C(31)-C(32)-C(37)	115.6(6)
H(16E)-C(16B)-H(16F)	109.5	C(31)-C(32)-C(33)	123.7(6)
C(14)-C(17B)-H(17D)	109.5	C(37)-C(32)-C(33)	120.7(6)
C(14)-C(17B)-H(17E)	109.5	C(35)-C(33)-C(32)	111.1(6)
H(17D)-C(17B)-H(17E)	109.5	C(35)-C(33)-C(36)	107.9(8)
C(14)-C(17B)-H(17F)	109.5	C(32)-C(33)-C(36)	112.2(7)
C(35)-C(33)-C(34)	107.6(8)	H(43A)-C(43)-H(43C)	109.5
C(32)-C(33)-C(34)	107.2(6)	H(43B)-C(43)-H(43C)	109.5
C(36)-C(33)-C(34)	110.9(8)	C(42)-C(44)-H(44A)	109.5
C(33)-C(34)-H(34A)	109.5	C(42)-C(44)-H(44B)	109.5
C(33)-C(34)-H(34B)	109.5	H(44A)-C(44)-H(44B)	109.5
H(34A)-C(34)-H(34B)	109.5	C(42)-C(44)-H(44C)	109.5
C(33)-C(34)-H(34C)	109.5	H(44A)-C(44)-H(44C)	109.5
H(34A)-C(34)-H(34C)	109.5	H(44B)-C(44)-H(44C)	109.5
H(34B)-C(34)-H(34C)	109.5	C(42)-C(45)-H(45A)	109.5
C(33)-C(35)-H(35A)	109.5	C(42)-C(45)-H(45B)	109.5
C(33)-C(35)-H(35B)	109.5	H(45A)-C(45)-H(45B)	109.5

H(35A)-C(35)-H(35B)	109.5	C(42)-C(45)-H(45C)	109.5
C(33)-C(35)-H(35C)	109.5	H(45A)-C(45)-H(45C)	109.5
H(35A)-C(35)-H(35C)	109.5	H(45B)-C(45)-H(45C)	109.5
H(35B)-C(35)-H(35C)	109.5	C(47)-C(46)-C(41)	121.0(6)
C(33)-C(36)-H(36A)	109.5	C(47)-C(46)-H(58)	119.5
C(33)-C(36)-H(36B)	109.5	C(41)-C(46)-H(58)	119.5
H(36A)-C(36)-H(36B)	109.5	N(4)-C(47)-C(46)	123.6(6)
C(33)-C(36)-H(36C)	109.5	N(4)-C(47)-H(59)	118.2
H(36A)-C(36)-H(36C)	109.5	C(46)-C(47)-H(59)	118.2
H(36B)-C(36)-H(36C)	109.5	O(4)-C(48)-Mn(2)	175.7(7)
C(38)-C(37)-C(32)	121.2(6)	O(5)-C(49)-Mn(2)	170.7(8)
C(38)-C(37)-H(61)	119.4	O(6)-C(50)-Mn(2)	178.9(7)
C(32)-C(37)-H(61)	119.4	C(52)-O(8)-C(51)	126.3(16)
N(3)-C(38)-C(37)	123.1(6)	C(51)-C(26)-C(27)	115.1(11)
N(3)-C(38)-C(39)	115.0(5)	C(51)-C(26)-H(26A)	108.5
C(37)-C(38)-C(39)	121.8(5)	C(27)-C(26)-H(26A)	108.5
N(4)-C(39)-C(40)	121.7(5)	C(51)-C(26)-H(26B)	108.5
N(4)-C(39)-C(38)	114.5(5)	C(27)-C(26)-H(26B)	108.5
C(40)-C(39)-C(38)	123.7(5)	H(26A)-C(26)-H(26B)	107.5
C(41)-C(40)-C(39)	121.7(6)	C(26)-C(51)-O(8)	109.1(13)
C(41)-C(40)-H(60)	119.2	C(26)-C(51)-H(51A)	109.9
C(39)-C(40)-H(60)	119.2	O(8)-C(51)-H(51A)	109.9
C(40)-C(41)-C(46)	115.1(6)	C(26)-C(51)-H(51B)	109.9
C(40)-C(41)-C(42)	123.6(6)	O(8)-C(51)-H(51B)	109.9
C(46)-C(41)-C(42)	121.2(6)	H(51A)-C(51)-H(51B)	108.3
C(44)-C(42)-C(43)	111.6(9)	O(8)-C(52)-C(53)	133.9(19)
C(44)-C(42)-C(41)	109.1(7)	O(8)-C(52)-H(52A)	103.7
C(43)-C(42)-C(41)	110.1(6)	C(53)-C(52)-H(52A)	103.7
C(44)-C(42)-C(45)	108.0(8)	O(8)-C(52)-H(52B)	103.7
C(43)-C(42)-C(45)	108.1(8)	C(53)-C(52)-H(52B)	103.7
C(41)-C(42)-C(45)	110.0(6)	H(52A)-C(52)-H(52B)	105.4
C(42)-C(43)-H(43A)	109.5	C(52)-C(53)-H(53A)	109.5
C(42)-C(43)-H(43B)	109.5	C(52)-C(53)-H(53B)	109.5
H(43A)-C(43)-H(43B)	109.5	H(53A)-C(53)-H(53B)	109.5
C(42)-C(43)-H(43C)	109.5	C(52)-C(53)-H(53C)	109.5
H(53A)-C(53)-H(53C)	109.5	H(53B)-C(53)-H(53C)	109.5

Table S4 Torsion angles [°] for **Mn-bpy^{OEt}**.

C(10)-N(1)-C(2)-C(3)	-0.9(11)	C(18)-C(19)-C(20)-C(21)	-83.5(14)
Mn(1)-N(1)-C(2)-C(3)	175.4(6)	C(19)-C(20)-C(21)-O(7)	-179.8(9)
N(1)-C(2)-C(3)-C(4)	-0.1(13)	C(22)-O(7)-C(21)-C(20)	-87.5(14)
C(2)-C(3)-C(4)-C(9)	1.3(11)	C(21)-O(7)-C(22)-C(23)	160.9(11)
C(2)-C(3)-C(4)-C(5)	-177.6(7)	C(38)-N(3)-C(27)-C(31)	-5.7(12)
C(9)-C(4)-C(5)-C(6)	103.8(9)	Mn(2)-N(3)-C(27)-C(31)	173.0(7)
C(3)-C(4)-C(5)-C(6)	-77.4(9)	C(38)-N(3)-C(27)-C(26)	167.9(10)
C(9)-C(4)-C(5)-C(8)	-136.2(7)	Mn(2)-N(3)-C(27)-C(26)	-13.4(14)
C(3)-C(4)-C(5)-C(8)	42.6(9)	N(3)-C(27)-C(31)-C(32)	1.3(14)
C(9)-C(4)-C(5)-C(7)	-16.7(10)	C(26)-C(27)-C(31)-C(32)	172.4(11)
C(3)-C(4)-C(5)-C(7)	162.1(7)	C(27)-C(31)-C(32)-C(37)	2.8(12)
C(3)-C(4)-C(9)-C(10)	-1.6(10)	C(27)-C(31)-C(32)-C(33)	-177.8(8)
C(5)-C(4)-C(9)-C(10)	177.3(6)	C(31)-C(32)-C(33)-C(35)	-129.7(9)
C(2)-N(1)-C(10)-C(9)	0.6(10)	C(37)-C(32)-C(33)-C(35)	49.7(10)
Mn(1)-N(1)-C(10)-C(9)	-176.0(5)	C(31)-C(32)-C(33)-C(36)	-8.9(12)
C(2)-N(1)-C(10)-C(11)	175.5(6)	C(37)-C(32)-C(33)-C(36)	170.5(8)
Mn(1)-N(1)-C(10)-C(11)	-1.2(7)	C(31)-C(32)-C(33)-C(34)	113.0(9)
C(4)-C(9)-C(10)-N(1)	0.6(10)	C(37)-C(32)-C(33)-C(34)	-67.5(9)
C(4)-C(9)-C(10)-C(11)	-173.8(6)	C(31)-C(32)-C(37)-C(38)	-2.3(11)
C(19)-N(2)-C(11)-C(12)	5.7(11)	C(33)-C(32)-C(37)-C(38)	178.2(6)
Mn(1)-N(2)-C(11)-C(12)	-173.4(5)	C(27)-N(3)-C(38)-C(37)	6.2(10)
C(19)-N(2)-C(11)-C(10)	-173.5(8)	Mn(2)-N(3)-C(38)-C(37)	-172.7(5)
Mn(1)-N(2)-C(11)-C(10)	7.5(7)	C(27)-N(3)-C(38)-C(39)	-169.3(7)
N(1)-C(10)-C(11)-N(2)	-4.3(8)	Mn(2)-N(3)-C(38)-C(39)	11.9(7)
C(9)-C(10)-C(11)-N(2)	170.5(6)	C(32)-C(37)-C(38)-N(3)	-2.3(10)
N(1)-C(10)-C(11)-C(12)	176.5(6)	C(32)-C(37)-C(38)-C(39)	172.9(6)
C(9)-C(10)-C(11)-C(12)	-8.7(9)	C(47)-N(4)-C(39)-C(40)	0.9(10)
N(2)-C(11)-C(12)-C(13)	-2.9(10)	Mn(2)-N(4)-C(39)-C(40)	-177.2(5)
C(10)-C(11)-C(12)-C(13)	176.2(6)	C(47)-N(4)-C(39)-C(38)	178.2(6)
C(11)-C(12)-C(13)-C(18)	-1.1(10)	Mn(2)-N(4)-C(39)-C(38)	0.1(7)
C(11)-C(12)-C(13)-C(14)	178.9(6)	N(3)-C(38)-C(39)-N(4)	-8.1(8)
C(12)-C(13)-C(14)-C(17A	-4(2)	C(37)-C(38)-C(39)-N(4)	176.4(6)
C(18)-C(13)-C(14)-C(17A	177(2)	N(3)-C(38)-C(39)-C(40)	169.1(6)
C(12)-C(13)-C(14)-C(15A	126(2)	C(37)-C(38)-C(39)-C(40)	-6.4(10)
C(18)-C(13)-C(14)-C(15A	-54(2)	N(4)-C(39)-C(40)-C(41)	1.9(10)
C(12)-C(13)-C(14)-C(16A	-119(2)	C(38)-C(39)-C(40)-C(41)	-175.2(6)
C(18)-C(13)-C(14)-C(16A	61(2)	C(39)-C(40)-C(41)-C(46)	-4.0(10)
C(12)-C(13)-C(14)-C(16B	-71.0(10)	C(39)-C(40)-C(41)-C(42)	177.7(6)
C(18)-C(13)-C(14)-C(16B	109.1(10)	C(40)-C(41)-C(42)-C(44)	92.7(9)
C(12)-C(13)-C(14)-C(17B	45.0(10)	C(46)-C(41)-C(42)-C(44)	-85.6(9)
C(18)-C(13)-C(14)-C(17B	134.9(10)	C(40)-C(41)-C(42)-C(43)	-144.6(9)
C(12)-C(13)-C(14)-C(15B	169.2(10)	C(46)-C(41)-C(42)-C(43)	37.1(11)
C(18)-C(13)-C(14)-C(15B	-10.7(13)	C(40)-C(41)-C(42)-C(45)	-25.6(10)
C(12)-C(13)-C(18)-C(19)	2.1(13)	C(46)-C(41)-C(42)-C(45)	156.1(8)
C(14)-C(13)-C(18)-C(19)	-177.9(9)	C(40)-C(41)-C(46)-C(47)	3.5(11)
C(11)-N(2)-C(19)-C(18)	-4.7(15)	C(42)-C(41)-C(46)-C(47)	-178.1(7)
Mn(1)-N(2)-C(19)-C(18)	174.2(8)	C(39)-N(4)-C(47)-C(46)	-1.4(12)
C(11)-N(2)-C(19)-C(20)	157.9(9)	Mn(2)-N(4)-C(47)-C(46)	176.6(6)
Mn(1)-N(2)-C(19)-C(20)	-23.2(15)	C(41)-C(46)-C(47)-N(4)	-0.9(13)
C(13)-C(18)-C(19)-N(2)	0.8(17)	N(3)-C(27)-C(26)-C(51)	123.2(15)
C(13)-C(18)-C(19)-C(20)	162.1(10)	C(31)-C(27)-C(26)-C(51)	-63(2)
N(2)-C(19)-C(20)-C(21)	113.0(13)	C(27)-C(26)-C(51)-O(8)	179.6(15)
C(52)-O(8)-C(51)-C(26)	-140(2)		
C(51)-O(8)-C(52)-C(53)	3(5)		

Table S5 Crystal data and structure refinement for **Mn-bpy^{diOMe}**.

	Mn-bpy^{diOMe}
Identification code	**Mn-bpy^{diOMe}**
Empirical formula	C27 H36 Br Mn N2 O5
Formula weight	603.43
Temperature	296(2) K
Wavelength	0.71073 Å
Crystal system	Trigonal
Space group	$P3_2$
Unit cell dimensions	a= 13.4309(2) Å a = 90°
	b= 13.4309(2) Å b = 90°
	c= 14.4904(4) Å g= 120°
Volume	2263.71(9) Å3
Z	3
Density (calculated)	1.328 g/cm3
Absorption coefficient	1.796 mm-1
F(000)	936
Crystal size	0.650 ×0.520 ×0.220 mm3
Theta range for data collection	2.245 to 25.960°
Index ranges	-16≤h≤16, -16≤k≤16, -17≤l≤16
Reflections collected	36142
Independent reflections	5780 [R(int) = 0.0419]
Completeness to theta = 25.242°	99.8 %
Absorption correction	Semi-empirical from equivalents
Max. and min. transmission	0.7492 and 0.2412
Refinement method	Full-matrix least-squares on F2
Data / restraints / parameters	5780 / 38 / 354
Goodness-of-fit on F2	1.045
Final R indices [I>2sigma(I)]	R_1=0.0375,wR_2=0.1053
R indices (all data)	R_1=0.0387,wR_2=0.1064
Absolute structure parameter	0.045(11)
Largest diff. peak and hole	0.607 and -0.259 e.Å-3

[a] $R_1 = \sum||F_o|-|F_c|| / \sum|F_o|$ (based on reflections with $F_o^2 > 2\sigma F^2$), [b] $wR_2 = [\sum[w (F_o^2-F_c^2)^2] / \sum[w (F_o^2)^2]]^{1/2}$; $w = 1/[\sigma^2 (F_o^2) + (0.095P)^2]$; $P = [\max(F_o^2, 0) + 2F_c^2]/3$(also with $F_o^2>2\sigma F^2$)

Table S6 Bond lengths [Å] for **Mn-bpy^{diOMe}**.

Br(1)-Mn(1)	2.5328(8)	C(12)-C(14)	1.562(13)
Mn(1)-C(1)	1.798(5)	C(13)-H(13A)	0.9600
Mn(1)-C(21)	1.801(5)	C(13)-H(13B)	0.9600
Mn(1)-C(22)	1.830(6)	C(13)-H(13C)	0.9600
Mn(1)-N(1)	2.072(3)	C(14)-H(14A)	0.9600
Mn(1)-N(2)	2.082(4)	C(14)-H(14B)	0.9600
O(1)-C(1)	1.146(7)	C(14)-H(14C)	0.9600
O(2)-C(20)	1.264(19)	C(15)-H(15A)	0.9600
O(2)-C(19)	1.406(10)	C(15)-H(15B)	0.9600
O(3)-C(21)	1.165(7)	C(15)-H(15C)	0.9600
O(4)-C(22)	1.064(8)	C(16)-C(17A)	1.418(15)
O(5)-C(10)	1.336(13)	C(16)-C(27B)	1.470(19)
O(5)-C(11)	1.387(17)	C(16)-C(26B)	1.540(18)
N(1)-C(2)	1.353(5)	C(16)-C(24)	1.513(6)
N(1)-C(4)	1.355(5)	C(16)-C(17B)	1.582(19)
N(2)-C(5)	1.357(5)	C(16)-C(27A)	1.56(2)
N(2)-C(8)	1.360(5)	C(16)-C(26A)	1.62(2)
C(2)-C(3)	1.383(6)	C(18)-C(19)	1.476(11)
C(2)-C(18)	1.519(6)	C(18)-H(18A)	0.9700
C(3)-C(24)	1.392(7)	C(18)-H(18B)	0.9700
C(3)-H(1)	0.9300	C(19)-H(19A)	0.9700
C(4)-C(23)	1.372(5)	C(19)-H(19B)	0.9700
C(4)-C(5)	1.486(5)	C(20)-H(20A)	0.9600
C(5)-C(6)	1.375(6)	C(20)-H(20B)	0.9600
C(6)-C(7)	1.382(6)	C(20)-H(20C)	0.9600
C(6)-H(16)	0.9300	C(23)-C(24)	1.391(6)
C(7)-C(25)	1.389(7)	C(23)-H(23)	0.9300
C(7)-C(12)	1.525(7)	C(25)-H(25)	0.9300
C(8)-C(25)	1.357(8)	C(17A)-H(17A)	0.9600
C(8)-C(9)	1.515(6)	C(17A)-H(17B)	0.9600
C(9)-C(10)	1.506(10)	C(17A)-H(17C)	0.9600
C(9)-H(3)	0.9700	C(26A)-H(26A)	0.9600
C(9)-H(2)	0.9700	C(26A)-H(26B)	0.9600
C(10)-H(10A)	0.9700	C(26A)-H(26C)	0.9600
C(10)-H(10B)	0.9700	C(27A)-H(27A)	0.9600
C(11)-H(11A)	0.9600	C(27A)-H(27B)	0.9600
C(11)-H(11B)	0.9600	C(27A)-H(27C)	0.9600
C(11)-H(11C)	0.9600	C(17B)-H(17D)	0.9600
C(12)-C(15)	1.498(9)	C(17B)-H(17E)	0.9600
C(12)-C(13)	1.519(10)	C(17B)-H(17F)	0.9600
C(26B)-H(26D)	0.9600	C(27B)-H(27D)	0.9600
C(26B)-H(26E)	0.9600	C(27B)-H(27E)	0.9600
C(26B)-H(26F)	0.9600	C(27B)-H(27F)	0.9600

Table S7 Angles [°] for **Mn-bpy^{diOMe}**.

C(1)-Mn(1)-C(21)	82.2(3)	C(8)-C(9)-H(3)	109.1
C(1)-Mn(1)-C(22)	90.6(3)	C(10)-C(9)-H(3)	109.1
C(21)-Mn(1)-C(22)	92.2(3)	C(8)-C(9)-H(2)	109.1
C(1)-Mn(1)-N(1)	173.9(3)	C(10)-C(9)-H(2)	109.1
C(21)-Mn(1)-N(1)	98.7(2)	H(3)-C(9)-H(2)	107.8
C(22)-Mn(1)-N(1)	95.38(19)	O(5)-C(10)-C(9)	112.4(8)
C(1)-Mn(1)-N(2)	99.9(2)	O(5)-C(10)-H(10A)	109.1
C(21)-Mn(1)-N(2)	172.8(2)	C(9)-C(10)-H(10A)	109.1
C(22)-Mn(1)-N(2)	94.6(2)	O(5)-C(10)-H(10B)	109.1
N(1)-Mn(1)-N(2)	78.45(12)	C(9)-C(10)-H(10B)	109.1
C(1)-Mn(1)-Br(1)	88.3(2)	H(10A)-C(10)-H(10B)	107.9
C(21)-Mn(1)-Br(1)	85.53(19)	O(5)-C(11)-H(11A)	109.5
C(22)-Mn(1)-Br(1)	177.63(18)	O(5)-C(11)-H(11B)	109.5
N(1)-Mn(1)-Br(1)	85.77(10)	H(11A)-C(11)-H(11B)	109.5
N(2)-Mn(1)-Br(1)	87.68(10)	O(5)-C(11)-H(11C)	109.5
C(20)-O(2)-C(19)	119.1(13)	H(11A)-C(11)-H(11C)	109.5
C(10)-O(5)-C(11)	117.0(13)	H(11B)-C(11)-H(11C)	109.5
C(2)-N(1)-C(4)	116.9(3)	C(15)-C(12)-C(13)	112.3(8)
C(2)-N(1)-Mn(1)	130.4(3)	C(15)-C(12)-C(7)	113.0(4)
C(4)-N(1)-Mn(1)	112.1(2)	C(13)-C(12)-C(7)	109.8(6)
C(5)-N(2)-C(8)	116.6(4)	C(15)-C(12)-C(14)	105.2(7)
C(5)-N(2)-Mn(1)	112.2(2)	C(13)-C(12)-C(14)	107.1(8)
C(8)-N(2)-Mn(1)	131.0(3)	C(7)-C(12)-C(14)	109.3(6)
O(1)-C(1)-Mn(1)	173.1(7)	C(12)-C(13)-H(13A)	109.5
N(1)-C(2)-C(3)	122.0(4)	C(12)-C(13)-H(13B)	109.5
N(1)-C(2)-C(18)	120.9(4)	H(13A)-C(13)-H(13B)	109.5
C(3)-C(2)-C(18)	117.0(4)	C(12)-C(13)-H(13C)	109.5
C(2)-C(3)-C(24)	121.3(4)	H(13A)-C(13)-H(13C)	109.5
C(2)-C(3)-H(1)	119.3	H(13B)-C(13)-H(13C)	109.5
C(24)-C(3)-H(1)	119.3	C(12)-C(14)-H(14A)	109.5
N(1)-C(4)-C(23)	122.6(3)	C(12)-C(14)-H(14B)	109.5
N(1)-C(4)-C(5)	114.9(3)	H(14A)-C(14)-H(14B)	109.5
C(23)-C(4)-C(5)	122.1(3)	C(12)-C(14)-H(14C)	109.5
N(2)-C(5)-C(6)	122.7(3)	H(14A)-C(14)-H(14C)	109.5
N(2)-C(5)-C(4)	114.8(3)	H(14B)-C(14)-H(14C)	109.5
C(6)-C(5)-C(4)	122.1(3)	C(12)-C(15)-H(15A)	109.5
C(7)-C(6)-C(5)	120.5(4)	C(12)-C(15)-H(15B)	109.5
C(7)-C(6)-H(16)	119.7	H(15A)-C(15)-H(15B)	109.5
C(5)-C(6)-H(16)	119.7	C(12)-C(15)-H(15C)	109.5
C(6)-C(7)-C(25)	116.0(4)	H(15A)-C(15)-H(15C)	109.5
C(6)-C(7)-C(12)	123.9(5)	H(15B)-C(15)-H(15C)	109.5
C(25)-C(7)-C(12)	120.0(4)	C(27B)-C(16)-C(26B)	111.3(17)
N(2)-C(8)-C(25)	122.1(4)	C(17A)-C(16)-C(24)	116.7(6)
N(2)-C(8)-C(9)	120.0(4)	C(27B)-C(16)-C(24)	116.9(10)

C(25)-C(8)-C(9)	117.9(4)	C(26B)-C(16)-C(24)	108.2(6)
C(8)-C(9)-C(10)	112.5(5)	C(27B)-C(16)-C(17B)	109.1(16)
C(26B)-C(16)-C(17B)	103.3(14)	C(16)-C(17A)-H(17A)	109.5
C(24)-C(16)-C(17B)	107.1(7)	C(16)-C(17A)-H(17B)	109.5
C(17A)-C(16)-C(27A)	111.8(16)	H(17A)-C(17A)-H(17B)	109.5
C(24)-C(16)-C(27A)	107.1(8)	C(16)-C(17A)-H(17C)	109.5
C(17A)-C(16)-C(26A)	116.4(13)	H(17A)-C(17A)-H(17C)	109.5
C(24)-C(16)-C(26A)	106.2(8)	H(17B)-C(17A)-H(17C)	109.5
C(27A)-C(16)-C(26A)	96.5(14)	C(16)-C(26A)-H(26A)	109.5
C(19)-C(18)-C(2)	114.4(6)	C(16)-C(26A)-H(26B)	109.5
C(19)-C(18)-H(18A)	108.7	H(26A)-C(26A)-H(26B)	109.5
C(2)-C(18)-H(18A)	108.7	C(16)-C(26A)-H(26C)	109.5
C(19)-C(18)-H(18B)	108.7	H(26A)-C(26A)-H(26C)	109.5
C(2)-C(18)-H(18B)	108.7	H(26B)-C(26A)-H(26C)	109.5
H(18A)-C(18)-H(18B)	107.6	C(16)-C(27A)-H(27A)	109.5
O(2)-C(19)-C(18)	107.1(8)	C(16)-C(27A)-H(27B)	109.5
O(2)-C(19)-H(19A)	110.3	H(27A)-C(27A)-H(27B)	109.5
C(18)-C(19)-H(19A)	110.3	C(16)-C(27A)-H(27C)	109.5
O(2)-C(19)-H(19B)	110.3	H(27A)-C(27A)-H(27C)	109.5
C(18)-C(19)-H(19B)	110.3	H(27B)-C(27A)-H(27C)	109.5
H(19A)-C(19)-H(19B)	108.5	C(16)-C(17B)-H(17D)	109.5
O(2)-C(20)-H(20A)	109.5	C(16)-C(17B)-H(17E)	109.5
O(2)-C(20)-H(20B)	109.5	H(17D)-C(17B)-H(17E)	109.5
H(20A)-C(20)-H(20B)	109.5	C(16)-C(17B)-H(17F)	109.5
O(2)-C(20)-H(20C)	109.5	H(17D)-C(17B)-H(17F)	109.5
H(20A)-C(20)-H(20C)	109.5	H(17E)-C(17B)-H(17F)	109.5
H(20B)-C(20)-H(20C)	109.5	C(16)-C(26B)-H(26D)	109.5
O(3)-C(21)-Mn(1)	173.7(5)	C(16)-C(26B)-H(26E)	109.5
O(4)-C(22)-Mn(1)	176.5(6)	H(26D)-C(26B)-H(26E)	109.5
C(4)-C(23)-C(24)	121.2(4)	C(16)-C(26B)-H(26F)	109.5
C(4)-C(23)-H(23)	119.4	H(26D)-C(26B)-H(26F)	109.5
C(24)-C(23)-H(23)	119.4	H(26E)-C(26B)-H(26F)	109.5
C(23)-C(24)-C(3)	115.5(4)	C(16)-C(27B)-H(27D)	109.5
C(23)-C(24)-C(16)	122.4(4)	C(16)-C(27B)-H(27E)	109.5
C(3)-C(24)-C(16)	122.0(4)	H(27D)-C(27B)-H(27E)	109.5
C(8)-C(25)-C(7)	121.8(4)	C(16)-C(27B)-H(27F)	109.5
C(8)-C(25)-H(25)	119.1	H(27D)-C(27B)-H(27F)	109.5
C(7)-C(25)-H(25)	119.1	H(27E)-C(27B)-H(27F)	109.5

Table S8 Torsion angles [°] for **Mn-bpy^{diOMe}.**

C(4)-N(1)-C(2)-C(3)	-6.1(6)	C(25)-C(7)-C(12)-C(15)	-173.7(7)
Mn(1)-N(1)-C(2)-C(3)	164.4(4)	C(6)-C(7)-C(12)-C(13)	-117.9(8)
C(4)-N(1)-C(2)-C(18)	170.7(5)	C(25)-C(7)-C(12)-C(13)	60.1(9)
Mn(1)-N(1)-C(2)-C(18)	-18.8(7)	C(6)-C(7)-C(12)-C(14)	125.0(7)
N(1)-C(2)-C(3)-C(24)	0.2(8)	C(25)-C(7)-C(12)-C(14)	-57.0(8)
C(18)-C(2)-C(3)-C(24)	-176.8(5)	N(1)-C(2)-C(18)-C(19)	117.4(6)
C(2)-N(1)-C(4)-C(23)	7.6(6)	C(3)-C(2)-C(18)-C(19)	-65.6(7)
Mn(1)-N(1)-C(4)-C(23)	-164.6(3)	C(20)-O(2)-C(19)-C(18)	-158.1(19)
C(2)-N(1)-C(4)-C(5)	-165.9(4)	C(2)-C(18)-C(19)-O(2)	-177.5(7)
Mn(1)-N(1)-C(4)-C(5)	21.9(4)	N(1)-C(4)-C(23)-C(24)	-3.1(6)
C(8)-N(2)-C(5)-C(6)	-6.3(6)	C(5)-C(4)-C(23)-C(24)	169.9(4)
Mn(1)-N(2)-C(5)-C(6)	169.5(3)	C(4)-C(23)-C(24)-C(3)	-2.9(7)
C(8)-N(2)-C(5)-C(4)	166.7(4)	C(4)-C(23)-C(24)-C(16)	-178.7(5)
Mn(1)-N(2)-C(5)-C(4)	-17.5(4)	C(2)-C(3)-C(24)-C(23)	4.3(7)
N(1)-C(4)-C(5)-N(2)	-2.9(5)	C(2)-C(3)-C(24)-C(16)	-179.8(5)
C(23)-C(4)-C(5)-N(2)	-176.4(4)	C(17A)-C(16)-C(24)-C(23)	-8.8(16)
N(1)-C(4)-C(5)-C(6)	170.2(4)	C(27B)-C(16)-C(24)-C(23)	-172.5(17)
C(23)-C(4)-C(5)-C(6)	-3.4(6)	C(26B)-C(16)-C(24)-C(23)	61.0(14)
N(2)-C(5)-C(6)-C(7)	4.1(7)	C(17B)-C(16)-C(24)-C(23)	-49.8(11)
C(4)-C(5)-C(6)-C(7)	-168.4(4)	C(27A)-C(16)-C(24)-C(23)	-134.9(13)
C(5)-C(6)-C(7)-C(25)	0.8(7)	C(26A)-C(16)-C(24)-C(23)	122.8(11)
C(5)-C(6)-C(7)-C(12)	178.9(5)	C(17A)-C(16)-C(24)-C(3)	175.7(15)
C(5)-N(2)-C(8)-C(25)	3.7(7)	C(27B)-C(16)-C(24)-C(3)	11.9(18)
Mn(1)-N(2)-C(8)-C(25)	-171.2(4)	C(26B)-C(16)-C(24)-C(3)	-114.6(13)
C(5)-N(2)-C(8)-C(9)	-176.5(4)	C(17B)-C(16)-C(24)-C(3)	134.7(10)
Mn(1)-N(2)-C(8)-C(9)	8.7(7)	C(27A)-C(16)-C(24)-C(3)	49.5(14)
N(2)-C(8)-C(9)-C(10)	-103.3(6)	C(26A)-C(16)-C(24)-C(3)	-52.8(12)
C(25)-C(8)-C(9)-C(10)	76.6(7)	N(2)-C(8)-C(25)-C(7)	1.1(8)
C(11)-O(5)-C(10)-C(9)	-176.0(13)	C(9)-C(8)-C(25)-C(7)	-178.7(5)
C(8)-C(9)-C(10)-O(5)	-71.6(8)	C(6)-C(7)-C(25)-C(8)	-3.4(8)
C(6)-C(7)-C(12)-C(15)	8.3(10)	C(12)-C(7)-C(25)-C(8)	178.5(5)

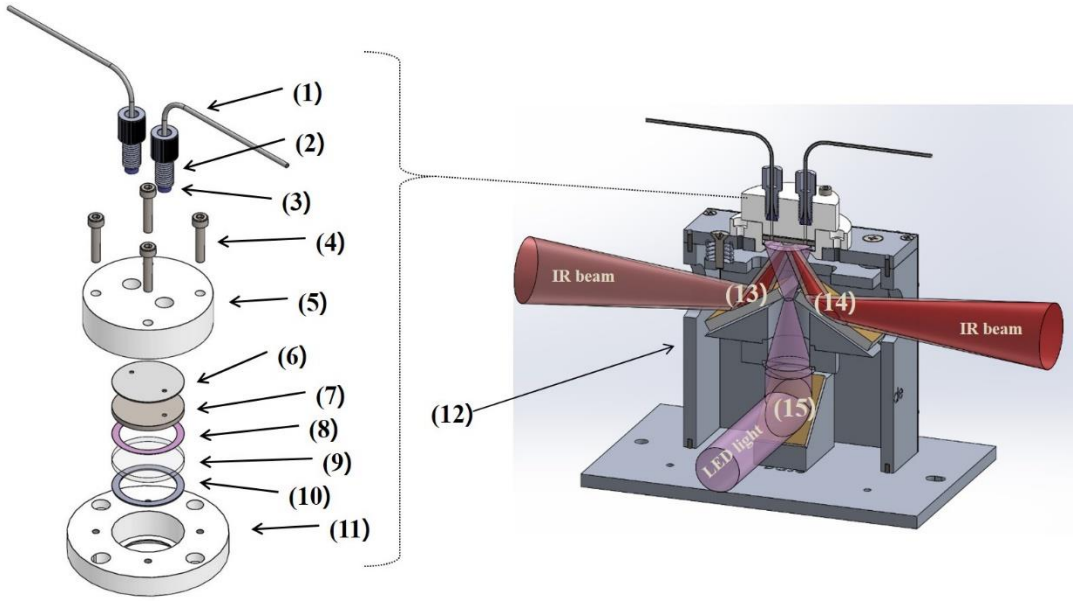

Fig. S1 Disassembled view of the in-situ FTIR cell. (1) Solution injection Tube (PTFE). (2) XP-230 PEEK fittings. (3) P-200 PTFE gasket. (4) M3 Hex Screw required to tighten the cell. (5) PEEK cell cover. (6) PEEK Gasket for overflow prevention. (7) Sample plate for reflect IR beam. (8) Teflon spacer determines the path length (0.1 mm) of the cell. (9) Calcium fluoride window (OD 25 mm, T 2 mm). (10) PTFE gasket type ring. (11) Cell base body (PEEK). (12) Three mirror reflectance accessory. (13~15) Mirrors.

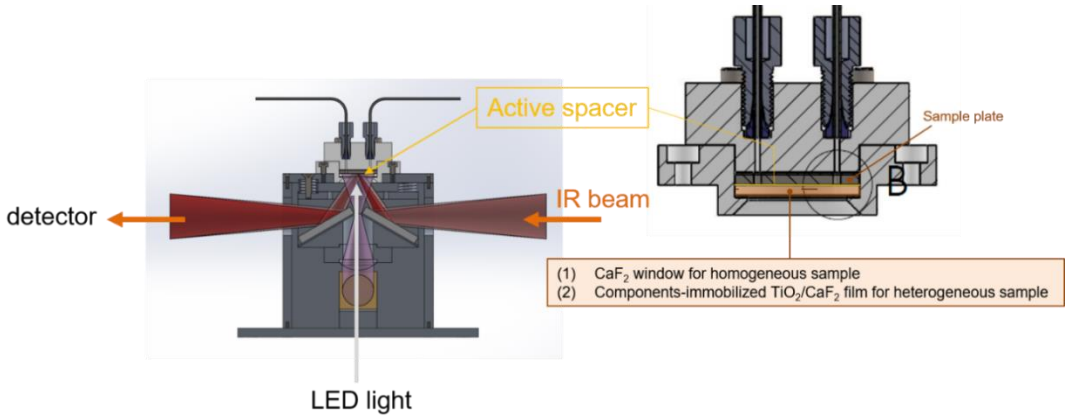

Fig. S2 Cross-sectional drawing of the cell. The Teflon spacer, through which the IR-beam pass, has 0.1 mm pass length and 0.03 mL total volume.

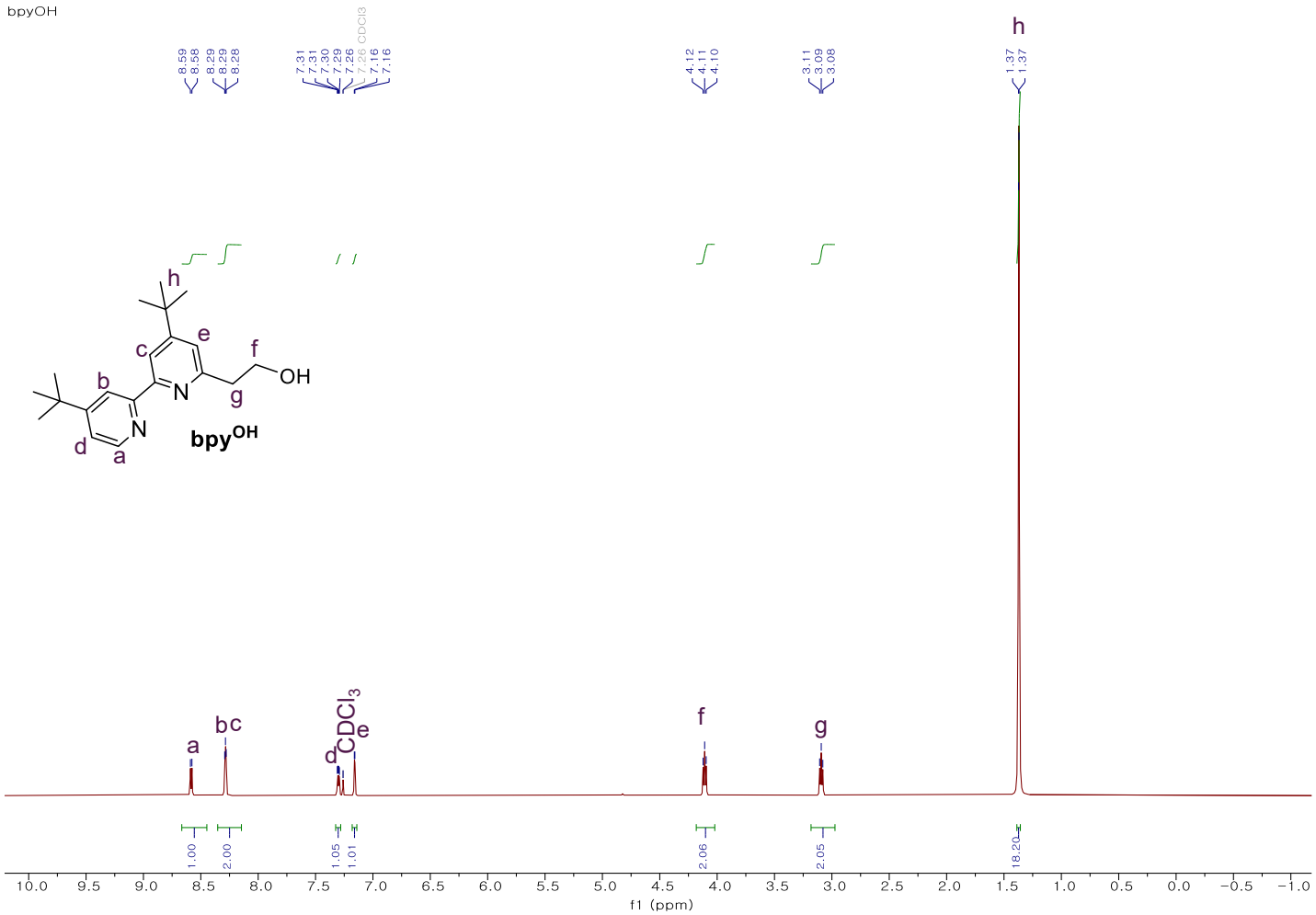

Fig. S3 ^{1}H-NMR spectroscopic view of **bpy^{OH}** in $CHCl_3$-d_1.

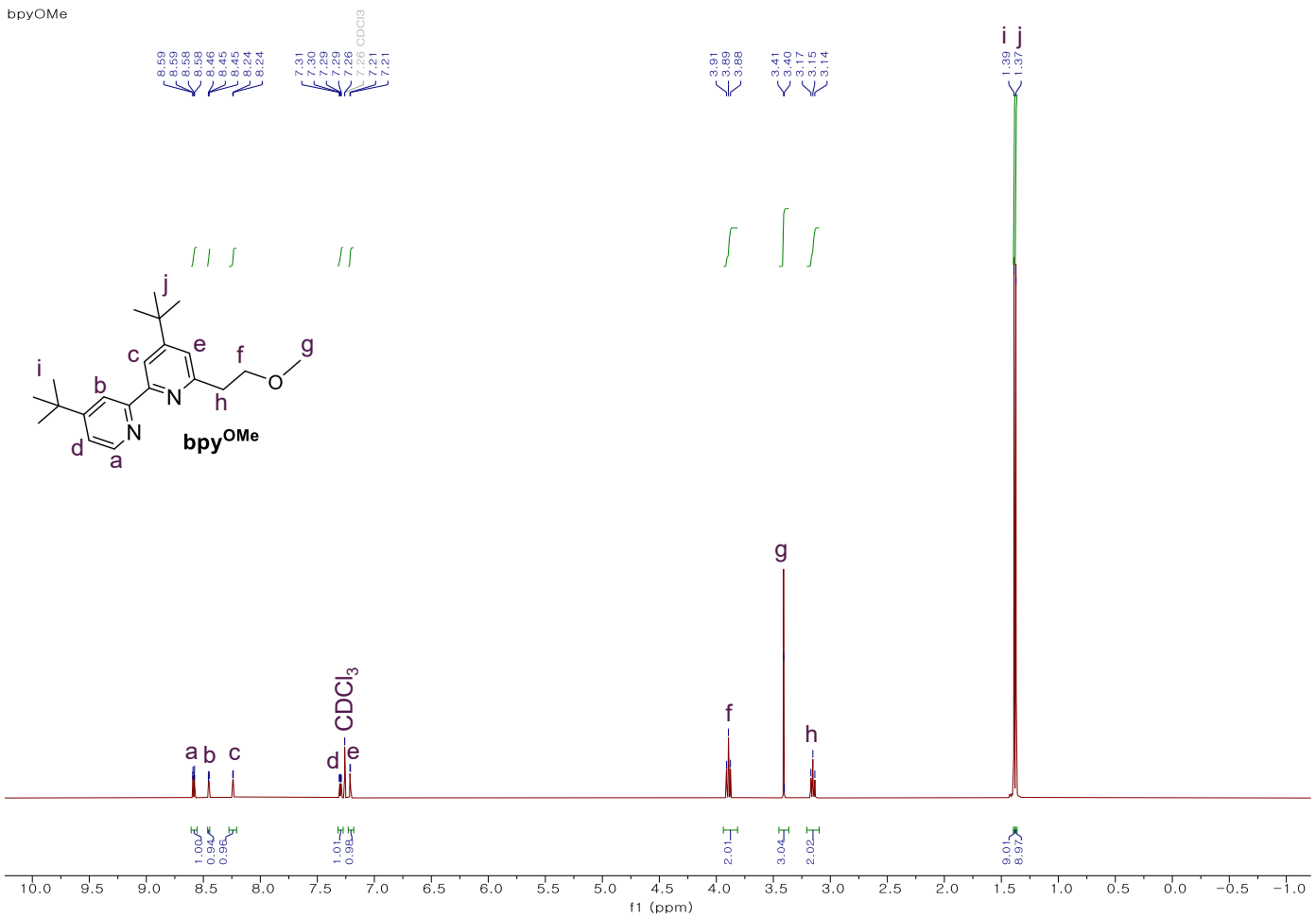

Fig. S4 ^{1}H-NMR spectroscopic view of **bpy^{OMe}** in $CHCl_3$-d_1.

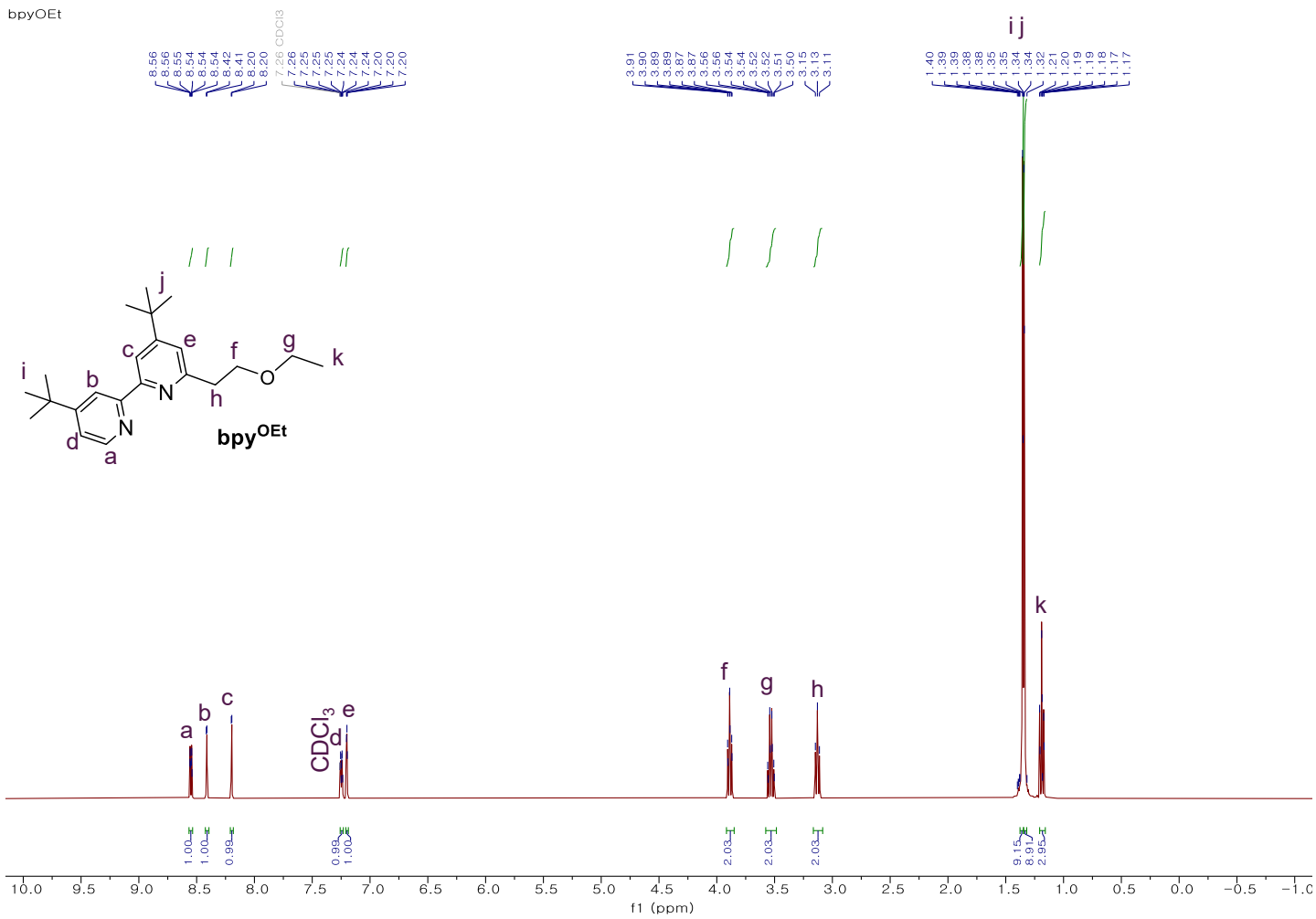

Fig. S5 ^{1}H-NMR spectroscopic view of **bpy^{OEt}** in $CHCl_3$-d_1.

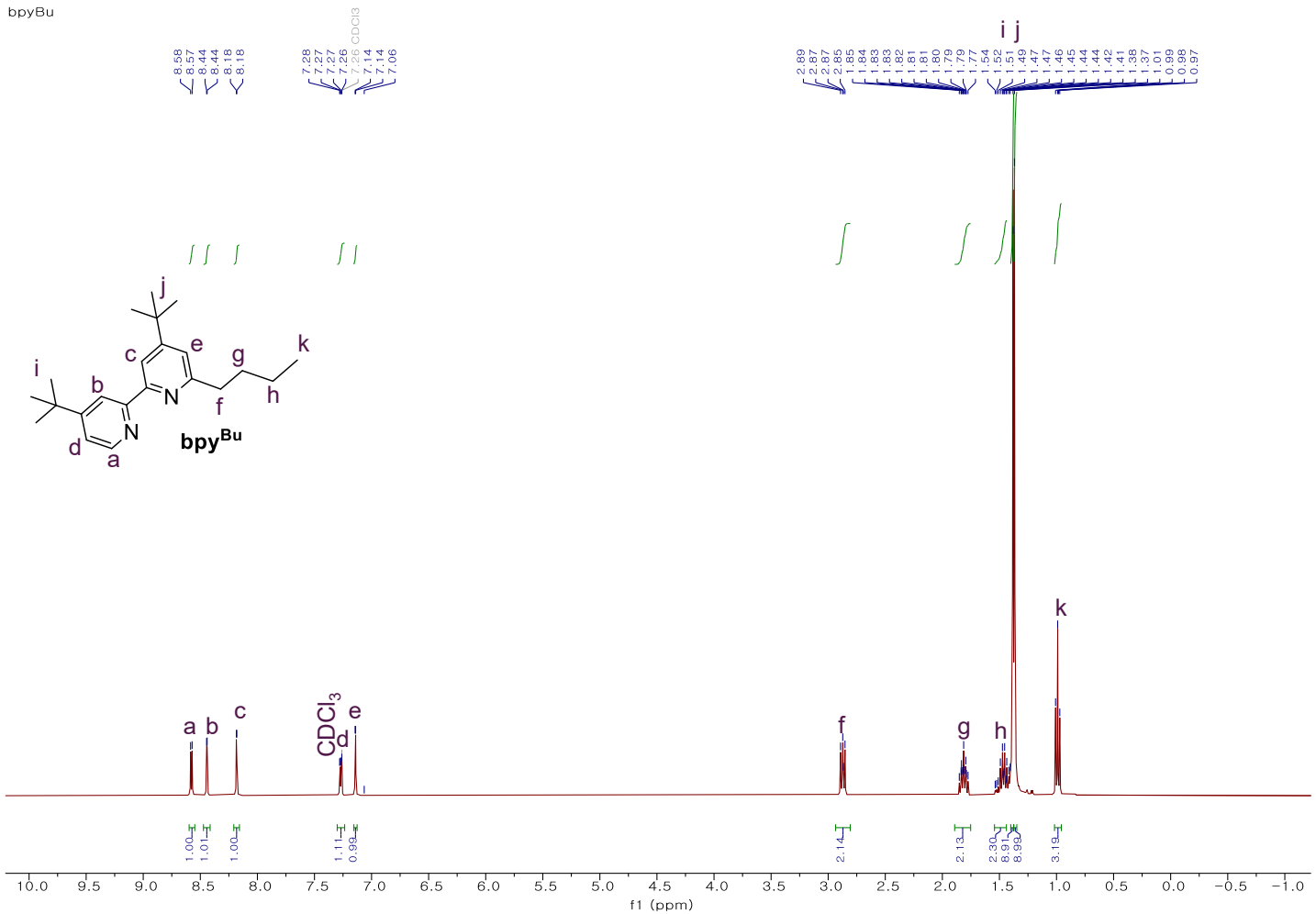

Fig. S6 ^{1}H-NMR spectroscopic view of **bpy^{Bu}** in $CHCl_3$-d_1.

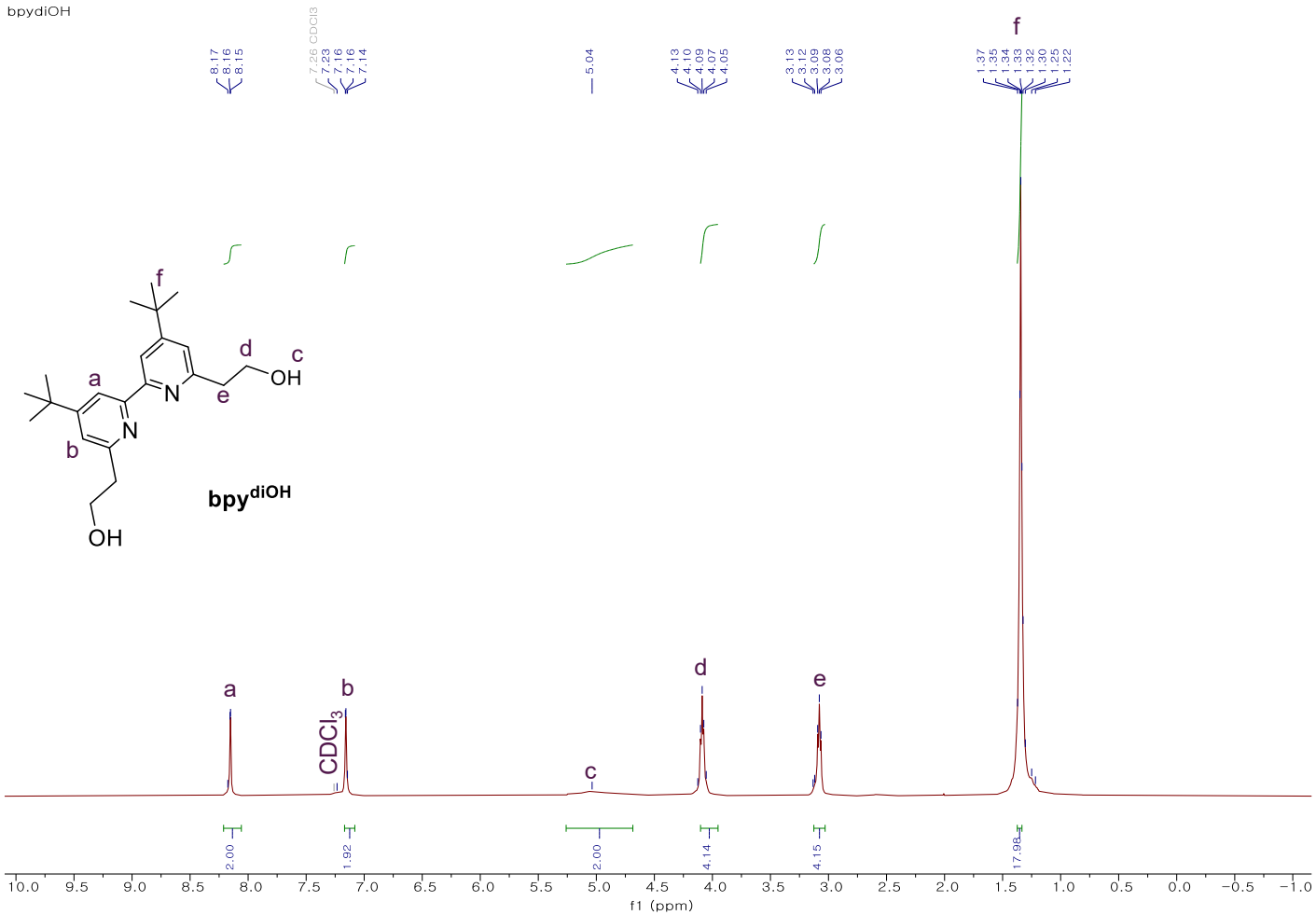

Fig. S7 ^{1}H-NMR spectroscopic view of **bpy^{diOH}** in $CHCl_3$-d_1.

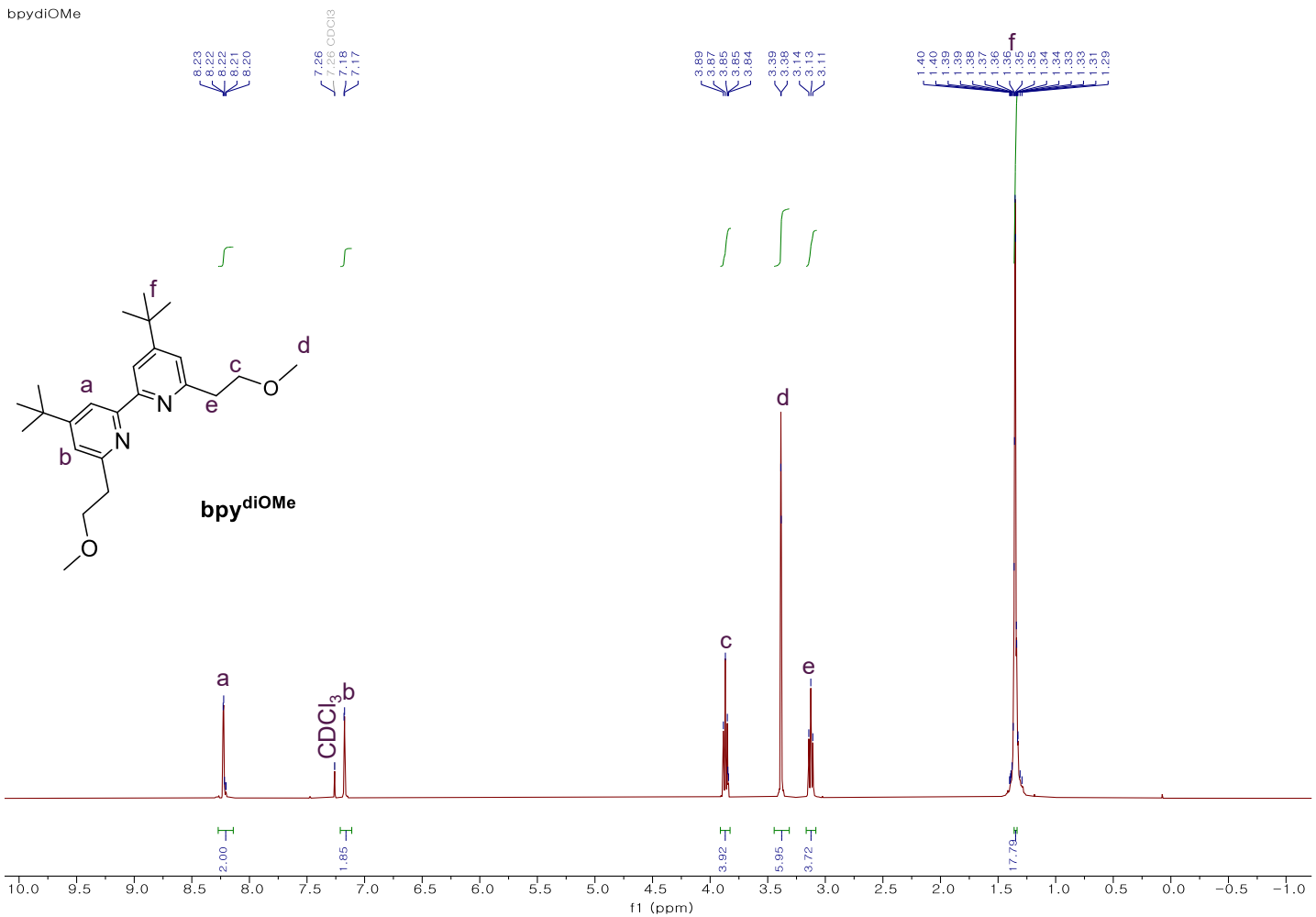

Fig. S8 ^{1}H-NMR spectroscopic view of **bpy^{diOMe}** in $CHCl_3$-d_1.

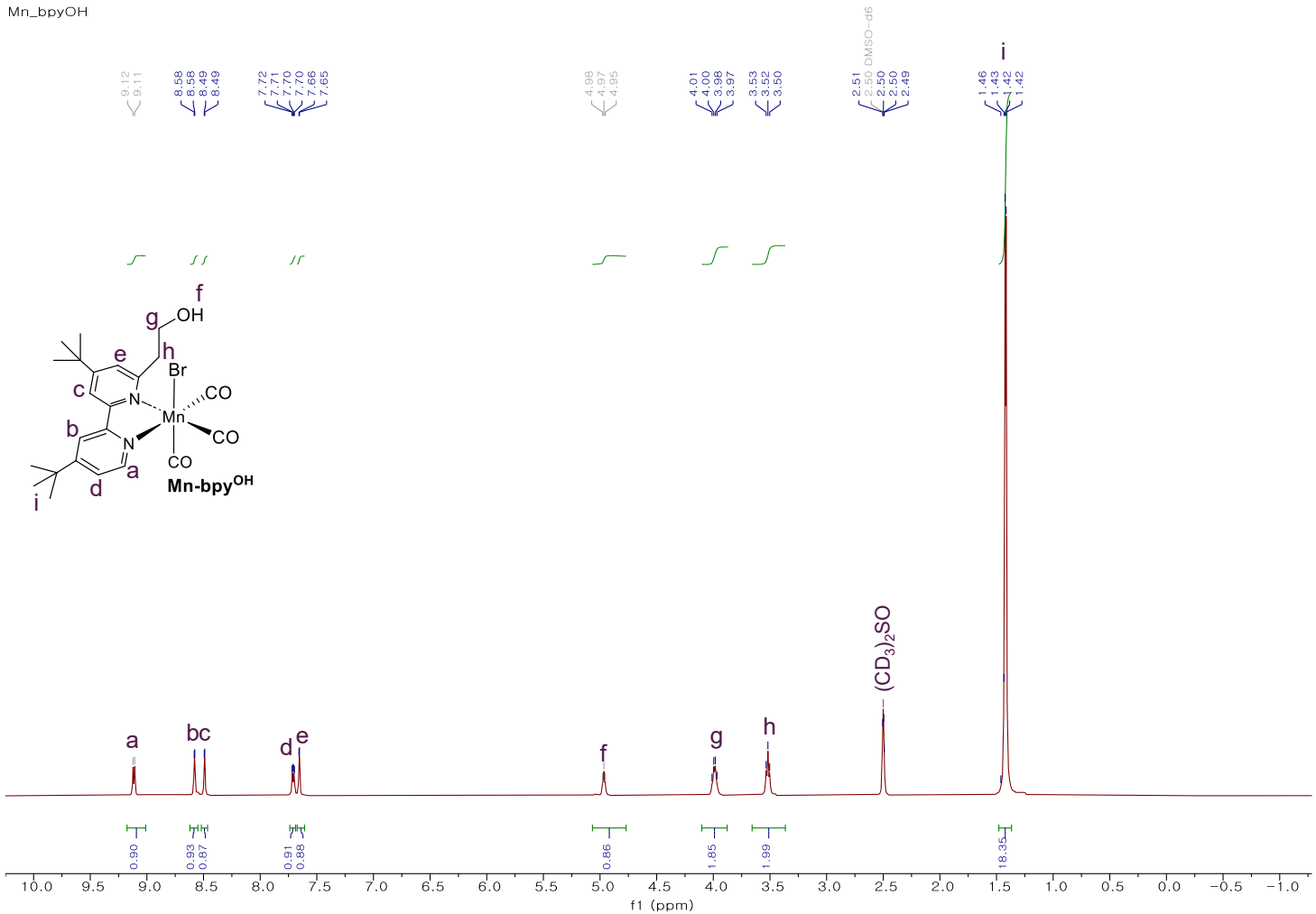

Fig S9 ^{1}H-NMR spectroscopic view of **Mn-bpy^{OH}** in DMSO-d_6.

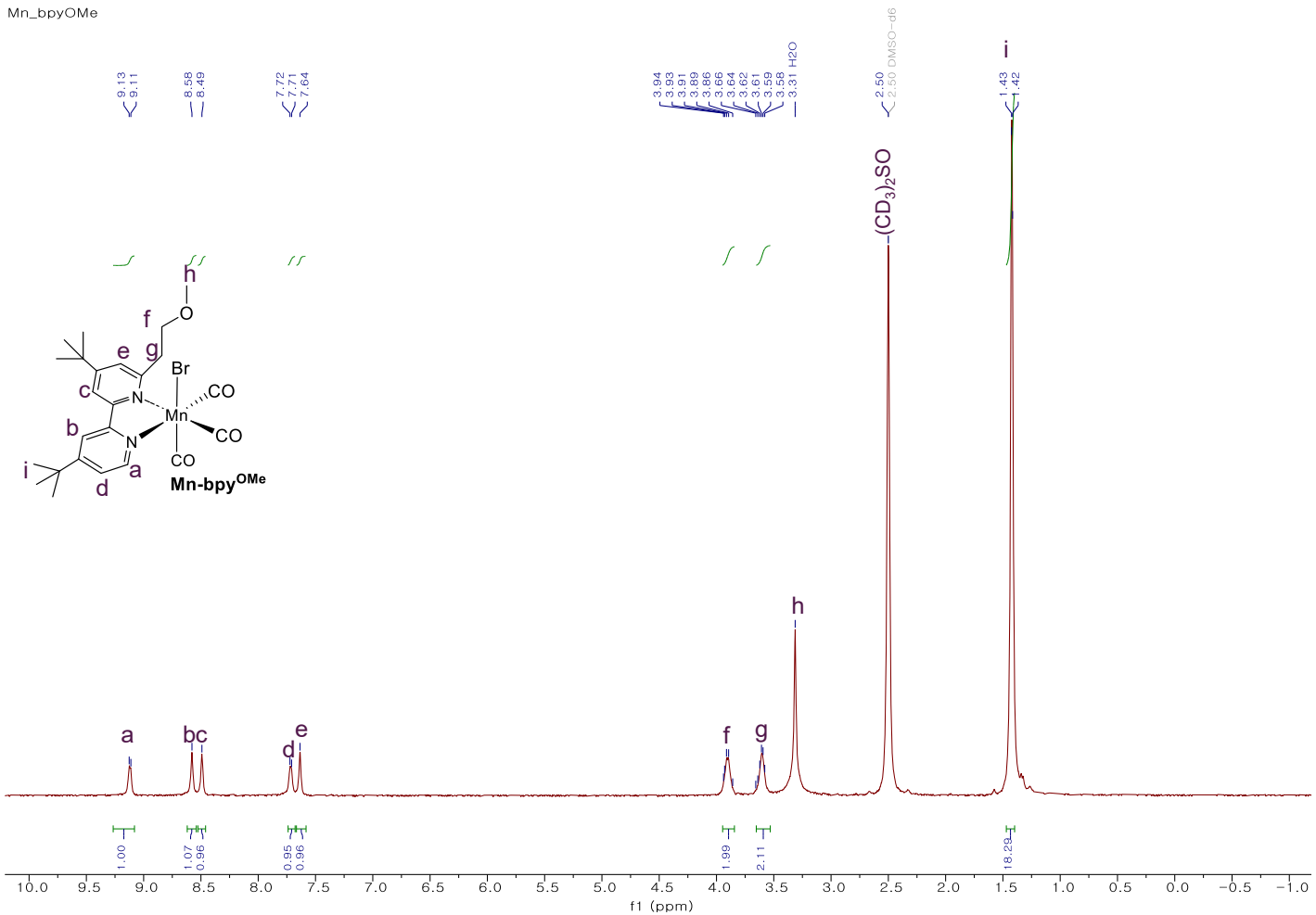

Fig. S10 ^{1}H-NMR spectroscopic view of **Mn-bpy^{OMe}** in DMSO-d_6.

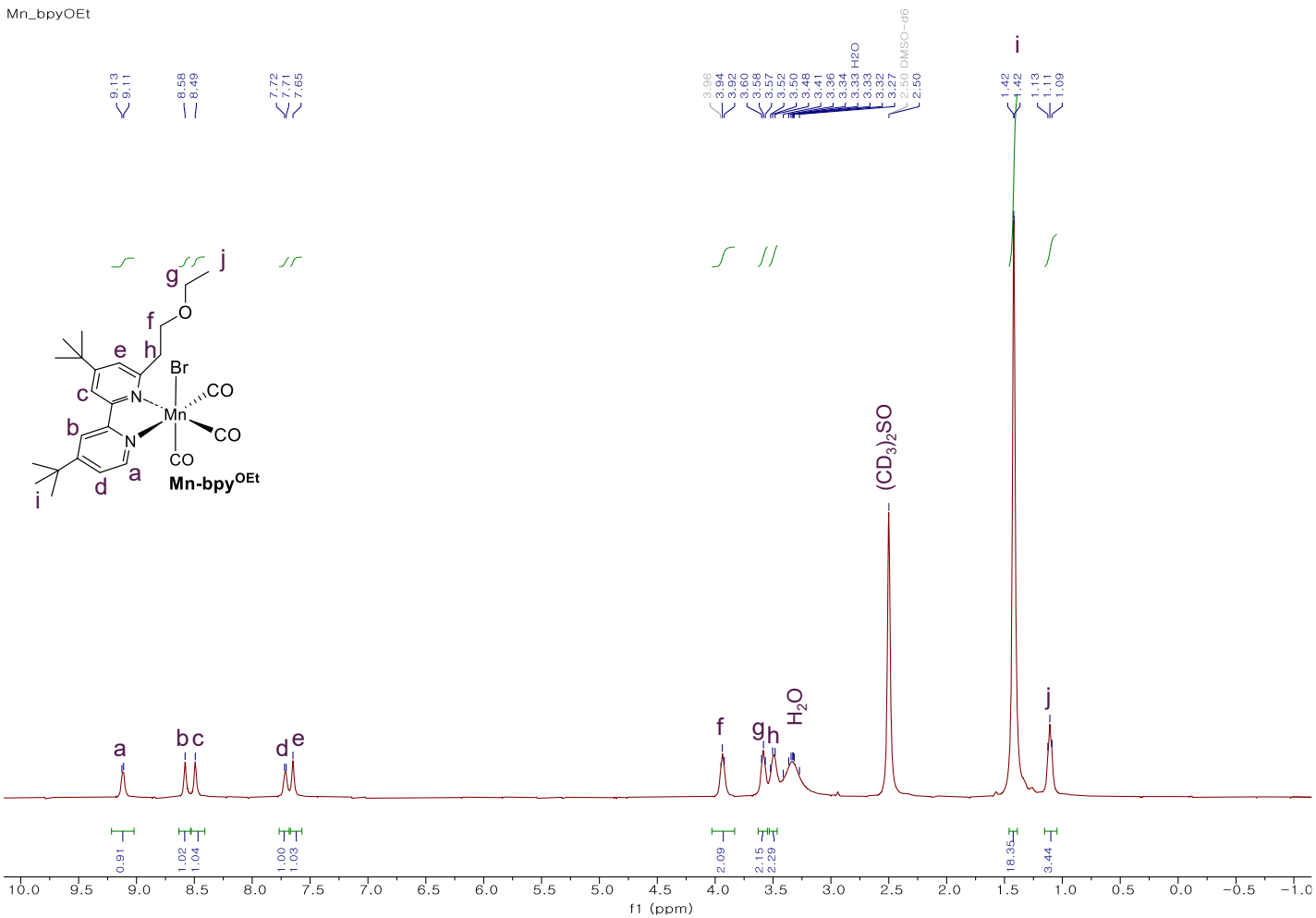

Fig. S11 ^{1}H-NMR spectroscopic view of **Mn-bpy^{OEt}** in DMSO-d_6.

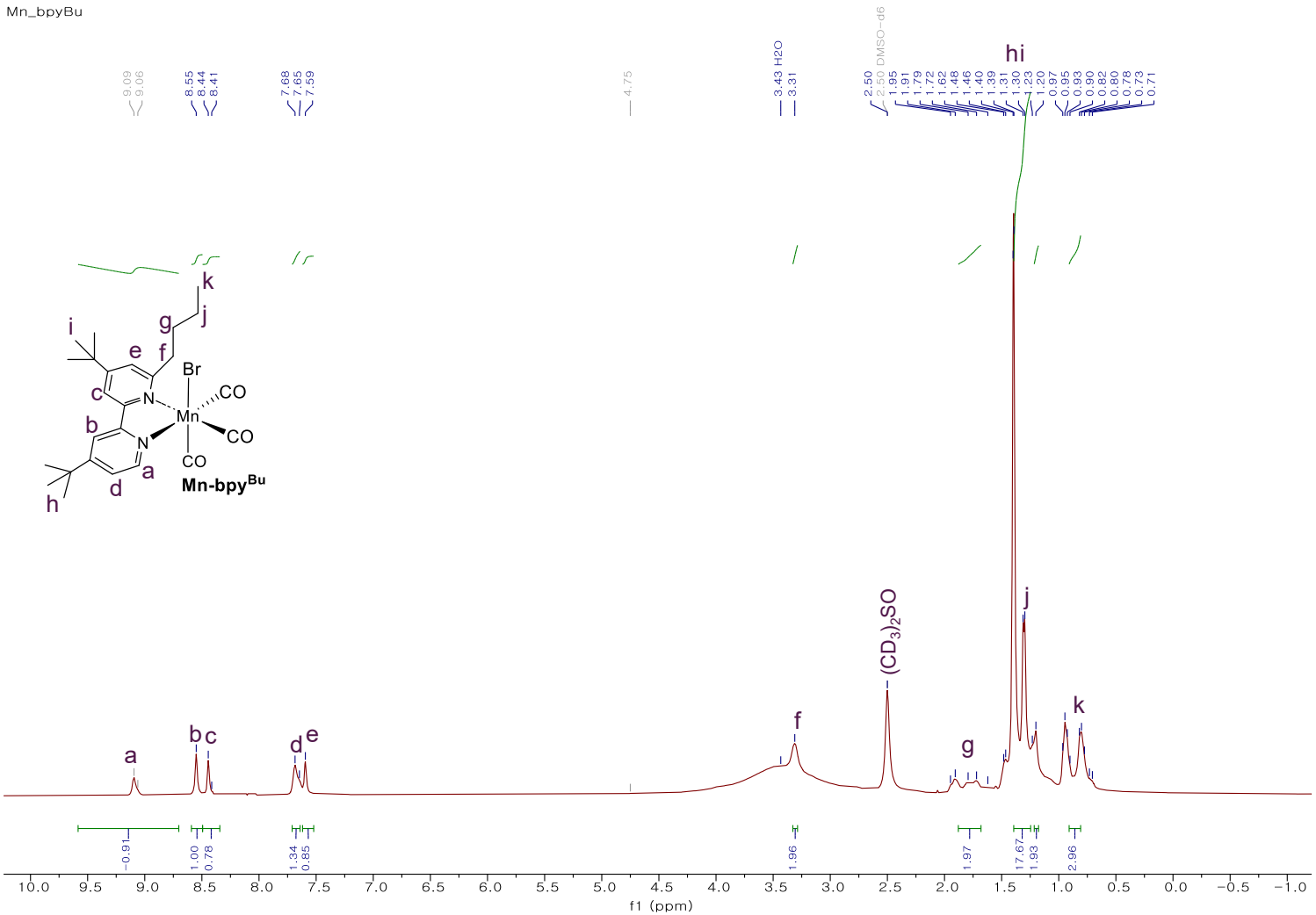

Fig. S12 ^{1}H-NMR spectroscopic view of **Mn-bpy^{Bu}** in DMSO-d_6.

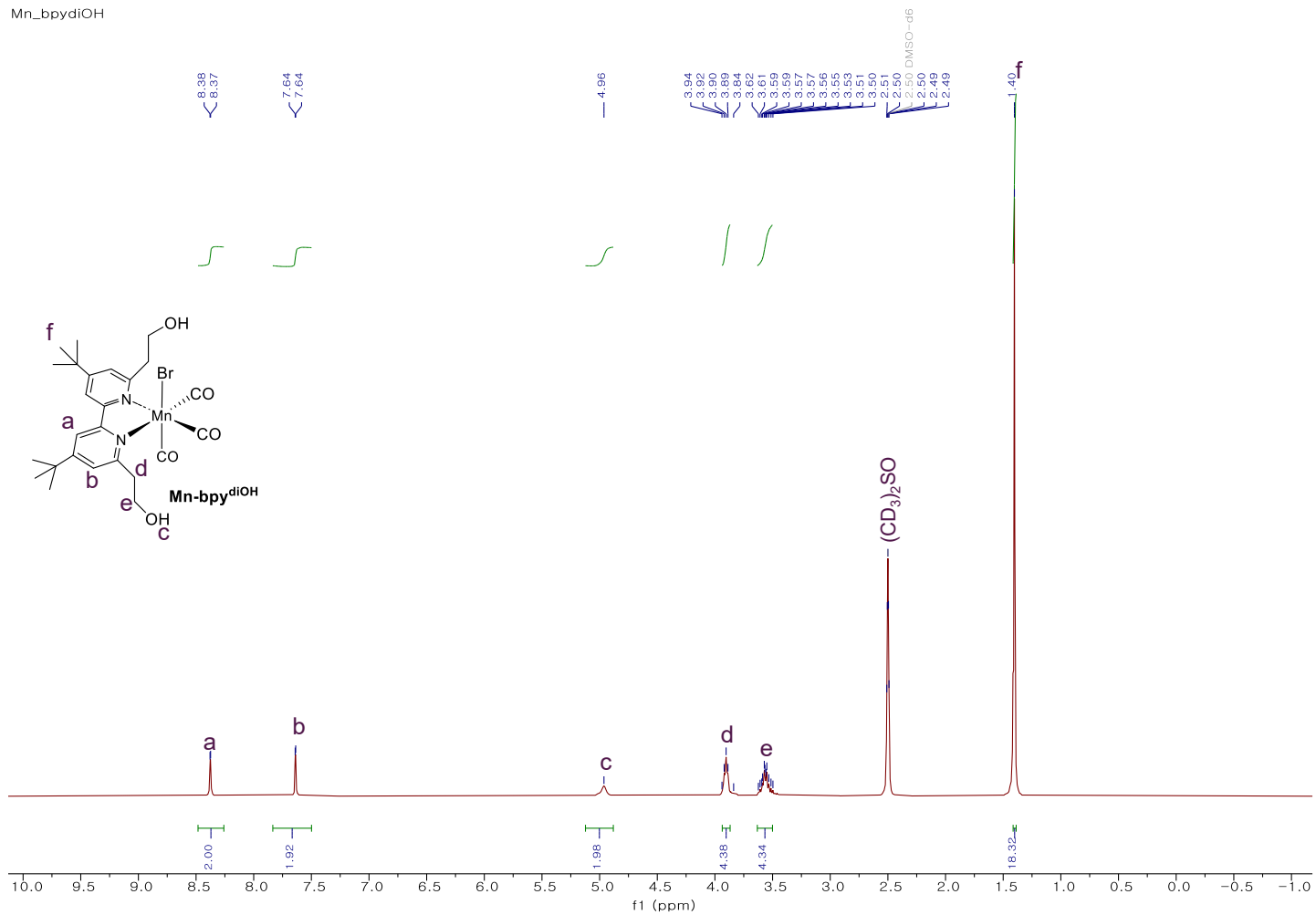

Fig. S13 ^{1}H-NMR spectroscopic view of **Mn-bpy^{diOH}** in DMSO-d_6.

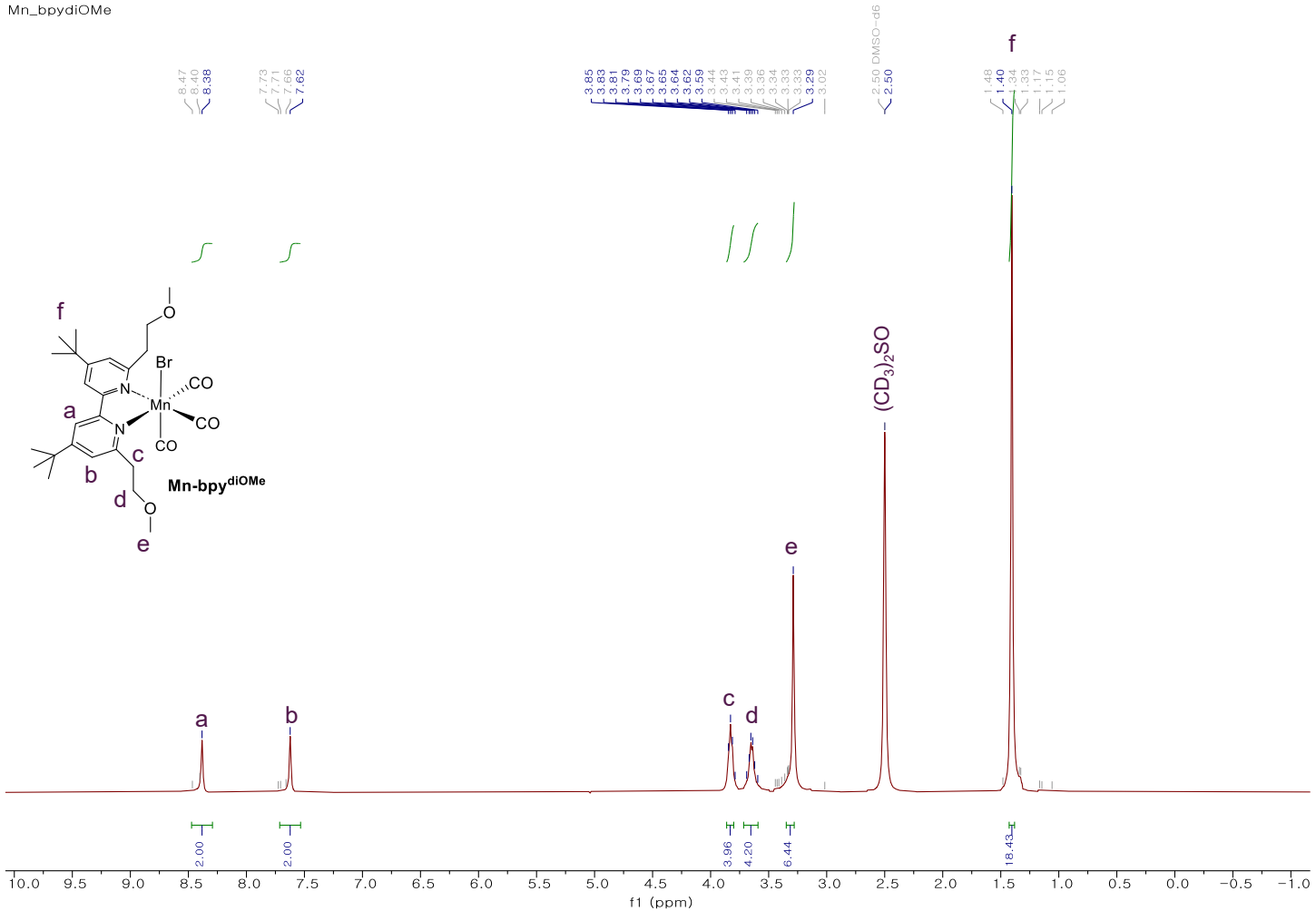

Fig. S14 ^{1}H-NMR spectroscopic view of **Mn-bpy^{diOMe}** in DMSO-d_6.

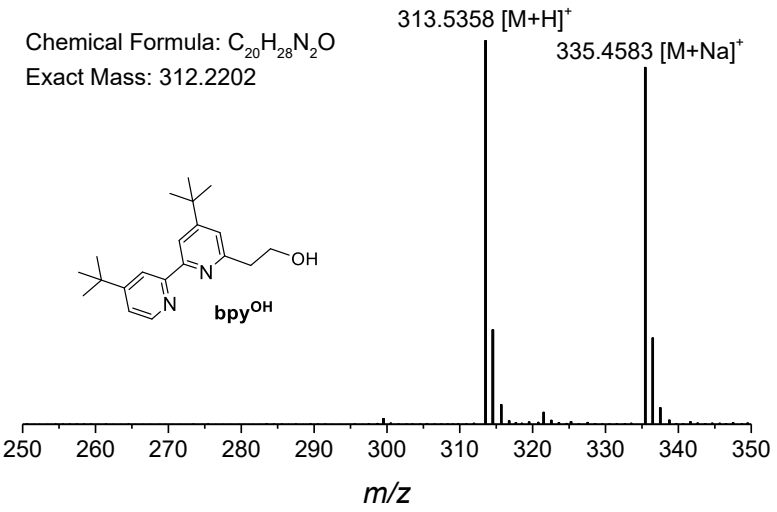

Fig. S15 ESI-Mass spectra of **bpy^{OH}**.

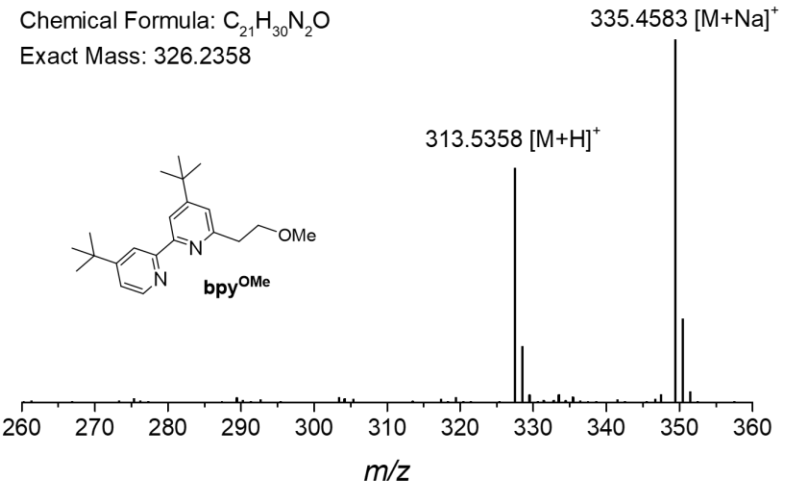

Fig. S16 ESI-Mass spectra of **bpy^{OMe}**.

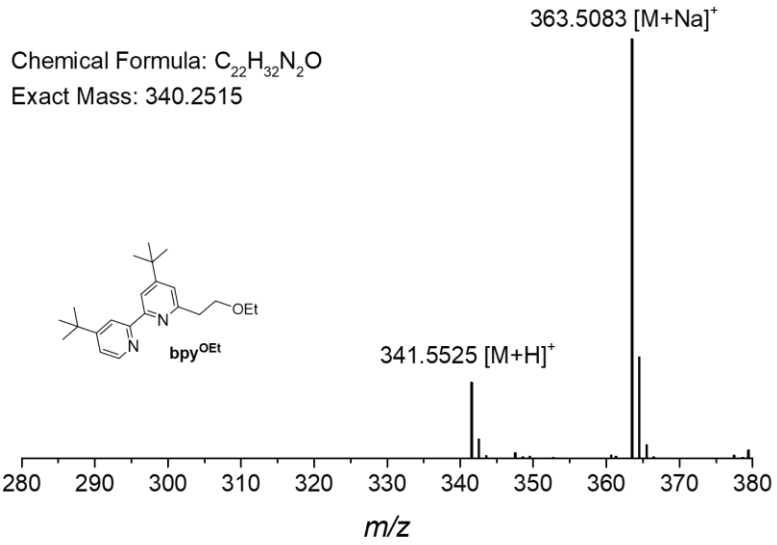

Fig. S17 ESI-Mass spectra of **bpy**$^{\mathbf{OEt}}$.

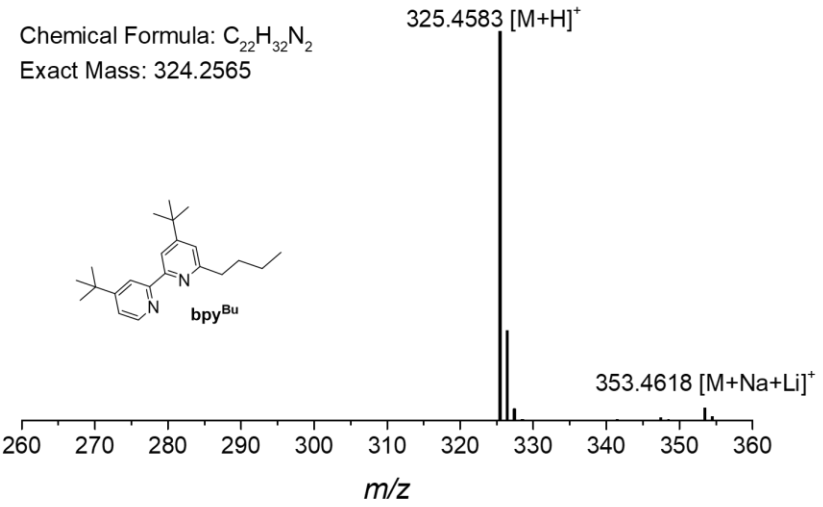

Fig. S18 ESI-Mass spectra of **bpy**$^{\mathbf{Bu}}$.

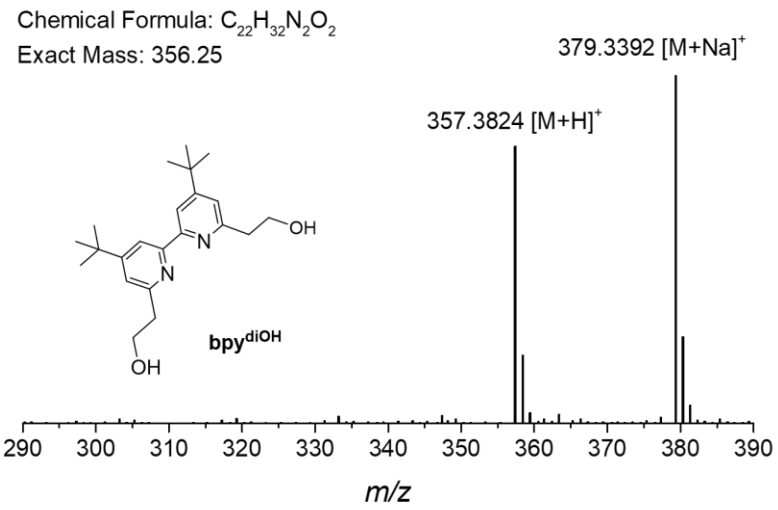

Fig. S19 ESI-Mass spectra of **bpy^{diOH}**.

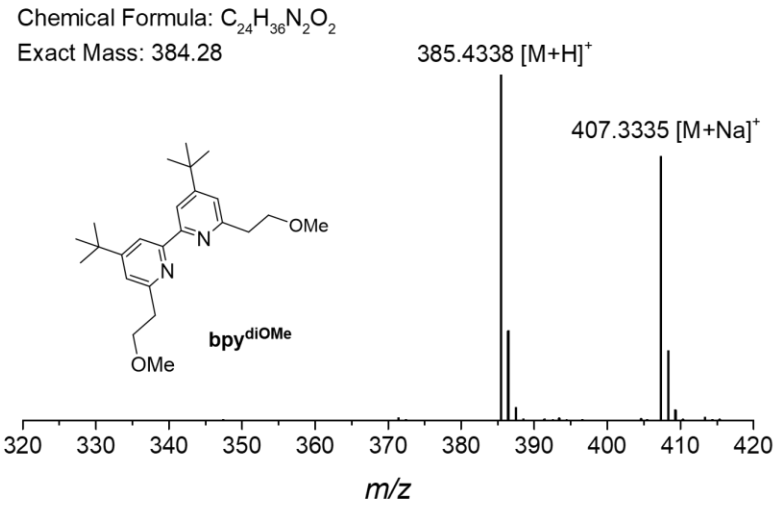

Fig. S20 ESI-Mass spectra of **bpy^{diOMe}**.

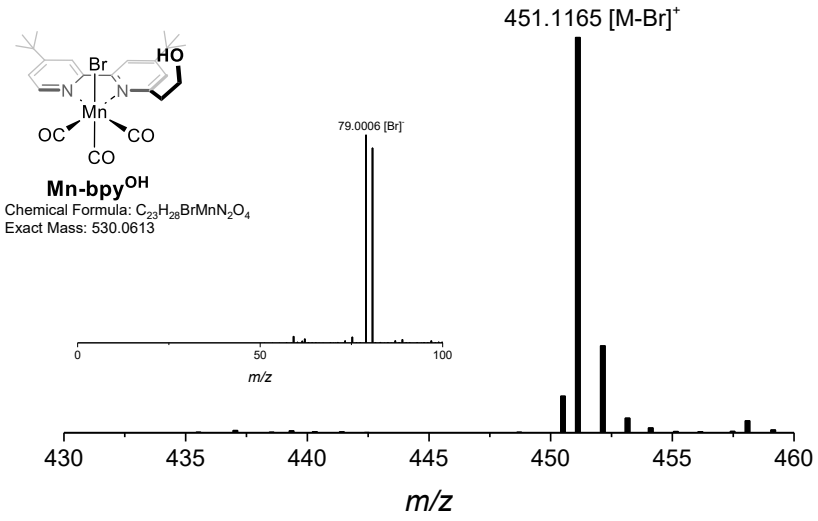

Fig. S21 ESI-Mass spectra of **Mn-bpy^{OH}**.

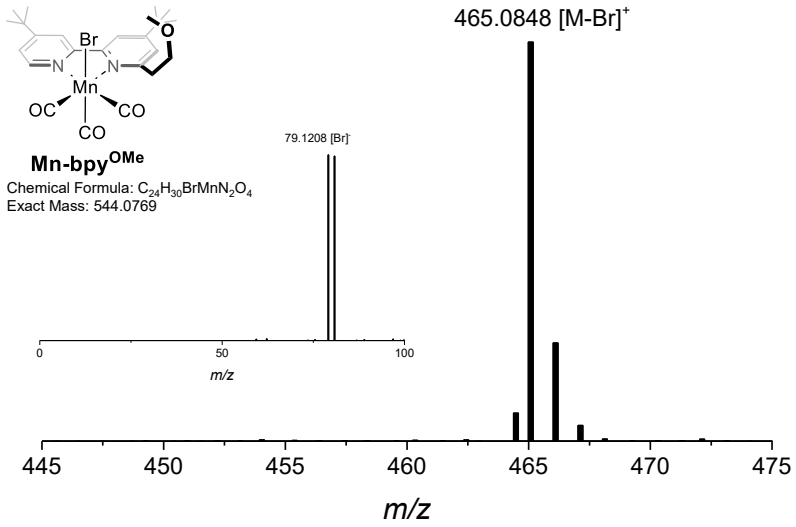

Fig. S22 ESI-Mass spectra of **Mn-bpy^{OMe}**.

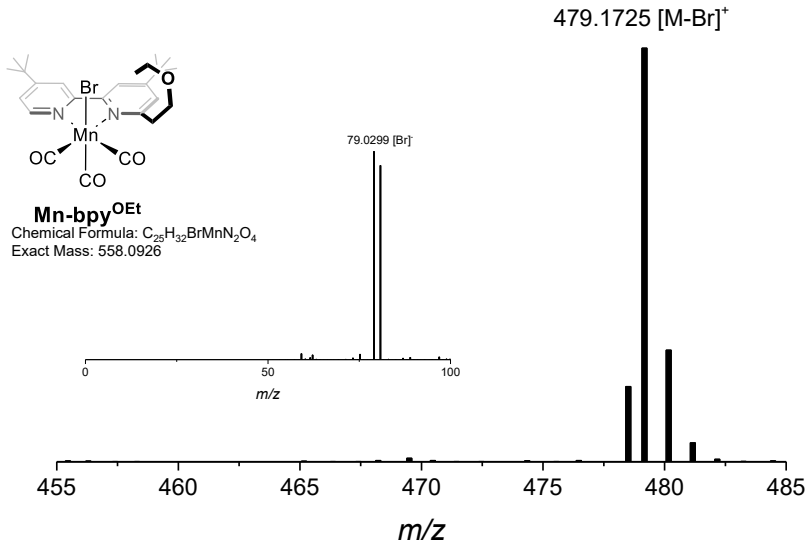

Fig. S23 ESI-Mass spectra of **Mn-bpy^{OEt}**.

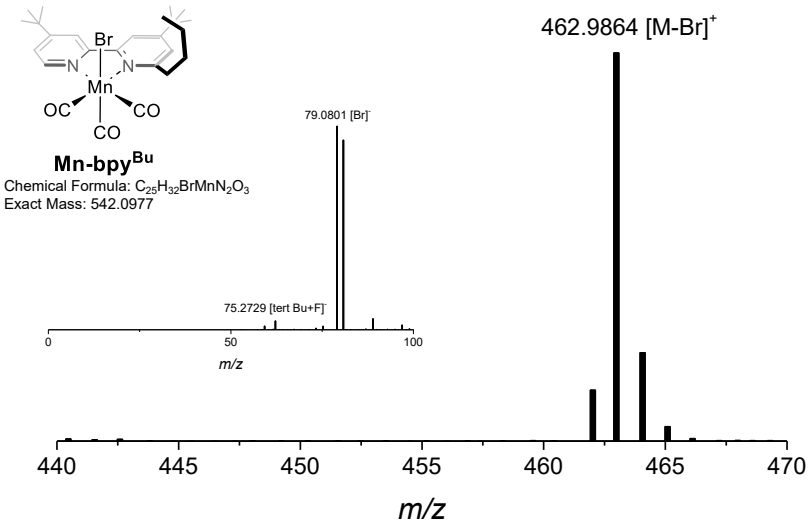

Fig. S24 ESI-Mass spectra of **Mn-bpy^{Bu}**.

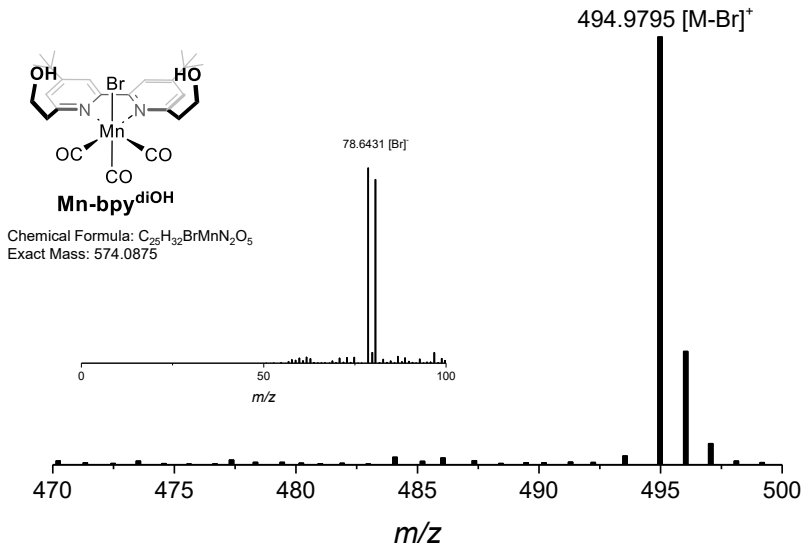

Fig. S25 ESI-Mass spectra of **Mn-bpy^{diOH}**.

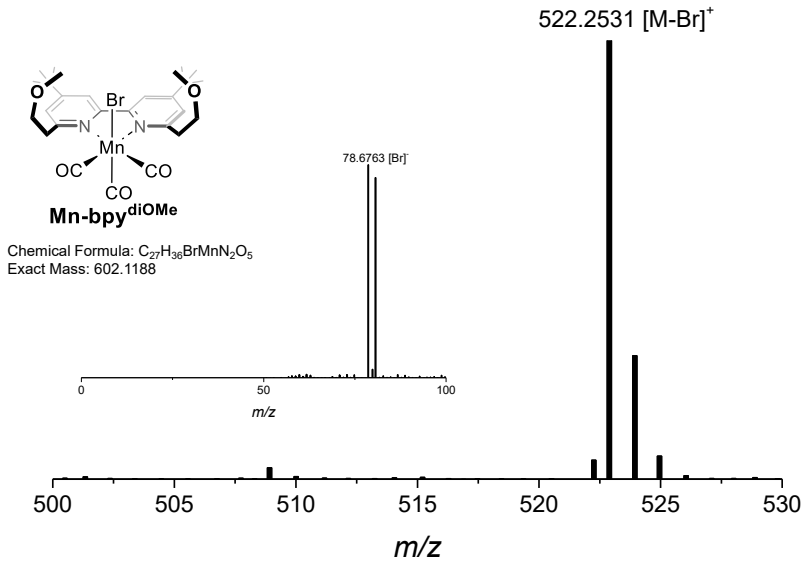

Fig. S26 ESI-Mass spectra of **Mn-bpy^{diOMe}**.

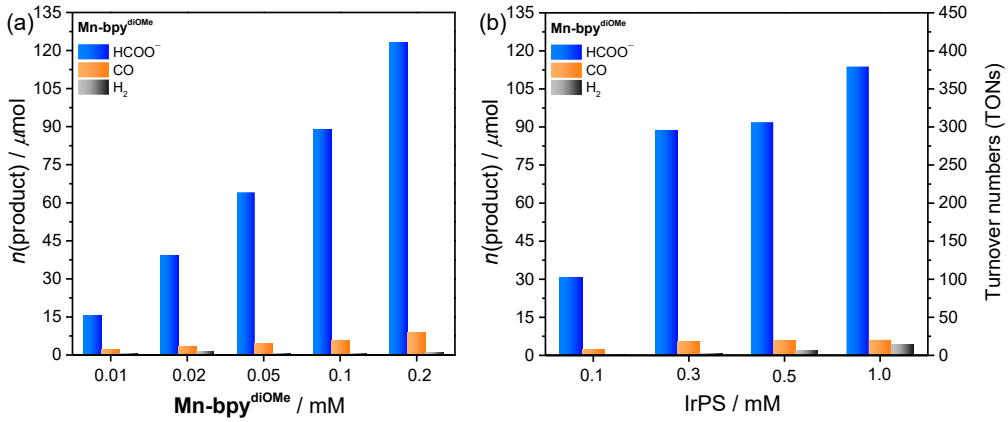

Fig. S27 Photolysis results after 3 h irradiation of mixed homogeneous system ((a) IrPS (0.3 mM) + **Mn-bpy^{diOMe}** (0.01–0.2 mM) and (b) IrPS (0.1–1.0 mM) + **Mn-bpy^{diOMe}** (0.1 mM)) in CO_2-saturated DMA/TEOA solution (16.7 vol% TEOA) containing 0.1 M BIH under λ >500 nm light at 298 K.

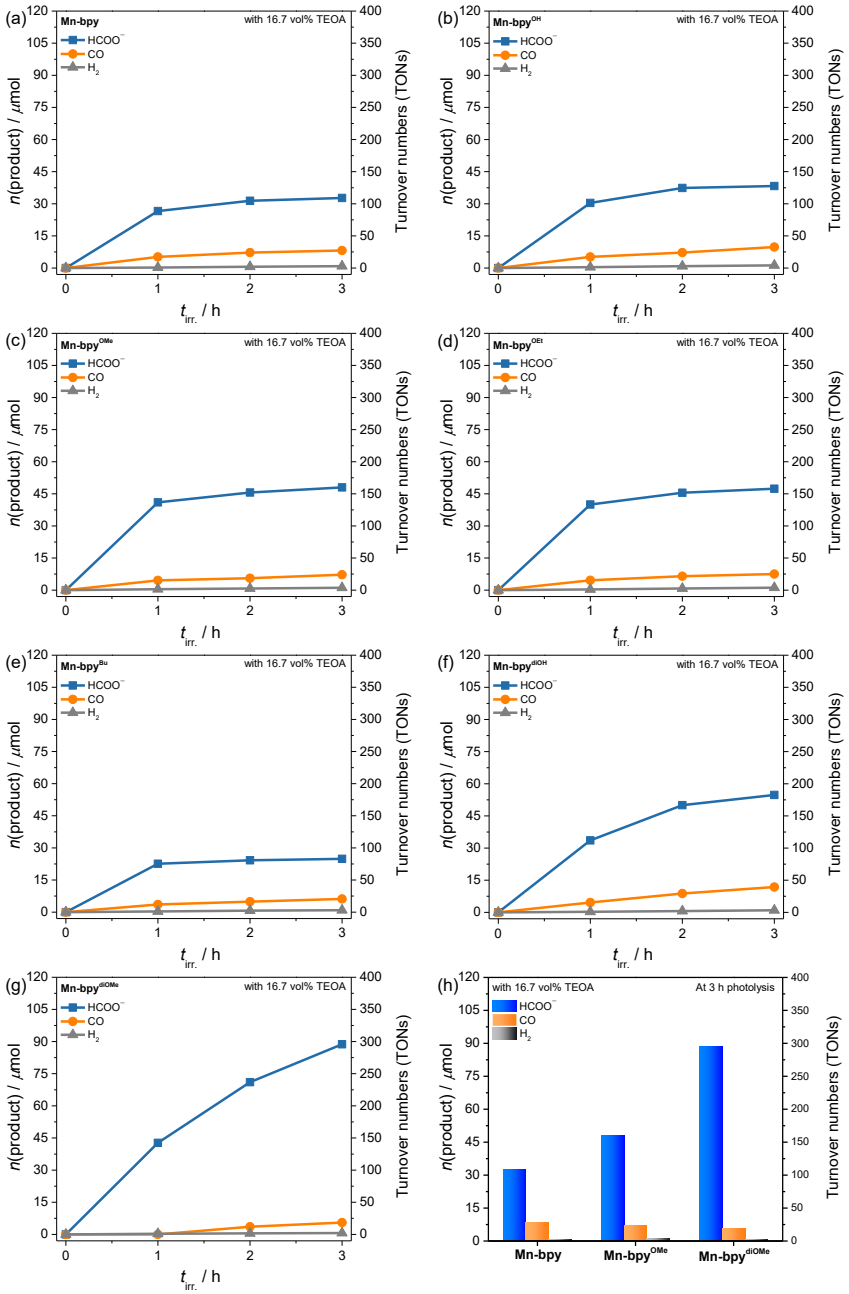

Fig. S28 Plots of formate/CO/H_2 formation versus irradiation time for 0.3 mM IrPS + 0.1 mM Mn(I) catalyst ((a) **Mn-bpy**, (b) **Mn-bpy^{OH}**, (c) **Mn-bpy^{OMe}**, (d) **Mn-bpy^{OEt}**, (e) **Mn-bpy^{Bu}**, (f) **Mn-bpy^{diOH}**, and (g) **Mn-bpy^{diOMe}**) and (h) product distribution of **Mn-bpy**, **Mn-bpy^{OMe}**, and **Mn-bpy^{diOMe}** in CO_2-saturated DMA/TEOA (16.7 vol% TEOA) solution containing 0.1 M BIH; irradiation at λ >500 nm at 298 K.

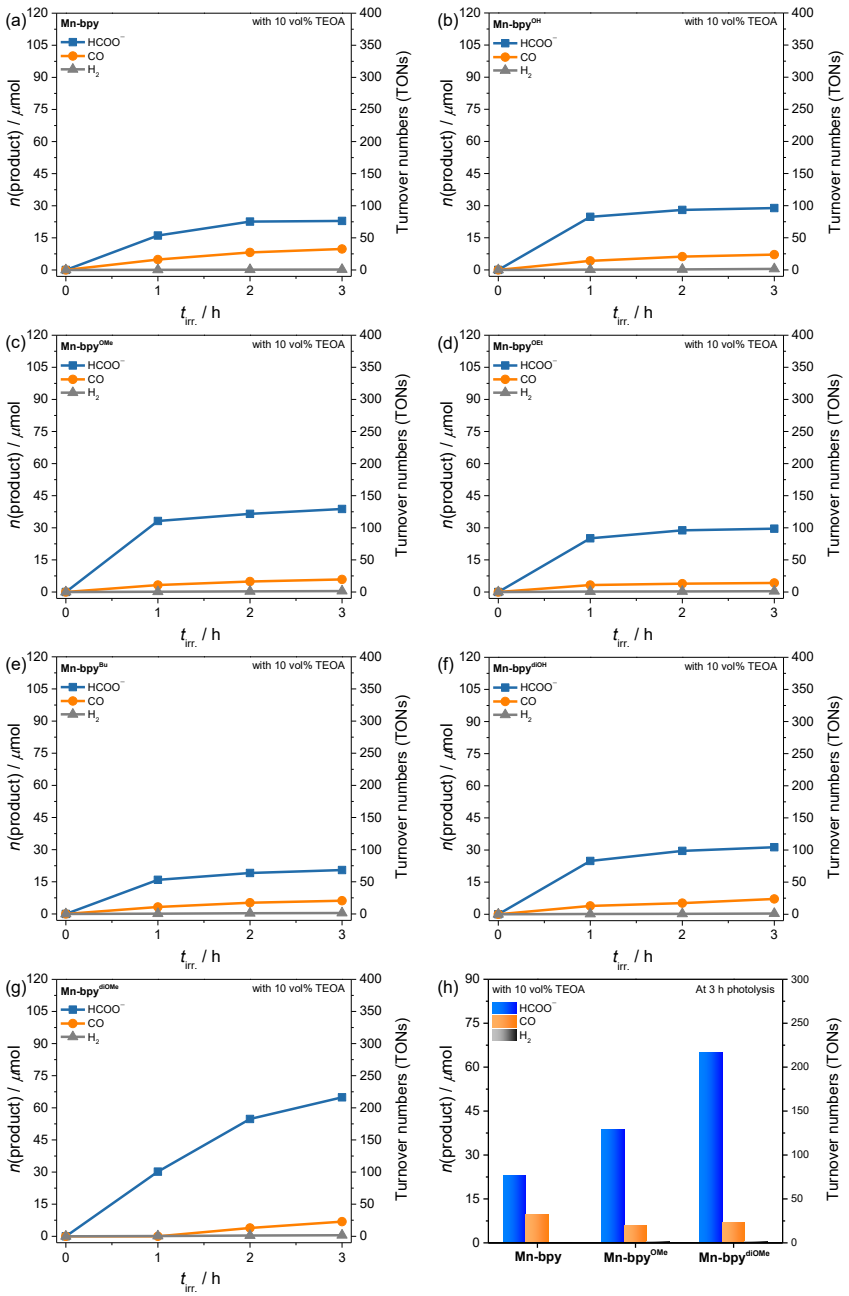

Fig. S29 Plots of formate/CO/H_2 formation versus irradiation time for 0.3 mM IrPS + 0.1 mM Mn(I) catalyst ((a) **Mn-bpy**, (b) **Mn-bpy^{OH}**, (c) **Mn-bpy^{OMe}**, (d) **Mn-bpy^{OEt}**, (e) **Mn-bpy^{Bu}**, (f) **Mn-bpy^{diOH}**, and (g) **Mn-bpy^{diOMe}**) and (h) product distribution of **Mn-bpy**, **Mn-bpy^{OMe}**, and **Mn-bpy^{diOMe}** in CO_2-saturated DMA/TEOA (10 vol% TEOA) solution containing 0.1 M BIH; irradiation at λ >500 nm at 298 K.

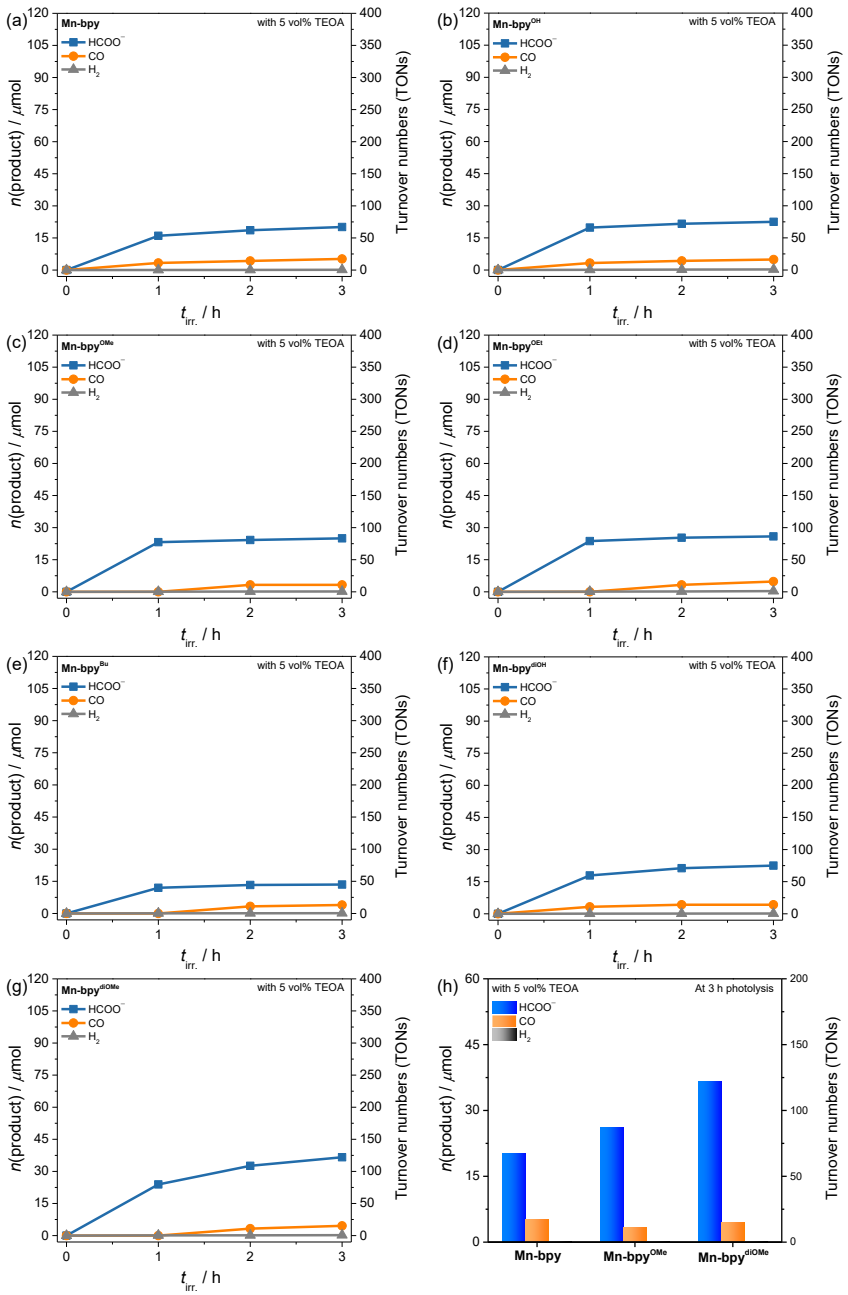

Fig. S30 Plots of formate/CO/H_2 formation versus irradiation time for 0.3 mM IrPS + 0.1 mM Mn(I) catalyst ((a) **Mn-bpy**, (b) **Mn-bpy^{OH}**, (c) **Mn-bpy^{OMe}**, (d) **Mn-bpy^{OEt}**, (e) **Mn-bpy^{Bu}**, (f) **Mn-bpy^{diOH}**, and (g) **Mn-bpy^{diOMe}**) and (h) product distribution of **Mn-bpy**, **Mn-bpy^{OMe}**, and **Mn-bpy^{diOMe}** in CO_2-saturated DMA/TEOA (5 vol% TEOA) solution containing 0.1 M BIH; irradiation at λ >500 nm at 298 K.

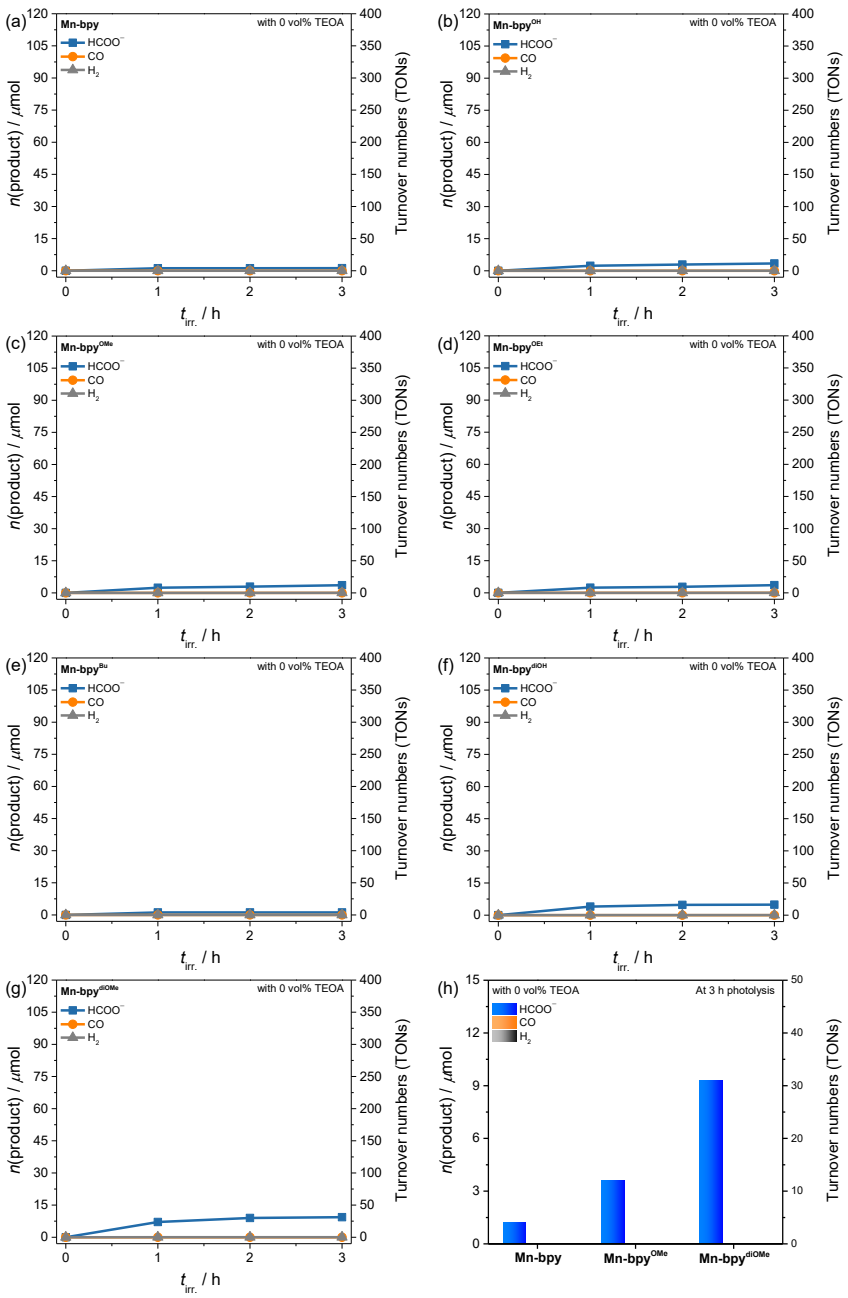

Fig. S31 Plots of formate/CO/H_2 formation versus irradiation time for 0.3 mM IrPS + 0.1 mM Mn(I) catalyst ((a) **Mn-bpy**, (b) **Mn-bpy^{OH}**, (c) **Mn-bpy^{OMe}**, (d) **Mn-bpy^{OEt}**, (e) **Mn-bpy^{Bu}**, (f) **Mn-bpy^{diOH}**, and (g) **Mn-bpy^{diOMe}**) and (h) product distribution of Mn(I) catalyst (**Mn-bpy**, **Mn-bpy^{OMe}**, and **Mn-bpy^{diOMe}**) in CO_2-saturated DMA solution containing 0.1 M BIH; irradiation at λ >500 nm at 298 K.

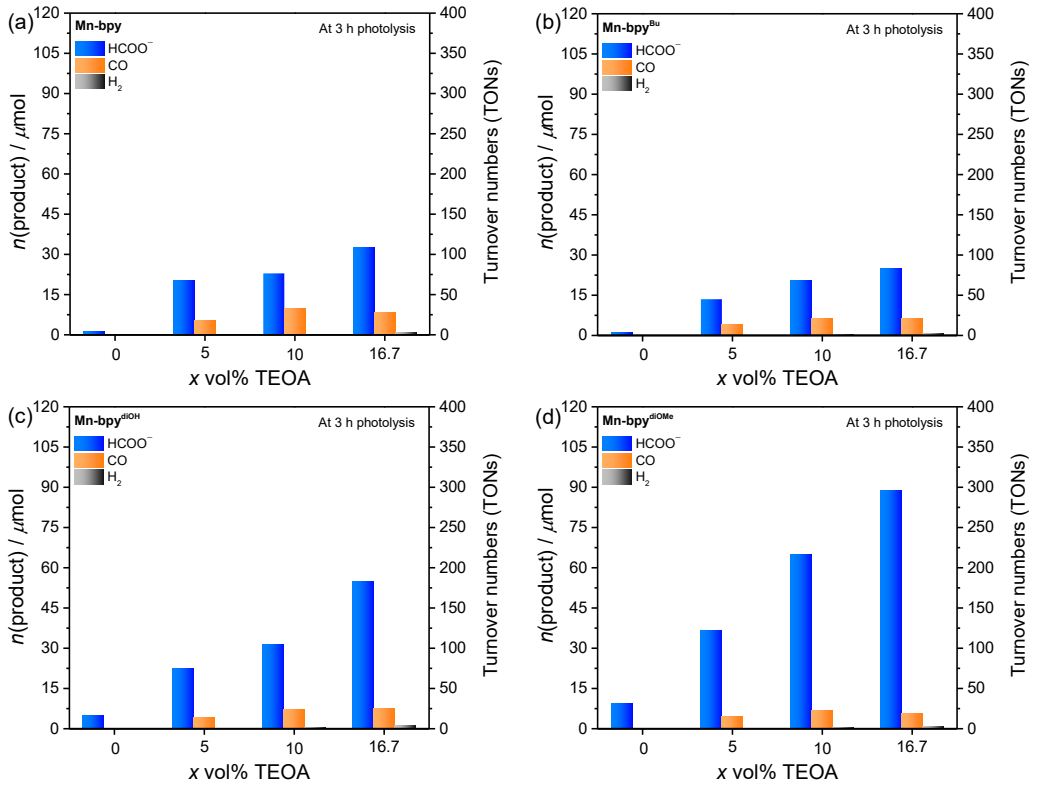

Fig. S32 Plots of formate/CO/H_2 formation versus irradiation time for 0.3 mM IrPS + 0.1 mM Mn(I) catalyst ((a) **Mn-bpy**, (b) **Mn-bpy^{Bu}**, (c) **Mn-bpy^{diOH}**, and (d) **Mn-bpy^{diOMe}**) in CO_2-saturated DMA or DMA/TEOA (5 to 16.7 vol% TEOA), with 0.1 M BIH, under irradiation at λ >500 nm at 298 K. Dependencies of TON and net formation amounts on the variation of TEOA content (0−16.7 vol%) in the DMA reaction solvent.

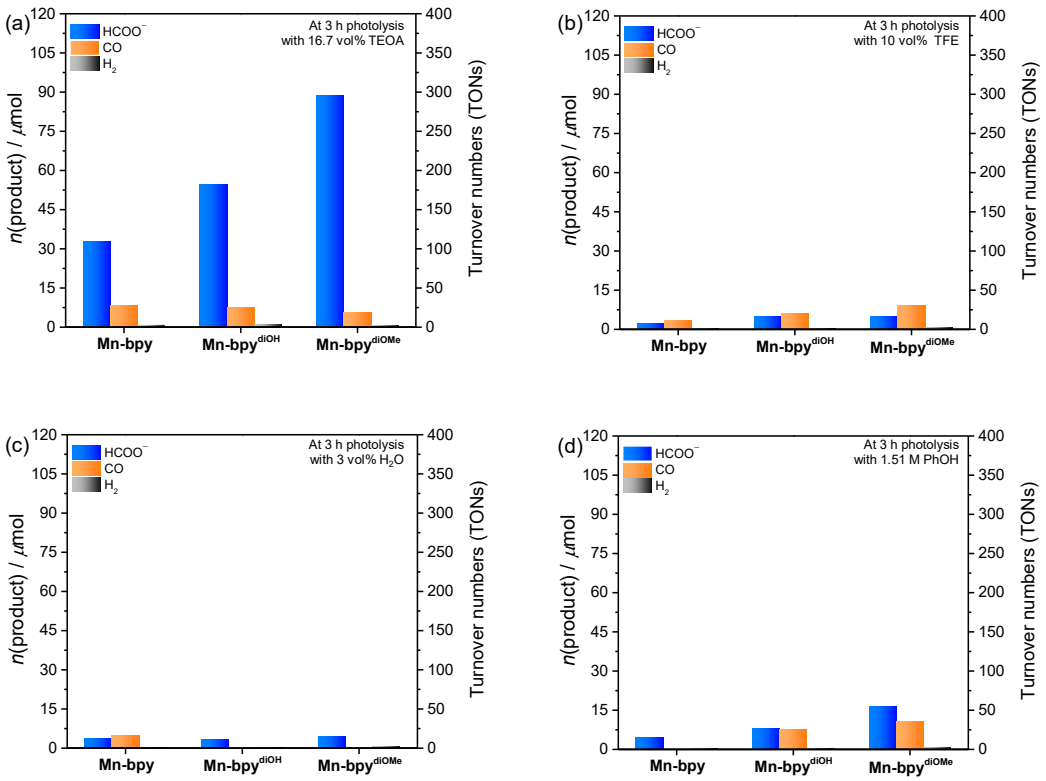

Fig. S33 Photolysis results of mixed homogeneous system (0.3 mM IrPS + 0.1 mM Mn(I) catalyst) in CO_2-saturated DMA/additive solution (additive = (a) 16.7 vol% TEOA, (b) 10 vol% TFE, (c) 3 vol% H_2O, and (d) 1.51 M PhOH) containing 0.1 M BIH; irradiation at λ >500 nm at 298 K.

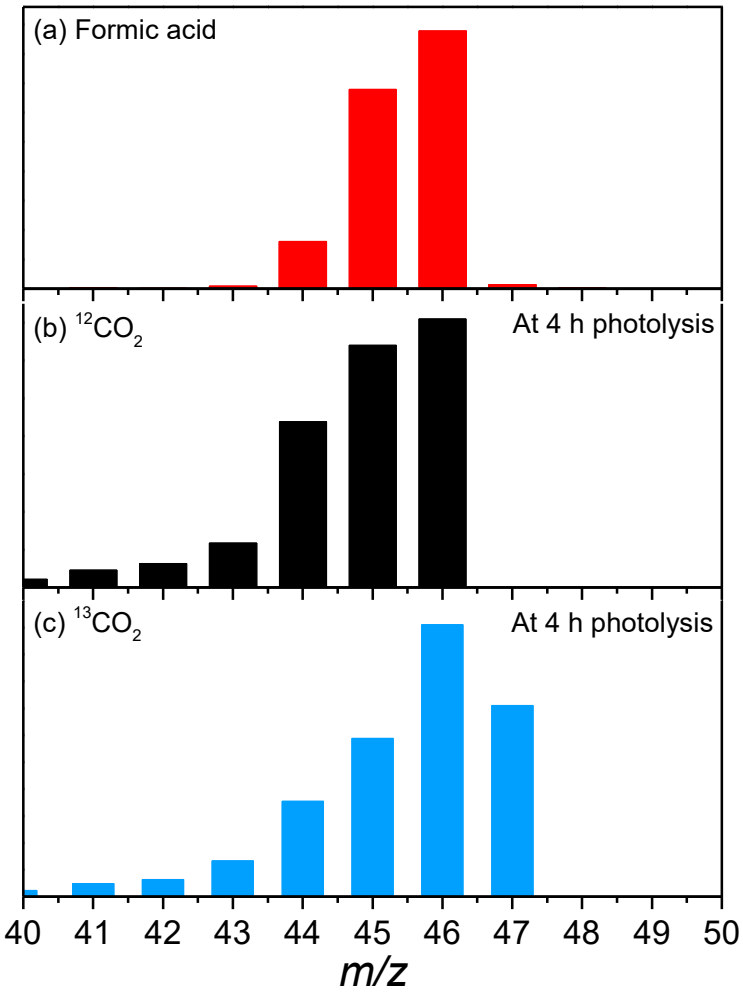

Fig. S34 GC–MS spectra of (a) pure formic acid reagent and the liquid phase of the photocatalytic reaction after 4 h irradiation of (b) $^{12}CO_2$- and (c) $^{13}CO_2$-saturated DMA/TEOA (16.7 vol% TEOA) solution containing 0.3 mM IrPS, 0.1 mM **Mn-bpy**$^{\mathbf{diOMe}}$, and 0.1 M BIH at 298 K under λ >500 nm.

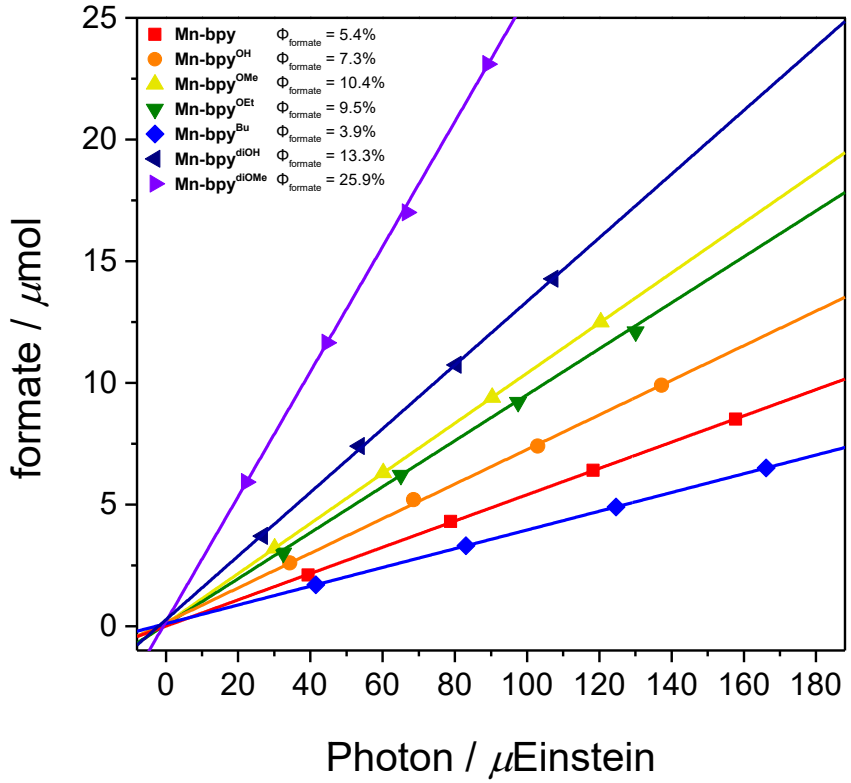

Fig. S35 Photocatalytic production of formate using 0.3 mM IrPS and 0.1 mM Mn(I) catalysts ((a) **Mn-bpy**, (b) **Mn-bpy^{OH}**, (c) **Mn-bpy^{OMe}**, (d) **Mn-bpy^{OEt}**, (e) **Mn-bpy^{Bu}**, (f) **Mn-bpy^{diOH}**, and (g) **Mn-bpy^{diOMe}**) in a CO_2-saturated DMA/TEOA (16.7 vol% TEOA) solution containing 0.1 M BIH. The samples were irradiated with light at 495–505 nm using a 300 W Xe lamp.

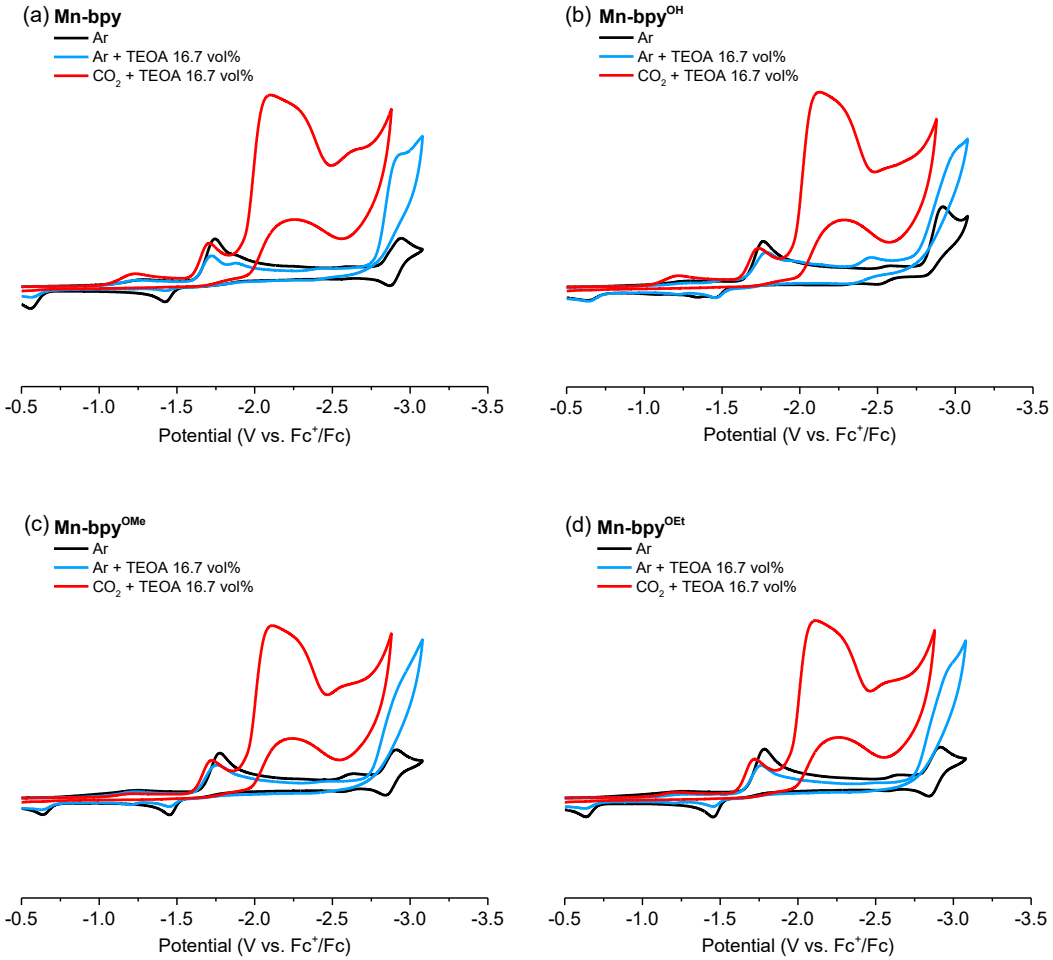

Fig. S36 Cyclic voltammograms of Mn(I) catalyst ((a) **Mn-bpy**, (b) **Mn-bpy^{OH}**, (c) **Mn-bpy^{OMe}** and (d) **Mn-bpy^{OEt}**) (1 mM) in Ar or CO_2-saturated DMF or DMF/TEOA (16.7 vol% TEOA) containing 0.1 M TBAP.

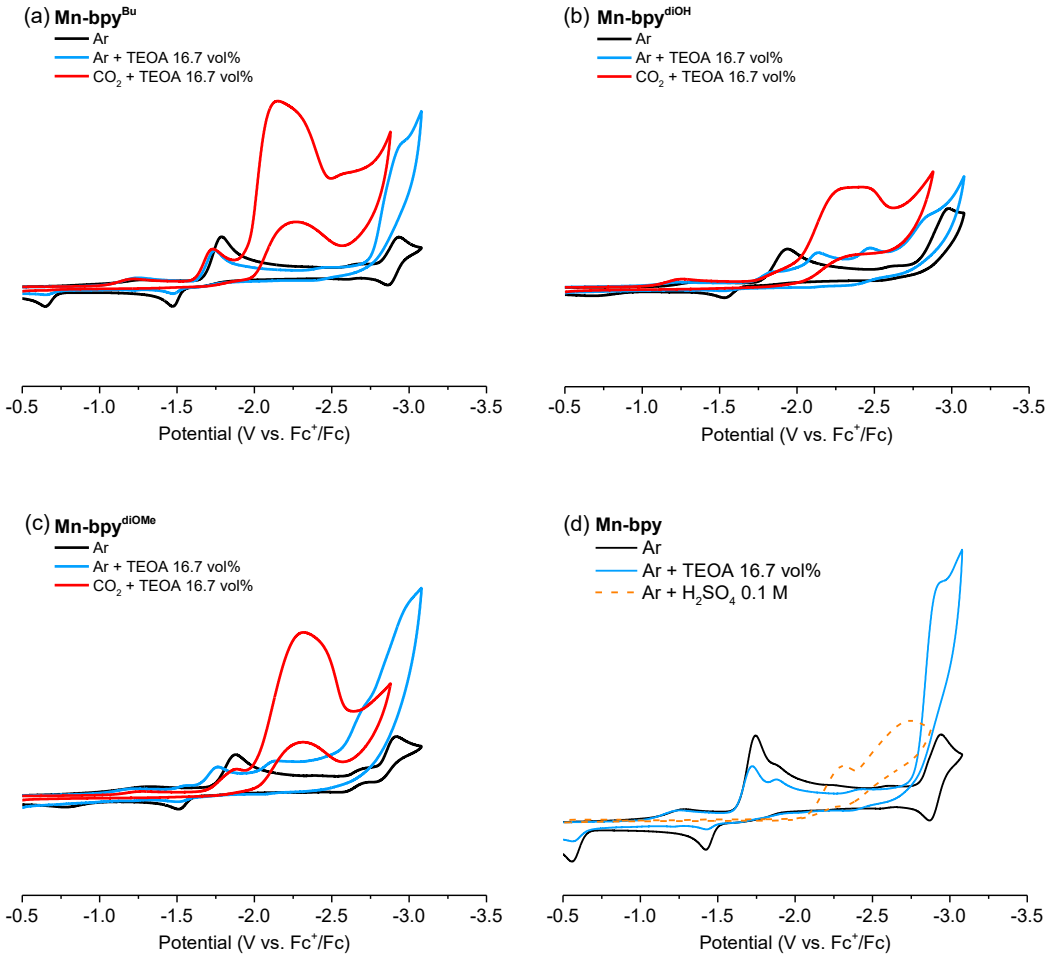

Fig. S37 Cyclic voltammograms of Mn(I) catalyst ((a) **Mn-bpy^{Bu}**, (b) **Mn-bpy^{diOH}**, (c) **Mn-bpy^{diOMe}**) (1 mM) in Ar or CO_2-saturated DMF or DMF/TEOA (16.7 vol% TEOA) and (d) **Mn-bpy** (1 mM) in Ar-saturated DMF or DMF with additives (16.7 vol% TEOA or 0.1 M H_2SO_4) containing 0.1 M TBAP.

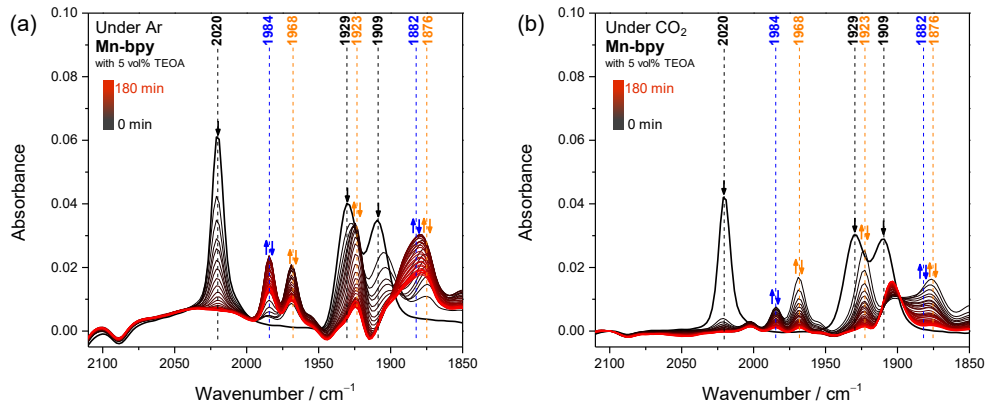

Fig. S38 FTIR spectral changes following irradiation time for 1 mM IrPS + 1 mM **Mn-bpy** in 0.03 mL of DMA/TEOA solution (5 vol% TEOA) containing 0.1 M BIH under (a) Ar and (b) CO_2 atmospheres.

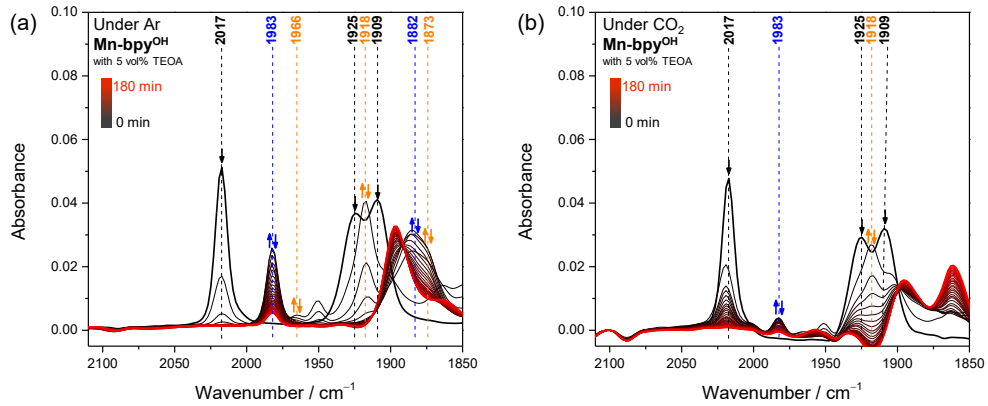

Fig. S39 FTIR spectral changes following irradiation time for 1 mM IrPS + 1 mM **Mn-bpy^{OH}** in 0.03 mL of DMA/TEOA solution (5 vol% TEOA) containing 0.1 M BIH under (a) Ar and (b) CO_2 atmospheres.

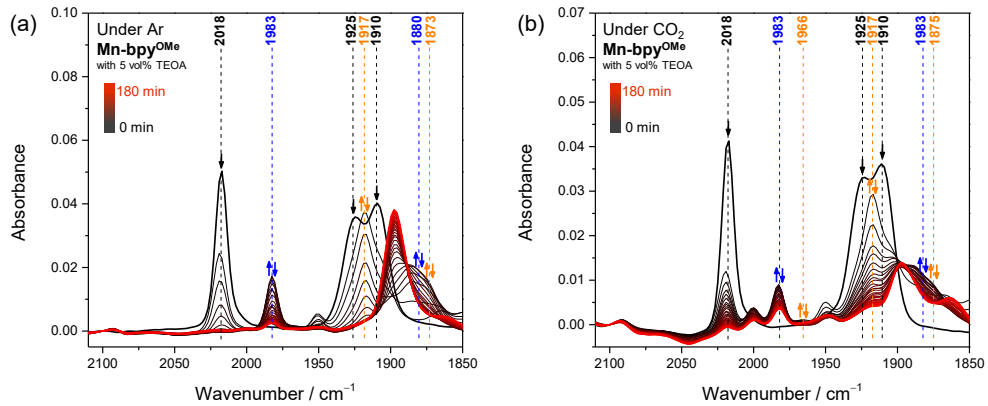

Fig. S40 FTIR spectral changes following irradiation time for 1 mM IrPS + 1 mM **Mn-bpy^{OMe}** in 0.03 mL of DMA/TEOA solution (5 vol% TEOA) containing 0.1 M BIH under (a) Ar and (b) CO_2 atmospheres.

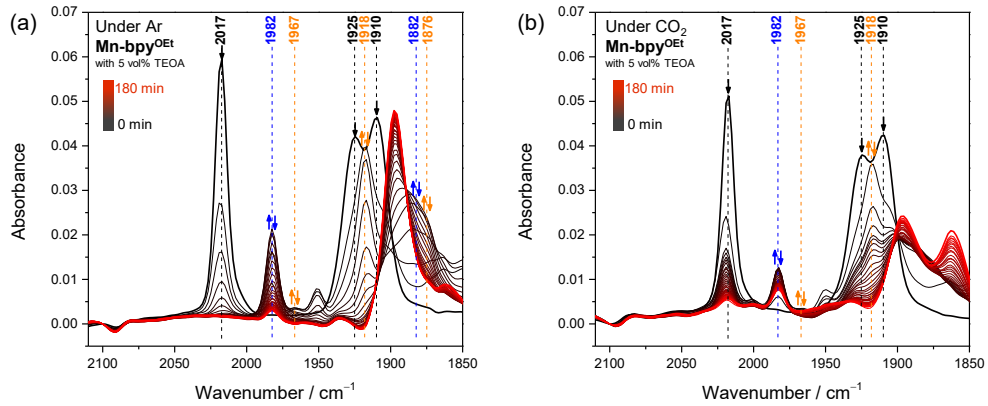

Fig. S41 FTIR spectral changes following irradiation time for 1 mM IrPS + 1 mM **Mn-bpy^{OEt}** in 0.03 mL of DMA/TEOA solution (5 vol% TEOA) containing 0.1 M BIH under (a) Ar and (b) CO_2 atmospheres.

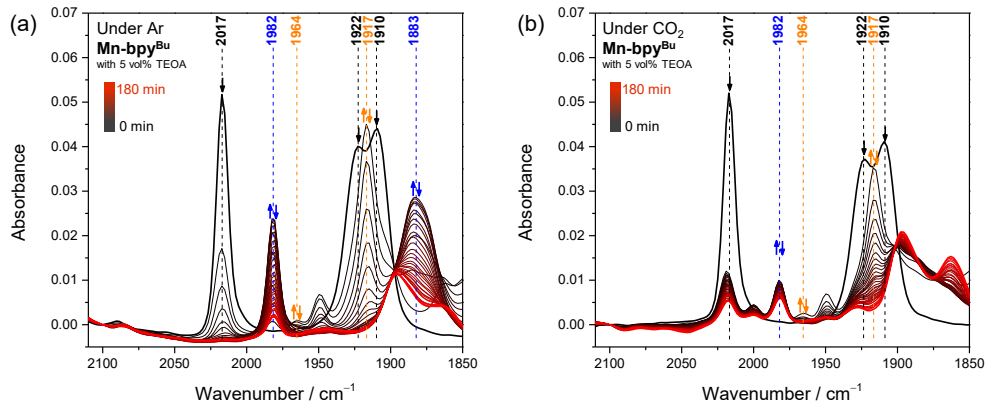

Fig. S42 FTIR spectral changes following irradiation time for 1 mM IrPS + 1 mM **Mn-bpy^{Bu}** in 0.03 mL of DMA/TEOA solution (5 vol% TEOA) containing 0.1 M BIH under (a) Ar and (b) CO_2 atmospheres.

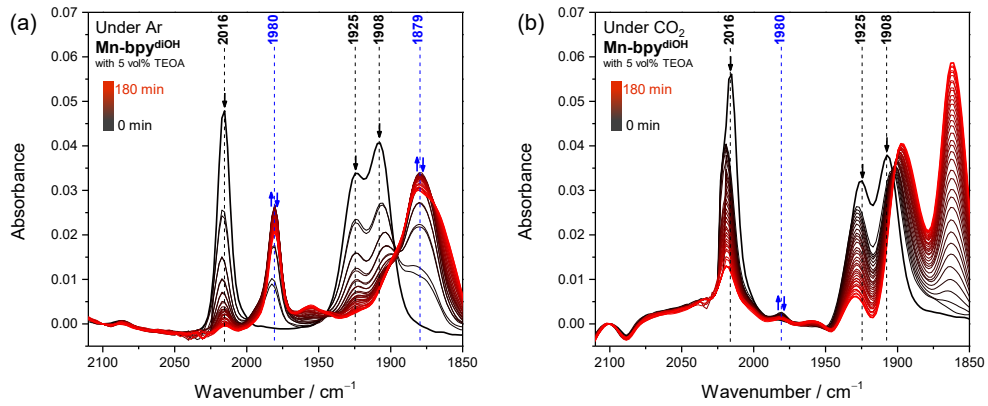

Fig. S43 FTIR spectral changes following irradiation time for 1 mM IrPS + 1 mM **Mn-bpy^{diOH}** in 0.03 mL of DMA/TEOA solution (5 vol% TEOA) containing 0.1 M BIH under (a) Ar and (b) CO_2 atmospheres.

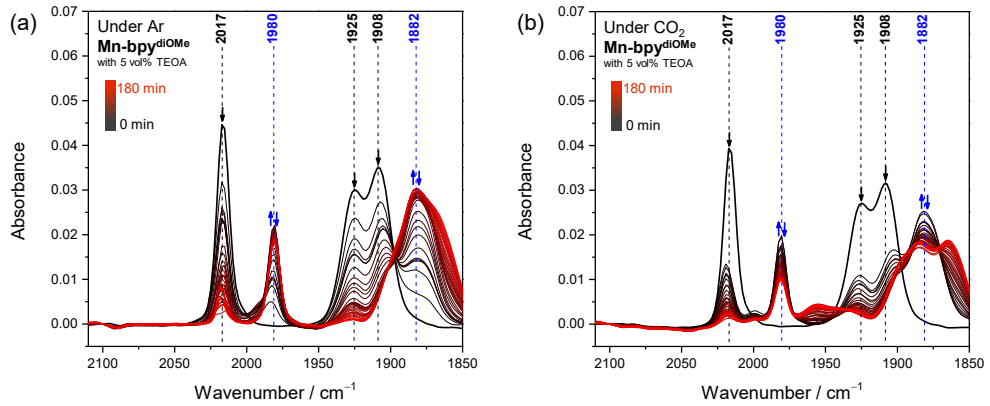

Fig. S44 FTIR spectral changes following irradiation time for 1 mM IrPS + 1 mM **Mn-bpy^{diOMe}** in 0.03 mL of DMA/TEOA solution (5 vol% TEOA) containing 0.1 M BIH under (a) Ar and (b) CO_2 atmospheres.

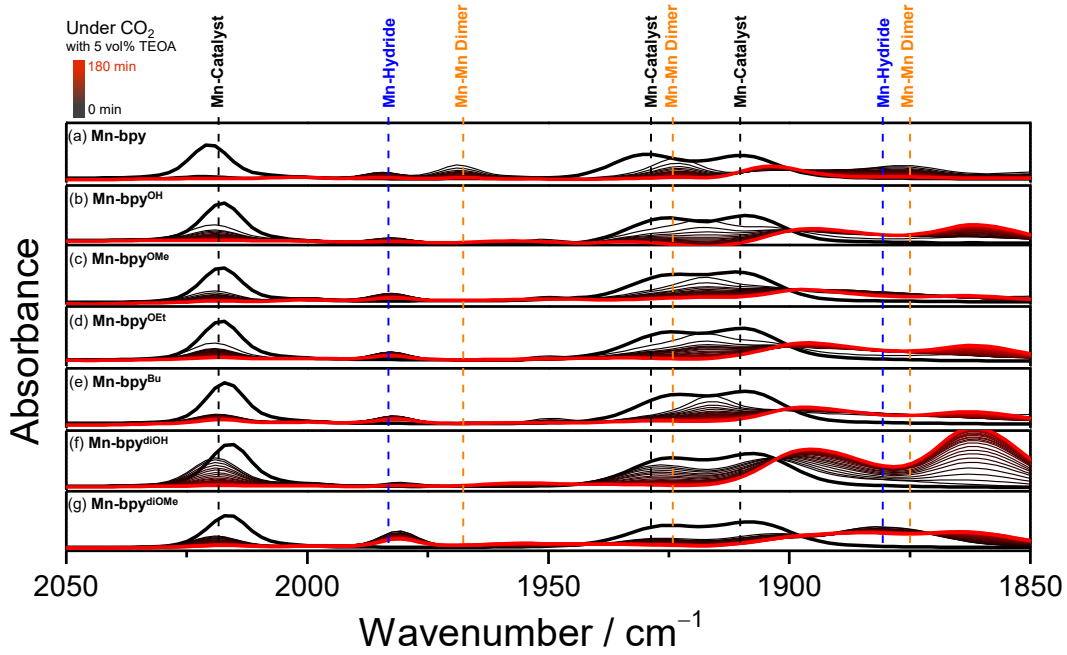

Fig. S45 Time-resolved FTIR spectra collected over 3 h of photolysis for a solution containing 1 mM IrPS and 1 mM Mn(I) catalyst in 0.03 mL of CO_2-saturated DMA/TEOA (5 vol%) with 0.1 M BIH. Spectral changes reflect the dynamic evolution of catalytic intermediates under CO_2 atmosphere.

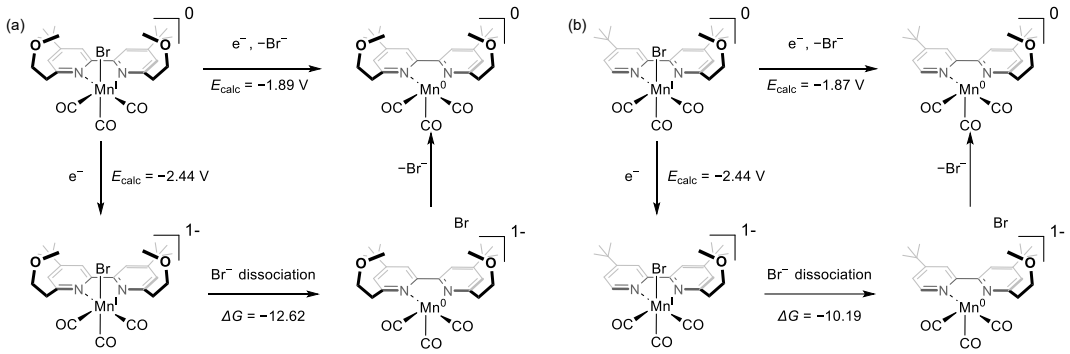

Fig. S46 Computational study on the first reduction of (a) **Mn-bpy^{diOMe}** and (b) **Mn-bpy^{OMe}**.

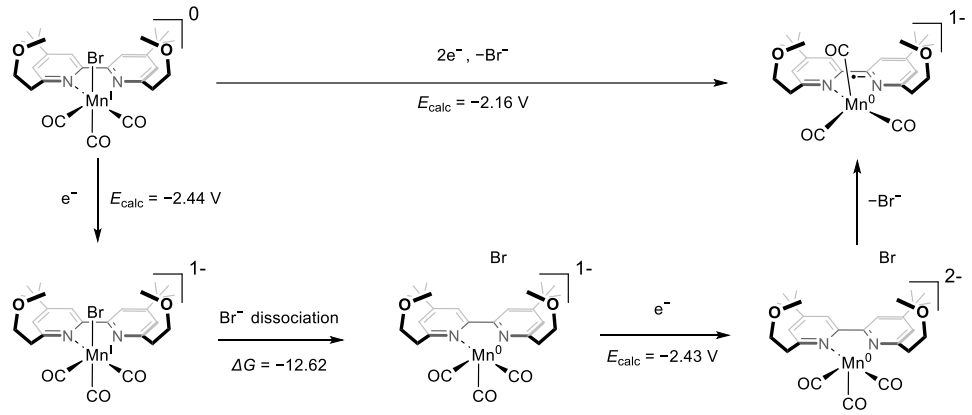

Fig. S47 Computational study on the two-electron reduction of **Mn-bpy^{diOMe}**.

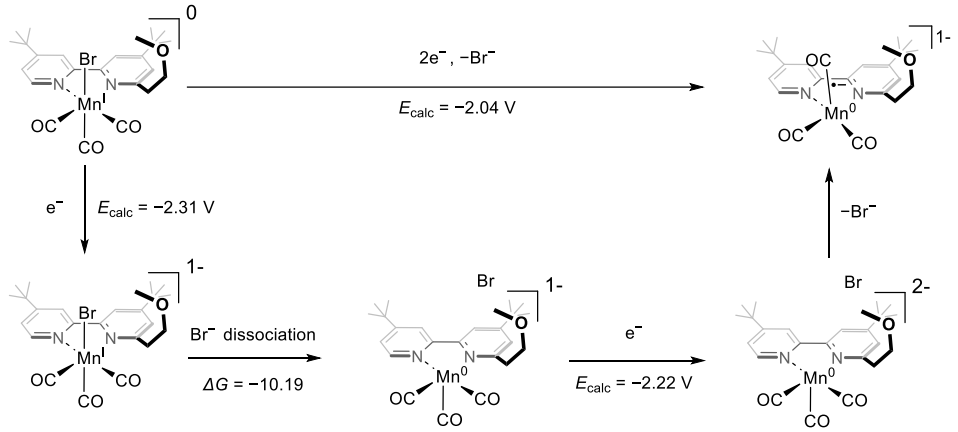

Fig. S48 Computational study on the two-electron reduction of **Mn-bpy^{OMe}**.

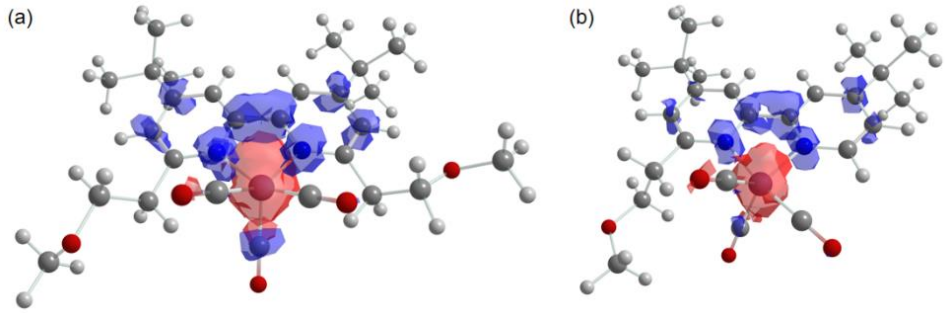

Fig. S49 Löwdin Spin density of $MnL^{\bullet-}$_0_-1_1 (isovalue: 0.003 a.u.) in (a) **Mn-bpy^{diOMe}** and (b) **Mn-bpy^{OMe}**. Red and blue colors indicate α and β spin electron density, respectively.

Table S9. UHF spin contamination of Mn_-1_1 in UKS or BS.

Mn-bpy^{diOMe}	Expectation value of <S**2>	Ideal value of S*(S+1)	Deviation	ΔG
Mn_-1_1_BS ($MnL^{\bullet-}$_0_-1_1)	2.0336	2.0	0.0336	0
Mn_-1_1_UKS	0	0	0	0.84
Mn_-1_3_UKS	2.0421	2.0	0.0421	4.49

Table S10 Mulliken spin density distributions for selected **Mn-bpy^{diOMe}** complex states.[a]

Mn-bpy^{diOMe}	Mn	C	N	Sum of atomic spin populations
Mn_0_0_2	1.034	0.133	−0.163	1.000
$MnL^{\bullet-}$_0_-1_1	1.049	0.808	0.145	2.000
Mn_I_O_2CH_-1_2	−0.025	0.752	0.256	1.000
Mn_I_CO_2H_-1_2	−0.023	0.733	0.313	1.000
Mn_0_CO_0_2	0.500	0.339	0.046	1.000
TS-2b	−0.062	0.791	0.331	1.000

[a]Mn_I_H_0_1, Mn_I_HCO_2_0_1, Mn_I_O_2CH_0_1, Mn_I_CO_2_-1_1, Mn_I_CO_2H_0_1, TS-1a, TS-2a, TS-3a, and TS-1b are omitted due to zero atomic spin populations.

Table S11 Mulliken spin density distributions for selected **Mn-bpy^{OMe}** complex states.[a]

Mn-bpy^{OMe}	Mn	C	N	Sum of atomic spin populations
Mn_0_0_2	0.875	0.278	−0.150	1.000
MnL$^{\bullet-}$_0_-1_1	0.945	0.933	0.123	2.000
Mn_I_O_2CH_-1_2	0.023	0.715	0.183	1.000
Mn_I_CO_2H_-1_2	−0.091	0.778	0.378	1.000
Mn_0_CO_0_2	0.003	0.701	0.280	1.000
TS-2b’	−0.232	0.527	0.921	1.000

[a]Mn_I_H_0_1, Mn_I_HCO_2_0_1, Mn_I_O_2CH_0_1, Mn_I_CO_2_-1_1, Mn_I_CO_2H_0_1, TS-1a’, TS-2a’, TS-3a’, and TS-1b’ are omitted due to zero atomic spin populations.

Table S12 Relative energies for formate pathway in kcal/mol from **Mn-bpy^{diOMe}**.[a]

Mn-bpy^{diOMe}	ΔDef2-SVP	$\Delta\Delta$Def2-TZVPPD	ΔE_{total}[b]	ΔZ_0	$\Delta\Delta E_{thermal}$[c]	$-T\Delta S$	ΔDisp	ΔG^o	ΔG[d]
Mn_0_0_2	0.00	0.00	0.00	0.00	0.00	0.00	0.00		0.00
MnL$^{\bullet-}$_0_-1_1	-56.41	-2.95	-59.36	-1.67	-0.04	0.44	-0.18		-60.82
IRC_TS-1a	-72.21	12.44	-59.77	1.52	0.04	17.82	-20.45	-1.89	-62.73
TS-1a	-59.25	9.80	-49.44	-2.58	-0.25	18.53	-25.48	-1.89	-61.12
Mn_I_H_0_1	-84.70	-1.35	-86.05	-4.49	-0.20	1.00	3.14		-86.60
TS-2a	-79.42	0.36	-79.06	-4.78	0.51	11.11	-2.62	-1.89	-76.72
Mn_I_HCO_2_0_1	-82.62	-1.19	-83.81	-2.76	0.52	11.39	-7.08	-1.89	-83.63
TS-3a	-76.19	-3.33	-79.52	-2.51	0.43	11.16	-8.40	-1.89	-80.73
Mn_I_O_2CH _0_1	-101.91	-0.11	-102.03	-1.40	0.53	11.14	-2.30	-1.89	-95.95
Mn_0_O_2CH_-1_2	-155.73	-2.56	-158.29	-3.70	0.71	10.45	-2.10	-1.89	-154.82
Mn_0_0_2	-148.28	-16.81	-165.09	-4.50	0.16	-2.03	1.13		-170.33

[a]Naming scheme that encodes the oxidation state (x), global charge (y), and spin multiplicity (z) in the format Mn_x_y_z. [b]Electronic energy = sum of the previous two columns. [c] T = 298.15 K [d]Gibb’s free energy = sum of the previous six columns.

Table S13 Relative energies for CO pathway in kcal/mol from **Mn-bpy^{diOMe}**.[a]

Mn-bpy^{diOMe}	ΔDef2-SVP	ΔΔDef2-TZVPPD	ΔE_{total}[b]	ΔZ_0	$\Delta\Delta E_{thermal}$[c]	$-T\Delta S$	ΔDisp	ΔG^{o}	ΔG[d]
Mn_0_0_2	0.00	0.00	0.00	0.00	0.00	0.00	0.00		0.00
MnL$^{\bullet-}$_0_-1_1	-56.41	-2.95	-59.36	-1.67	-0.04	0.44	-0.18		-60.82
TS-1b	-56.33	-0.49	-56.83	-0.87	0.31	11.81	-8.76	-1.89	-56.23
Mn_I_CO_2_-1_1	-60.92	-5.16	-66.08	0.59	0.18	12.22	-6.34	-1.89	-61.32
Mn_I_CO_2H_0_1	-85.84	0.79	-85.05	-1.06	0.26	11.78	-4.77	-1.89	-80.74
Mn_0_CO_2H_-1_2	-138.54	-1.30	-139.85	-3.36	0.39	11.43	-4.39	-1.89	-137.67
TS-2b	-136.37	7.36	-129.01	-7.01	17.93	25.78	-14.32	-3.78	-126.75
Mn_0_CO_0_2	-142.20	-11.48	-153.69	-9.47	1.65	-0.92	0.59		-161.84
Mn_0_0_2	-140.81	-15.44	-156.25	-10.81	1.52	-12.07	3.39	1.89	-172.34

[a]Naming scheme that encodes the oxidation state (x), global charge (y), and spin multiplicity (z) in the format Mn_x_y_z. [b]Electronic energy = sum of the previous two columns. [c] T = 298.15 K [d]Gibb's free energy = sum of the previous six columns.

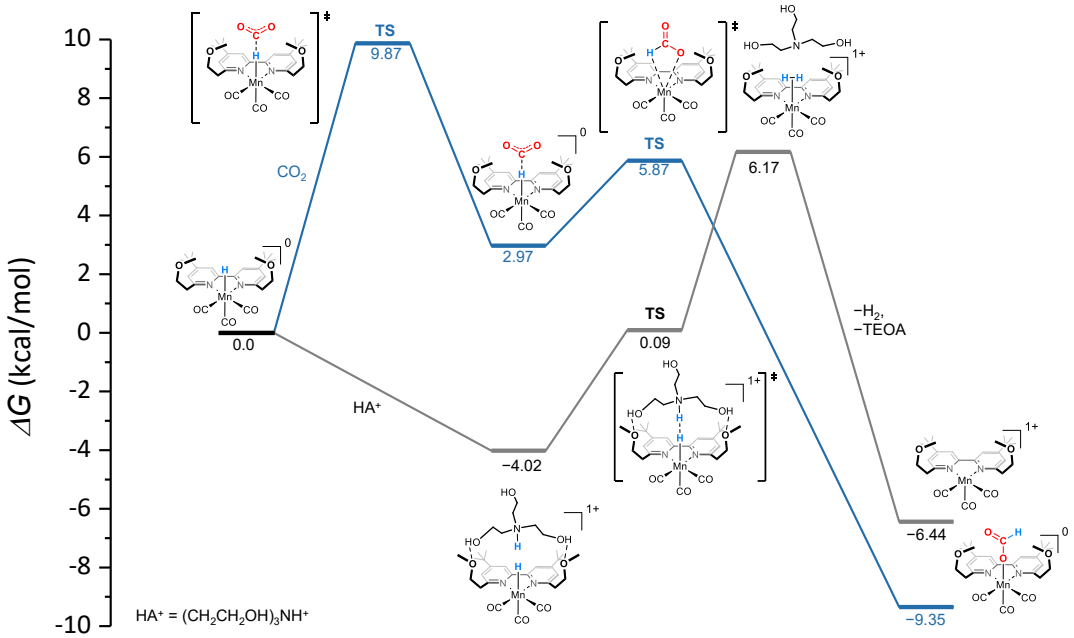

Fig. S50 Comparative energy diagrams for the CO_2 reduction pathway to formate (blue) and the H_2 evolution pathway (grey) mediated by **Mn-bpy^{diOMe}**.

Table S14 Relative energies for formate pathway in kcal/mol from **Mn-bpy^{OMe}**.[a]

Mn-bpy^{OMe}	ΔDef2-SVP	$\Delta\Delta$Def2-TZVPPD	ΔE_{total}[b]	ΔZ_0	$\Delta\Delta E_{thermal}$[c]	$-T\Delta S$	ΔDisp	ΔG^o	ΔG[d]
Mn_0_0_2	0.00	0.00	0.00	0.00	0.00	0.00	0.00		0.00
MnL$^{\bullet-}$_0_-1_1	-60.83	-2.89	-63.72	-1.34	-0.11	0.83	-0.32		-64.67
IRC_TS-1a'	-71.91	6.38	-65.53	0.67	0.37	16.87	-15.24	-1.89	-64.76
TS-1a'	-62.33	8.23	-54.10	-3.67	0.15	17.47	-20.11	-1.89	-62.15
Mn_I_H_0_1	-85.57	-1.18	-86.75	-4.79	-0.06	0.75	3.32		-87.52
TS-2a'	-80.34	0.61	-79.72	-4.87	0.57	11.06	-2.30	-1.89	-77.16
Mn_I_HCO_2_0_1	-83.50	-1.43	-84.93	-3.02	0.62	11.31	-4.19	-1.89	-82.10
TS-3a'	-76.88	-2.81	-79.69	-2.87	0.57	10.95	-7.75	-1.89	-80.68
Mn_I_O_2CH _0_1	-102.75	0.02	-102.73	-1.60	0.64	11.07	-1.74	-1.89	-96.25
Mn_0_O_2CH_-1_2	-158.31	-2.00	-160.31	-3.76	0.76	10.62	-1.68	-1.89	-156.27
Mn_0_0_2	-148.28	-16.81	-165.09	-4.50	0.16	-2.03	1.13		-170.33

[a]Naming scheme that encodes the oxidation state (x), global charge (y), and spin multiplicity (z) in the format Mn_x_y_z. [b]Electronic energy = sum of the previous two columns. [c] T = 298.15 K [d] Gibb's free energy = sum of the previous six columns.

Table S15 Relative energies for CO pathway in kcal/mol from **Mn-bpy^{OMe}**.[a]

Mn-bpy^{OMe}	ΔDef2-SVP	$\Delta\Delta$Def2-TZVPPD	ΔE_{total}[b]	ΔZ_0	$\Delta\Delta E_{thermal}$[c]	$-T\Delta S$	ΔDisp	ΔG^o	ΔG[d]
Mn_0_0_2	0.00	0.00	0.00	0.00	0.00	0.00	0.00		0.00
MnL$^{\bullet-}$_0_-1_1	-60.83	-2.89	-63.72	-1.34	-0.11	0.83	-0.32		-64.67
TS-1b'	-60.17	0.30	-59.87	-0.75	0.26	11.99	-8.43	-1.89	-58.69
Mn_I_CO_2_-1_1	-62.32	-4.64	-66.95	0.39	0.26	12.09	-5.39	-1.89	-61.49
Mn_I_CO_2H_0_1	-86.62	0.45	-86.17	-1.26	0.35	11.93	-3.72	-1.89	-80.76
Mn_0_CO_2H_-1_2	-140.15	-1.69	-141.84	-3.56	0.50	11.36	-3.58	-1.89	-139.01
TS-2b'	-137.97	8.47	-129.50	-7.22	14.64	25.88	-14.65	-3.78	-127.50
Mn_0_CO_0_2	-145.85	-9.21	-155.06	-9.63	1.56	-1.02	0.84		-163.32
Mn_0_0_2	-140.81	-15.44	-156.25	-10.81	1.52	-12.07	3.39	1.89	-172.34

[a]Naming scheme that encodes the oxidation state (x), global charge (y), and spin multiplicity (z) in the format Mn_x_y_z. [b]Electronic energy = sum of the previous two columns. [c] T = 298.15 K [d] Gibb's free energy = sum of the previous six columns.

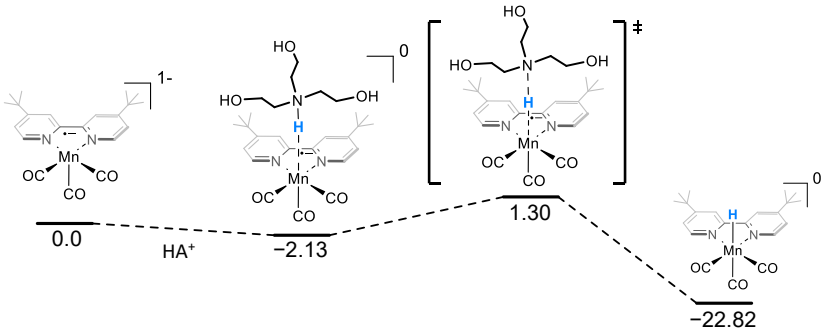

Fig. S51 Calculated reaction pathway for protonation of **Mn-bpy**.

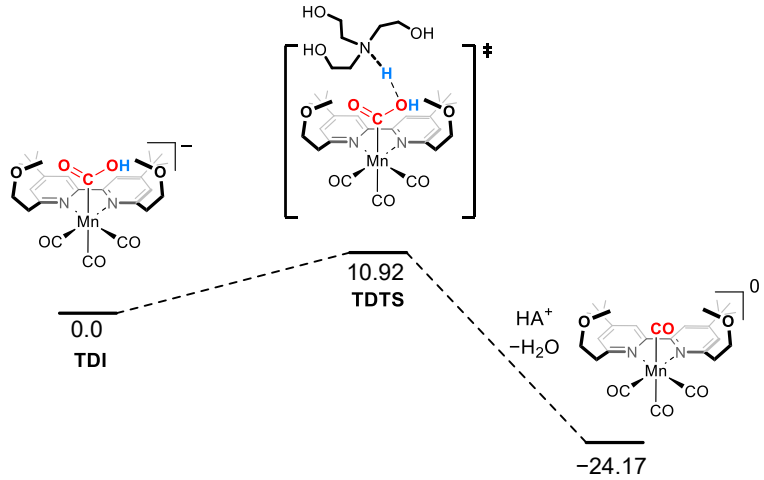

Fig. S52 TDI and TDTS for CO pathway of **Mn-bpy**$^{\mathbf{diOMe}}$.

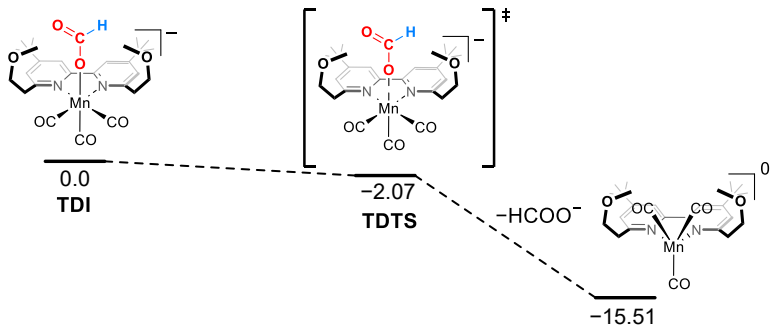

Fig. S53 TDI and TDTS for formate pathway of **Mn-bpy**$^{\mathbf{diOMe}}$.

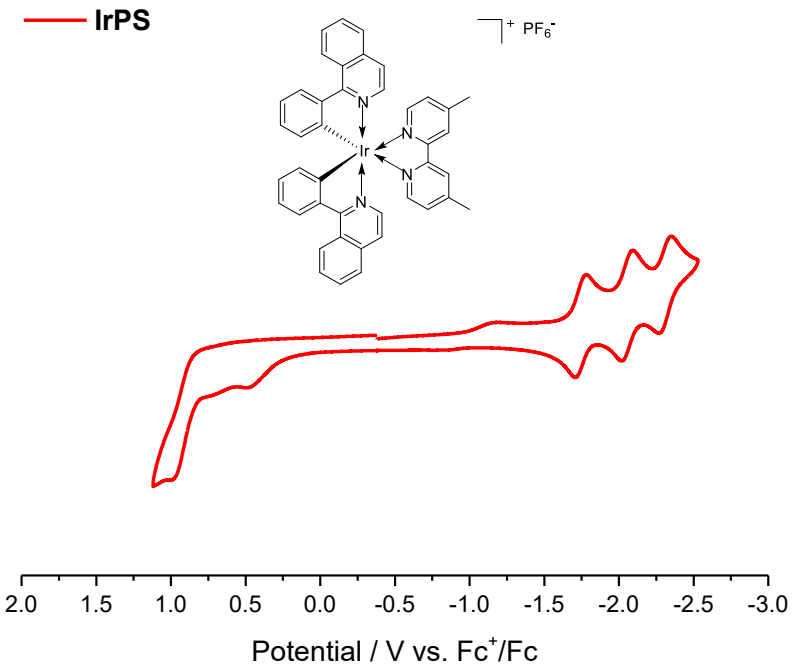

Fig. S54 Cyclic voltammograms of IrPS in Ar-saturated DMF containing 0.1 M TBAP.

Reference

S1. S. J. Liu, Q. Zhao, Q. L. Fan and W. Huang, A Series of Red-Light-Emitting Ionic Iridium Complexes: Structures, Excited State Properties, and Application in Electroluminescent Devices, *Eur. J. Inorg. Chem.*, 2008, **2008**, 2177–2185. DOI: 10.1002/ejic.200701184

S2. M. Gaydou, T. Moragas, F. Juliá-Hernández and R. Martin, Site-Selective Catalytic Carboxylation of Unsaturated Hydrocarbons with CO_2 and Water, *J. Am. Chem. Soc.*, 2017, **139**, 12161-12164. DOI: 10.1021/jacs.7b07637

S3. R. Ziessel, D. Matt and L. Toupet, Construction of a Phosphane-Based Metallo-Synthon Suitable for the Selective Formation of a Tetranuclear Ru_2–Cu_2 Macrocycle, *J. Chem. Soc., Chem. Commun.*, 1995, 2033–2035. DOI: 10.1039/C39950002033

S4. R. Ziessel, L. Toupet, S. Chardon-Noblat, A. Deronzier and D. Matt, Co-ordinative Properties of a Hybrid Phosphine–Bipyridine Ligand, *J. Chem. Soc., Dalton Trans.*, 1997, 3777–3784. DOI: 10.1039/A702463K

S5. R. A. Johnstone and M. E. Rose, A Rapid, Simple, and Mild Procedure for Alkylation of Phenols, Alcohols, Amides and Acids, *Tetrahedron*, 1979, **35**, 2169–2173. DOI: 10.1016/0040-4020(79)87035-0

S6. V. Hebbe-Viton, V. Desvergnes, J. J. Jodry, C. Dietrich-Buchecker, J.-P. Sauvage and J. Lacour, Chiral Spiro Cu(I) Complexes. Supramolecular Stereocontrol and Isomerisation Dynamics by the Use of TRISPHAT Anions, *Dalton Trans.*, 2006, 2058–2065. DOI: 10.1039/B515540A

S7. S.-Z. Sun, C. Romano and R. Martin, Site-Selective Catalytic Deaminative Alkylation of Unactivated Olefins, *J. Am. Chem. Soc.*, 2019, **141**, 16197-16201. DOI: 10.1021/jacs.9b07489

S8. X.-Q. Zhu, M.-T. Zhang, A. Yu, C.-H. Wang and J.-P. Cheng, Hydride, Hydrogen Atom, Proton, and Electron Transfer Driving Forces of Various Five-Membered Heterocyclic Organic Hydrides and Their Reaction Intermediates in Acetonitrile, *J. Am. Chem. Soc.*, 2008, **130**, 2501–2516. DOI: 10.1021/ja075523m

S9. M. Bourrez, F. Molton, S. Chardon-Noblat and A. Deronzier, [Mn(bpy)$(CO)_3$Br]: An Abundant Metal Carbonyl Complex as Efficient Electrocatalyst for CO_2 Reduction, *Angew. Chem. Int. Ed.*, 2011, **50**, 9903–9906. DOI: 10.1002/anie.201103006

S10. SMART and SAINT, Bruker Analytical X-Ray Division, Madison, WI, 2002.

S11. SHELXTL-PLUS Software Package, Bruker Analytical X-Ray Division, Madison, WI, 2002.

S12. S.-J. Woo, S. Choi, S.-Y. Kim, P. S. Kim, J. H. Jo, C. H. Kim, H.-J. Son, C. Pac and S. O. Kang, Highly Selective and Durable Photochemical CO_2 Reduction by Molecular Mn(I) Catalyst Fixed on a Particular Dye-Sensitized TiO_2 Platform, *ACS Catal.*, 2019, **9**, 2580–2593. DOI: 10.1021/acscatal.8b03816

S13. F. Neese, The ORCA Program System, *Wiley Interdiscip. Rev.: Comput. Mol. Sci.*, 2012, **2**, 73–78. DOI: 10.1002/wcms.81

S14. V. Barone and M. Cossi, Quantum Calculation of Molecular Energies and Energy Gradients in Solution by a Conductor Solvent Model, *J. Phys. Chem. A*, 1998, **102**, 1995–2001. DOI: 10.1021/jp9716997

S15. A. Bondi, van der Waals Volumes and Radii, *J. Phys. Chem.*, 1964, **68**, 441–451. DOI: 10.1021/j100785a001
S16. M. Cossi, N. Rega, G. Scalmani and V. Barone, Energies, Structures, and Electronic Properties of Molecules in Solution with the C-PCM Solvation Model, *J. Comput. Chem.*, 2003, **24**, 669–681. DOI: 10.1002/jcc.10189
S17. F. Weigend and R. Ahlrichs, Balanced Basis Sets of Split Valence, Triple Zeta Valence and Quadruple Zeta Valence Quality for H to Rn: Design and Assessment of Accuracy, *Phys. Chem. Chem. Phys.*, 2005, **7**, 3297–3305. DOI: 10.1039/B508541A
S18. S. C. L. Kamerlin and A. Warshel, The EVB as a Quantitative Tool for Formulating Simulations and Analyzing Biological and Chemical Reactions, *Faraday Discuss.*, 2010, **145**, 71–106. DOI: 10.1039/B907354J
S19. T. Fogeron, J.-P. Porcher, M. Gomez-Mingot, T. K. Todorova, L.-M. Chamoreau, C. Mellot-Draznieks, Y. Li and M. Fontecave, A Cobalt Complex with a Bioinspired Molybdopterin-like Ligand: a Catalyst for Hydrogen Evolution, *Dalton Trans.*, 2016, **45**, 14754–14763. DOI: 10.1039/C6DT01824F
S20. M. Namazian, C. Y. Lin and M. L. Coote, Benchmark Calculations of Absolute Reduction Potential of Ferricinium/Ferrocene Couple in Nonaqueous Solutions, *J. Chem. Theory Comput.*, 2010, **6**, 2721–2725. DOI: 10.1021/ct1003252
S21. A. S. Kramarenko, D. I. Sharapa, E. A. Pidko and F. Studt, Ab Initio Kinetics of Electrochemical Reactions Using the Computational Fc^0/Fc^+ Electrode, *J. Phys. Chem. A*, 2024, **128**, 9063–9070. DOI: 10.1021/acs.jpca.4c04923